LOW TEMPERATURE TRANSPORT PROPERTIES OF SOME DILUTE COPPER ALLOYS

J. J. DE JONG

LOW TEMPERATURE TRANSPORT PROPERTIES OF SOME DILUTE COPPER ALLOYS

PROEFSCHRIFT

TER VERKRIJGING VAN DE GRAAD VAN DOCTOR IN DE WISKUNDE EN NATUURWETENSCHAPPEN AAN DE RIJKSUNIVERSITEIT TE LEIDEN, OP GEZAG VAN DE RECTOR MAGNIFICUS DR. A. E. COHEN, HOOGLERAAR IN DE FACULTEIT DER LETTEREN, VOLGENS BESLUIT VAN HET COLLEGE VAN DEKANEN TE VERDEDIGEN OP WOENSDAG 11 DECEMBER 1974 TE KLOKKE 16.15 UUR.

DOOR

JACOBUS JOHANNES DE JONG
GEBOREN TE SCHEVENINGEN IN 1946

1974
DRUKKERIJ J. H. PASMANS, 'S-GRAVENHAGE

PROMOTOR: Dr. G.J. van den Berg

COREFERENT: Dr. W.M. Star

This investigation is part of the research programs of the 'Stichting voor Fundamenteel Onderzoek der Materie (F.O.M.)', which is financially supported by the 'Nederlandse Organisatie voor Zuiver-Wetenschappelijk Onderzoek (Z.W.O.)' and by the 'Centrale Organisatie voor Toegepast Natuurwetenschappelijk Onderzoek (T.N.O.)'.

Aan mijn ouders

CONTENTS

CHAPTER I

GENERAL INTRODUCTION

The study of the transport phenomena of metals and their alloys is known to provide valuable information about the electronic structure of these metals. Throughout the years most attention has been given to the electrical conductivity, since this property can be measured and calculated in a relatively simple manner. Thermal conductivity, another important transport property, has received much less attention. This is not surprising, in view of the complicated structure of the thermal conductivity mechanism and of the experimental accuracy that can be achieved, i.e., some orders of magnitude less than can be obtained in electrical conductivity measurements. Besides, much information that can be extracted from thermal conductivity studies is already contained in electrical conductivity data. On the other hand a number of reasons can be put forward, which emphasize the importance of thermal conductivity studies, such as the need of a proper knowledge of this quantity for materials to be used in low temperature physics, and more recently, in modern technology (space research). From a theoretical point of view it appears that the additional information, obtained from thermal conductivity studies can enrich the knowledge about some aspects of the theory of metals.

The interpretation of experimental data on transport properties was and still is often hampered considerably by the occurrence of anomalies at low temperatures, of which the 'minimum in the electrical resistivity' is the most famous one. Originally considered as being annoying complications, these phenomena, which are associated with the presence of small traces of transition metal impurities in the host metal, have attracted the attention of many experimentalists (1) and later on also many theorists (2). The anomalies in various physical properties are now known in literature by the name 'Kondo effect', which formed an interesting field of research for many metal physicists during the past decade.

Actually, the original purpose of the work presented in this thesis, was to investigate the Kondo effect in copper dilutely alloyed with transition metal atoms with special emphasis on its influence on the thermal conductivity, since this aspect had been more or less neglected over the years. It soon appeared to be necessary to study nonmagnetic alloys and the pure metal as well. This now forms the framework of Chapter III of this thesis. A major part of this chapter deals with one of the most intriguing subjects in metal physics:the electron-phonon interaction. This interaction determines the coupling between the conduction electrons, which carry

charge and heat, and the lattice. In addition, the lattice also transports heat. The lattice thermal conductivity is affected by the same electron-phonon coupling and can therefore provide additional information about this interaction.

A parameter, which will be used frequently in this thesis, is the Lorenz number L defined as

$$L = \frac{\lambda}{\sigma T} \qquad (I.1)$$

where λ is the thermal conductivity, σ is the electrical conductivity and T is the temperature. The physical significance of comparing both conductivities by means of this ratio will be discussed in Section II.2. From a practical point of view it is important to note, that certain constants, the values of which are uncertain or difficult to calculate, cancel (e.g., the shapefactor, a quantity which is always difficult to determine precisely, cancels if λ and σ are measured on the same specimen).

After a brief introduction to transport theory in Section II,1 with emphasis on its qualitative aspects, the theory of the Lorenz number is presented in Section II.2. A more quantitative treatment of the behaviour of some transport phenomena at low temperatures (electrical and thermal conductivity and thermoelectric power) is found in Section II.3. We will exclude from this section the phenomena associated with the Kondo effect (Chapter IV). Experimental details, given in Section II.4, conclude Chapter II.

In Chapter III the experimental results on some nonmagnetic Cu-alloys and pure Cu are presented and discussed within the context of the theory given in the preceding chapter. Some of these results will be employed to analyse the transport properties of dilute magnetic Cu-alloys (copper dilutely alloyed with transition metal impurities) in Chapter IV. This chapter starts with a discussion of the various theoretical models, developed for dilute magnetic alloys. Subsequently the experimental results are presented, analysed and critically discussed.

It should be noted, that it was not possible to obtain a Cu specimen sufficiently free of magnetic impurities. Consequently, some experimental results, presented in Chapter III, exhibit small anomalies, illustrating the remarks, made above, about the problems, which arise if one tries to discuss the properties of pure metals at low temperatures.

References

1. The most up-to-date review paper concerning experiments on the Kondo effect is: C. Rizzuto, Reports on Progress in Physics, 37 (1974) 147.
2. Reviews of recent theoretical developments in the dilute magnetic alloy problem can be found in:
Magnetism, ed. H. Suhl (Academic Press, New York and London, 1973), Vol. V.
A more extensive list of review papers on both the experimental and theoretical aspects of the Kondo effect is given at the end of Chapter IV.

CHAPTER II

THEORETICAL CONSIDERATIONS AND EXPERIMENTAL DETAILS

II.1. Some aspects of the transport theory of metals.

In this section emphasis will be placed on the qualitative features of the theory, with particular application to the electrical and thermal conductivity at low temperatures. The mathematical derivation of the transport coefficients can be found in the textbooks covering this topic (1).

The metal is considered as an array of atoms in a crystal lattice embedded in a 'sea' of conduction electrons, which obey Fermi-Dirac statistics. The electron distribution function is given by

$$f_0 = \frac{1}{e^{\frac{(\varepsilon-\mu)}{k_B T}} + 1} \qquad \text{(II.1)}$$

where f_0 through ε depends on the wave-vector $\vec{k}$. The chemical potential μ is equal to the Fermi energy ε_F at $T = 0$. The periodicity of the crystal corresponds to a periodicity in wave-vector space. The most convenient unit cell of the reciprocal lattice is called the Brillouin zone. This unit cell is the smallest volume in $\vec{k}$ space, bounded by planes, bisecting the vectors which connect a fixed point of the reciprocal lattice with all other lattice points. The concept of Brillouin zones implies that physically there is no difference between states with wave-vector $\vec{k}$ and $\vec{k} + \vec{g}$, where $\vec{g}$ is a reciprocal lattice vector. All states can be described by wave-vectors in the fundamental Brilluoin zone with origin $\vec{k} = 0$.

The volume in wave-vector space, which contains the occupied electron states at $T = 0$, is enclosed by a surface of constant energy ε_F, called the Fermi Surface (FS). The FS is spherical, if the conduction electrons are considered to be free electrons with energy $\varepsilon = \hbar^2 k^2/2m$. This simple model, which disregards the periodicity of the lattice potential, formed one of the crucial breakthroughs in the understanding of the electronic structure of metals. In reality only very few metals behave according to the free electron model.

Taking into account the periodicity of the lattice potential the FS will become distorted from a sphere, especially in regions close to the zone boundaries. A surprisingly good description of many real metals is provided by the so-called nearly free electron model, which considers the lattice potential $V(\vec{r})$ as a weak

pertubation. The change in the ε-k relation can be accounted for in terms of an effective mass m* : $\varepsilon = \hbar^2 k^2/2m^*$. For the moment, the free electron model forms a useful starting point for our discussion of the transport phenomena in metals.

The flow of charge and/or heat under the influence of external force fields (electric field $\vec{E}$ and/or temperature gradient $\vec{\nabla}T$) is disturbed by scattering processes, which the carriers undergo. The stationary state is described by the Boltzmann equation

$$\left(\frac{\partial f}{\partial t}\right)_{field} + \left(\frac{\partial f}{\partial t}\right)_{coll.} = 0 \qquad \text{(II.2)}$$

where

$$\left(\frac{\partial f}{\partial t}\right)_{field} = -\vec{v}_k \cdot \vec{\nabla}_r f - \dot{\vec{k}} \cdot \vec{\nabla}_k f \qquad \text{(II.3)}$$

in which $\vec{v}_k$ is the group velocity of the conduction electrons and $\dot{\vec{k}} = e\vec{E}/\hbar$. The first term in the right-hand side of Eq.(II.3) arises from a possible variation in temperature: $df/d\vec{r} = (df/dT)\vec{\nabla}T$. Eq.(II.3) can be linearized under the assumption, that the applied electric field and temperature gradient are small and consequently the resulting electric and heat current are linear in $\vec{E}$ and $\vec{\nabla}T$. Eq.(II.3) then becomes

$$\left(\frac{\partial f}{\partial t}\right)_{field} = -\vec{v}_k \cdot \frac{df_0}{d\varepsilon}\left(e\vec{E} + \frac{\varepsilon_F - \varepsilon}{T}\vec{\nabla}T\right) \qquad \text{(II.4)}$$

where we have neglected the temperature dependence of μ.

The problem of solving Eq.(II.2) is considerably simplified by assuming that after removing the pertubation, the electron distribution relaxes exponentially back to its equilibrium value f_0

$$-\left(\frac{\partial f}{\partial t}\right)_{coll.} = \frac{f_0 - f}{\tau} \qquad \text{(II.5)}$$

where τ is the time characterizing this exponential decay.

It is shown in the next section, that the introduction of a relaxation time is not always justified and other methods, such as the variational method, must be employed to solve Eq.(II.2). This technique is based on finding the most rapid relaxation of f towards f_0 when the pertubation is removed, which is equivalent to maximizing the relaxation rate. The concept of a relaxation time has, however, a

clear physical meaning, since it can be shown from general considerations, that τ may be interpreted as the collision time of the conduction electrons $\tau = \ell/v$, where ℓ is the mean free path and v is the velocity of the electrons.

The new electron distribution function in the steady state can now be written as

$$f = f_0 - \tau \frac{df_0}{d\varepsilon} \vec{v}.(e\vec{E} + \frac{\varepsilon_F - \varepsilon}{T}\vec{\nabla}T) \qquad \text{(II.6)}$$

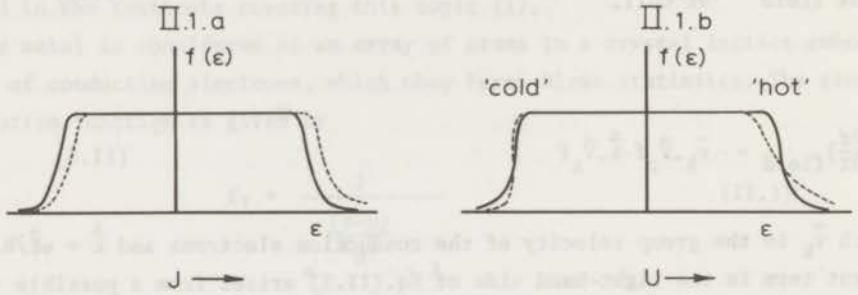

Fig.II.1. The energy distribution function for electronic conduction (a) and for thermal conduction (b) as a function of energy ε for two directions of $\vec{k}$ parallel to the electric field gradient and the temperature gradient, respectively.
——— equilibrium distribution
------ steady state distribution

The change in the distribution function is visualized in Fig. II.1. The response of the system to an applied electric field is shown in Fig. II.1.a. The shift in f corresponds to an electric current in the direction of the applied field. The departure of f from its equilibrium value, resulting from a temperature gradient, depends on the energy ε (Fig.II.1.b). At the 'hot' side of the FS, there are now more 'hot' electrons, whereas at the 'cold' side there is a surplus of 'cold' electrons. Since there are just as many hot electrons travelling in one direction as there are cold electrons travelling in the opposite direction only a flow of heat is produced.

The electric current density $\vec{J}$ and the heat currect density $\vec{U}$ are given by

$$\vec{J} = \frac{e}{4\pi^3} \int \vec{v}(f-f_0)d^3\vec{k} \qquad \text{(II.7)}$$

$$\vec{U} = \frac{1}{4\pi^3} \int \vec{v}(f-f_0)(\varepsilon-\varepsilon_F)d^3\vec{k} \qquad \text{(II.8)}$$

From the definition of the electrical conductivity σ : $\vec{J} = \sigma\vec{E}$ in the absence of a temperature gradient, and the thermal conductivity λ : $\vec{U} = -\lambda\vec{\nabla}T$ if $\vec{J} = 0$, the following expressions for the transport coefficients are obtained

$$\sigma = e^2 K_0 \tag{II.9}$$

$$\lambda = \frac{1}{T}\left(K_2 - \frac{K_1^2}{K_0}\right) \tag{II.10}$$

$$S = \frac{1}{eT}\frac{K_1}{K_0} \tag{II.11}$$

$$L = \frac{1}{e^2T^2}\left(\frac{K_2}{K_0}\right) - S^2 \tag{II.12}$$

where

$$K_n = -\frac{1}{4\pi^3\hbar^2}\int \left(\frac{\partial\varepsilon}{\partial k_x}\right)^2 \tau \frac{df_0}{d\varepsilon}(\varepsilon-\varepsilon_F)^n \, d^3\vec{k} \tag{II.13}$$

and $d^3\vec{k} = dSd\varepsilon\left|\vec{\nabla}_k\varepsilon\right|^{-1}$; dS is an element of the FS. The electrical field and the temperature gradient are taken along the x-direction. The third transport coefficient S (Eq.(II.11)) is the thermoelectric power and results from the fact that the non-equilibrium distribution produced by a heat current can lead to a net charge flow.

In the case of a spherical FS Eq.(II.13) reduces to:

$$K_n = -\frac{2}{3}\int v^2\tau n(\varepsilon)\frac{df_0}{d\varepsilon}(\varepsilon-\varepsilon_F)^n \, d\varepsilon \tag{II.14}$$

where the density of states is given by $n(\varepsilon) = (1/(8\pi^3))\int dS\left|\vec{\nabla}_k\varepsilon\right|^{-1}$.

The dependence of the transport coefficients on the transport integrals K_n reflects one of the characteristic differences between σ and λ. Because of the factor $df_0/d\varepsilon$, the integrand in Eq.(II.14) has a finite value only in a range of order k_BT about the Fermi energy. Furthermore, it can be seen that the second term in Eqs.(II.10) and (II.11) is in general very small, since $(\varepsilon-\varepsilon_F)(df_0/d\varepsilon)$ is an odd function of $(\varepsilon-\varepsilon_F)$. In Eq.(II.9) the relaxation time is measured at energies in the immediate vicinity of ε_F, whereas in Eq.(II.10) τ is measured at energies slightly below and above ε_F (Fig.II.2). This may have important consequences, if τ is strongly energy dependent near the Fermi energy, as will be discussed in the

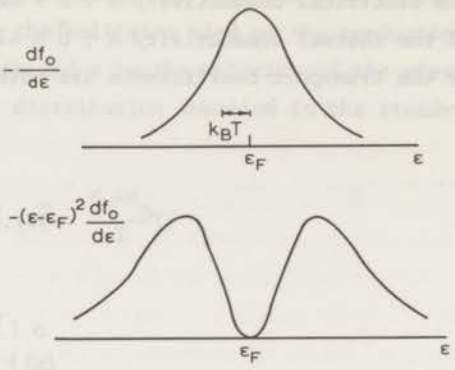

Fig.II.2. Schematic representation of the factors $df_0/d\varepsilon$ and $(\varepsilon - \varepsilon_F)^2\, df_0/d\varepsilon$ which are contained in the expressions of the electrical and thermal conductivity.

next section. If, however, $v^2\tau n$ does not vary markedly with energy, then this factor can be replaced by its value at ε_F. Since $\int(df_0/d\varepsilon)d\varepsilon = -1$ and $\int(df_0/d\varepsilon)(\varepsilon-\varepsilon_F)^2 d\varepsilon = -\pi^2 k_B{}^2T^2/3$, the following important relation is obtained:

$$\frac{\lambda}{\sigma T} = \frac{\pi^2}{3}\left(\frac{k_B}{e}\right)^2 \qquad \text{(II.15)}$$

This is the Wiedemann-Franz-Lorenz law (WFL law), where $L_0 = (\pi^2/3)(k_B/e)^2 = 2.443 \times 10^{-8}\ V^2/K^2$ is known as the Sommerfeld value of the Lorenz number. The WFL law is thus derived under the assumption that a relaxation time exists. It can be shown that this result also holds for a non-spherical FS.

II.2. The Lorenz number

In the preceding section we have introduced the concept of a relaxation time. It turned out that a simple relation exists between the electrical and thermal conductivity. As was noted, the use of such a relaxation time is not always justified. In order to show this, we will examine in more detail the collision term $(\partial f/\partial t)_{coll}$. Two types of scattering processes can be distinquished:elastic scattering involving only a change in electron momentum and inelastic scattering, in which both momentum and energy transfer may occur. We discuss the following scattering mechanisms: 1) electron-impurity scattering, 2) electron-phonon scattering and 3) electron-electron scattering. The latter process is generally not very important in simple metals, but is included in this discussion because of its interesting features. Moreover, we will again encounter this scattering process in Chapter IV.

II.2.a. Electron-impurity scattering

Electron-impurity scattering is an elastic scattering process. If we restrict ourselves for the moment to ordinary impurity scattering (potential scattering, arising from a local change in the lattice potential when impurities are added to the host metal) this process is characterized by a relaxation time which varies slowly with energy (typically $\tau \sim \varepsilon^{0.5}$). Because only the direction of the velocity of the electrons is changed, such a scattering event is equally effective in destroying an electric current and a heat current. At the end of the preceding section it was shown that in that case the WFL law holds.

When the scattering is strongly energy dependent, the WFL law breaks down. We consider the extreme case of a resonance in the scattering crossection at ε_F, superimposed on the background scattering (e.g., weakly energy dependent potential scattering with relaxation time τ_0) as shown in Fig.II.3.

$$\tau^{-1} = \tau_0^{-1} + A \frac{\Gamma^2}{(\varepsilon-\varepsilon_F)^2 + \Gamma^2} \qquad \text{(II.16)}$$

In the expression for σ (Eq.(II.9)) the relaxation time is strongly weighted at energies in the immediate vicinity of ε_F, whereas the thermal conductivity reflects τ at energies slightly below and above ε_F (Fig.II.2). Therefore, at a fixed temperature T, the particular shape of τ (Eq.(II.16)) leads to a relatively larger reduction of K_0 from its original value, viz., $(2/3)(v^2\tau_0(\varepsilon_F)n(\varepsilon_F))$ than the reduction of K_2 from the value $(2/3)(v^2\tau_0(\varepsilon_F)n(\varepsilon_F)\pi^2/3)(k_BT)^2$. Consequently, the Lorenz number will exceed L_0. If the temperature is low enough, so that the thermal layer of the FS becomes small compared to the width of the resonance then L decreases towards its theoretical value L_0. It should be noted that K_1 is very small again, since τ was taken to be symmetrical about the Fermi energy, but may become important

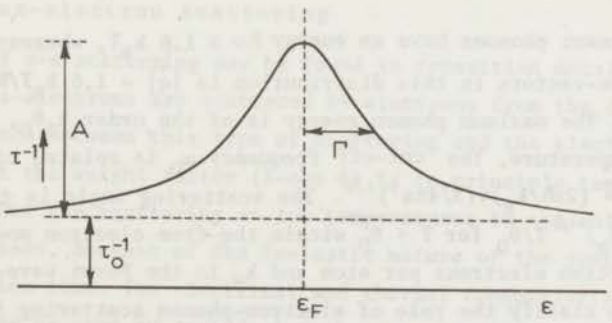

Fig.II.3. Resonance in the scattering amplitude at the Fermi energy.

if the scattering resonance occurs at energies slightly below or above ε_F('giant' thermopower, see Chapter IV). A possible temperature dependence of Γ may also influence the magnitude of the Lorenz number.

II.2.b. Electron-phonon scattering

Electron-phonon scattering arises from the interaction between the conduction electrons and the thermal vibrations of the lattice which disturbs the periodicity of the lattice potential. This interaction can be represented by

$$\vec{k} - \vec{k}' = \vec{q} + \vec{g} \qquad \text{(II.17)}$$

where $\vec{k}$ and $\vec{k}'$ are the wave-vectors of the electron before and after the collision, in which a phonon with wave-vector $\vec{q}$ is emitted or a phonon with wave-vector $-\vec{q}$ is absorbed. Since the electronic states are periodic in $\vec{k}$ (the period being a reciprocal lattice vector), two types of electron-phonon scattering processes can be distinquished. Processes in which $\vec{g} = 0$ are called Normal processes (N-processes). Processes with a non-zero $\vec{g}$ are called Umklapp processes (U-processes). The latter process, where after emission or absorption of a phonon the electron undergoes a Bragg reflection at the zone boundary, involves large momentum transfer. The distinction between large angle scattering (large momentum transfer) and small angle scattering (small momentum transfer) is useful in view of the inelastic nature of the electron-phonon scattering. The momentum and energy transfer is determined by the wave-vector and energy of the phonons involved in this scattering process. In the Debye model the number of phonons in a interval $d\omega$ is proportional to

$$\frac{(\hbar\omega/k_B T)^2}{e^{\hbar\omega/k_B T} - 1} \qquad \text{(II.18)}$$

so that the dominant phonons have an energy $\hbar\omega \approx 1.6\ k_B T$, whereas the magnitude of the dominant wave-vectors in this distribution is $|\vec{q}| = 1.6\ k_B T/\hbar v$, where v is the phonon velocity. The maximum phonon energy is of the order $k_B\theta_D$, where $\theta_D = \hbar\omega_D/k_B$ is the Debye temperature. The cut-off frequency ω_D is related to the interatomic distance a : $\theta_D = (2\pi\hbar/k_B)v(3/4\pi a^3)^{1/3}$. The scattering angle is given by the ratio $|\vec{q}|/2k_F \approx 1.6(4N_a)^{-1/3}\, T/\theta_D$ for $T < \theta_D$ within the free electron model. N_a is the number of conduction electrons per atom and k_F is the Fermi wave-vector.

In order to clarify the role of electron-phonon scattering in transport processes, we consider a monovalent metal ($N_a = 1$) within the free electron model.

The volume of the Fermi sphere is half the volume of the Brillouin zone and the FS closely approaches but does not touch the zone boundaries.

At low temperatures ($T \ll \theta_D$) the momentum transfer is very small ($|\vec{q}|/2k_F \ll 1$), whereas the energy transfer is of the order $k_B T$. This small angle scattering is therefore ineffective in destroying an electric current, since it takes many scattering events before the direction of motion of the electron is reversed. On the other hand, this type of scattering is highly effective in destroying a heat current, since the energy transfer is of the same order of magnitude as the thermal layer of the FS and can therefore change a hot electron into a cold electron or vice versa (Section II.1).

At high temperatures ($T > \theta_D$) the energy transfer ($\approx k_B \theta_D$) is smaller than the thermal layer ($\approx k_B T$) and the scattering can be treated as an elastic process, with typical momentum transfer $|\vec{q}| = |\vec{k} - \vec{k}'| \approx k_F$. This large angle quasi-elastic scattering affects both types of currents to the same extent. In the latter case a common relaxation time can again be defined, leading to the WFL law. In the former case ($T \ll \theta_D$) the concept of a relaxation time, as introduced in Section II.1 (Eq.II.5) has lost its meaning, since the relaxation of the electron distribution function now depends on the nature of the pertubation. It is of course permitted to use effective relaxation times describing the different conductivity processes, i.e., τ_σ and τ_λ. In the present case these characteristic times may be written as $\tau_\sigma^{-1} = \tau_0^{-1} \cdot (1-\cos\phi)$ and $\tau_\lambda^{-1} = \tau_0^{-1}$, where ϕ is the scattering angle (1). The weight factor $(1-\cos\phi)$ stresses the effectiveness of large angle scattering on the electrical conductivity. With increasing temperature this factor approaches the value 1. At low temperatures $(1-\cos\phi)$ can be replaced by $\phi^2/2 \simeq (1/2)(q/2k_F)^2 \sim (T/\theta_D)^2$. Hence the Lorenz number for electron-phonon scattering only is proportional to $(T/\theta_D)^2$ at low temperatures and approaches its theoretical value as T increases.

II.2.c. Electron-electron scattering

An example of e-e scattering may be found in transition metals, where the current carrying s-electrons are scattered by electrons from the d-band. The essential difference between this type of scattering and the electron-phonon scattering is that the weight factor $(1-\cos\phi)$ is in principle temperature independent, so that the scattering at low temperatures is not only governed by small angle processes. Because of the inelastic nature of the scattering, the effective relaxation times for electrical and thermal conductivity are stil different. This can be seen by considering the e-e scattering as a two-step process. First, the momentum of the electron changes in an elastic collission.

Then the energy of the electron is changed. The electrical conductivity is in principle only affected by the former process, whereas both steps influence the flow of heat. The Lorenz number arising from this type of scattering will have a value somewhere between zero and L_0 (typically $L_0/2$) depending on the relative effectiveness of both processes.

A remark is in order concerning the mutual interaction between the conduction electrons represented by $\vec{k}_1 + \vec{k}_2 \rightarrow \vec{k}_1' + \vec{k}_2'$. Since the total momentum and energy are conserved, this type of N-process will not produce resistance. The resistive nature of these e-e scattering processes arises from the inclusion of U-processes (Eq.(II.17)). However, in general only interactions between electrons belonging to different bands turn out to be important in transport problems.

In this section we have qualitatively discussed the effect of various scattering processes on the Lorenz number. It turned out that the Lorenz number arising from a particular interaction process is a very suitable quantity for obtaining information about the nature of the interaction. Unfortunately, because of the simultaneous occurrence of various scattering processes, the measured Lorenz number has a rather complicated structure. A well known example is the Lorenz number for combined electron-impurity and electron-phonon scattering in simple metals, shown in Fig.II.4. At high temperatures electron-phonon scattering dominates and because of the quasi-elastic nature of the scattering the WFL law holds. As T decreases, L is reduced below L_0, since the electrical conductivity is less affected by the interaction between electrons and long wavelength phonons, than is the thermal conductivity. In ideally pure metals L would approach zero at T = 0. In reality, electron-impurity scattering becomes important at low temperatures. Conse-

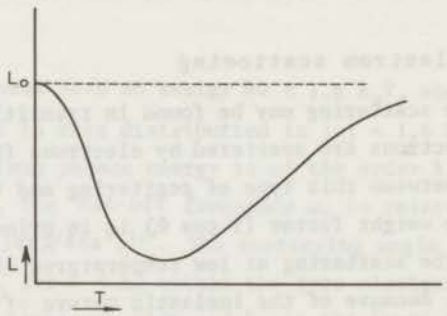

Fig.II.4. The Lorenz number for combined electron-impurity and electron-phonon scattering of a typical metal as a function of temperature.

quently, in a certain temperature region L starts to rise and reaches its theoretical value at T = 0. The depth of the minimum in L and the temperature at which this minimum occurs depend on the relative importance of both scattering processes.

The structure of L becomes even more complicated in alloys. Because of the importance of the lattice thermal conductivity compared to the electronic thermal conductivity, the measured Lorenz number is not solely determined by electron scattering processes anymore. This will considerably reduce the precision of the experimental values of specific Lorenz numbers, such as L_{imp} and L_{e-e} (Chapter IV).

II.3. Low temperature transport properties of metals and alloys

In this section we will examine in more detail the low temperature transport properties of metals. First, the electrical and thermal conductivity are discussed. Subsequently the lattice thermal conductivity is considered and some remarks about the thermoelectric power conclude this section.

II.3.a. Electronic conduction

II.3.a.1. Pure metals

Defining the resistivity as the reciprocal of the conductivity, the electrical resistivity (ρ) and the electronic thermal resistivity (W_e) can be written as: $\rho = \rho_0 + \rho_{id}$ and $W_e = W_0 + W_{id}$, where ρ_{id} and W_{id} are the resistivities arising from electron-phonon scattering ('ideal' resistivity). The resistivity components arising from electron-impurity scattering, ρ_0 and W_0, are related through the WFL law.

The quantitative theory of the ideal resistivity is based on the Bloch model for the electrical resistivity, which assumes a spherical FS, N-processes and a Debye spectrum for the phonons. The electrical and thermal resistivity due to electron-phonon scattering can be written as (1)

$$\rho_{id} = \frac{3\pi a^3 C^2 m^2}{e^2 \hbar N_a^2 k_B M\theta} \left(\frac{T}{\theta}\right)^5 J_5\left(\frac{\theta}{T}\right) \qquad \text{(II.19)}$$

$$W_{id} = \frac{27 m^2 a^3 C^2}{\pi^3 k_B^3 \hbar (2)^{2/3} N_a^{4/3} M\theta^2} \left(\frac{T}{\theta}\right)^2 \left[J_5\left(\frac{\theta}{T}\right) + \frac{2^{-1/3}}{N_a^{2/3}} \left(\frac{T}{\theta}\right)^2 \left(\frac{2\pi^2}{3} J_5\left(\frac{\theta}{T}\right) - \frac{1}{3} J_7\left(\frac{\theta}{T}\right)\right)\right] \qquad \text{(II.20)}$$

where a^3 is the atomic volume, e is the electronic charge, M is the atomic mass, θ

is the Debye temperature, C is the electron-phonon interaction constant with dimension energy and

$$J_n(z) = \int_0^z \frac{e^x x^n dx}{(e^x-1)^2} \qquad \text{(II.21)}$$

Referring to the discussion in Section II.2.b, one sees that the first term in Eq.(II.20) arises from small angle scattering. A comparison with Eq.(II.19) demonstrates the breakdown of the WFL law

$$L_{id} = 5.22\ L_0 \left(\frac{T}{\theta}\right)^2 N_a^{-2/3} \qquad \text{(II.22)}$$

The second term in W_{id} is due to large angle scattering and will eventually dominate the T^2-term. Comparison with Eq.(II.19) shows the validity of the WFL law for this type of scattering. The J_7-term is a correction term and results from the fact that large momentum transfer combined with large energy transfer should not produce resistance.

Eq.(II.20) is valid only in the limit of strong impurity scattering. For the inverse case ($W_{id} >> W_0$) Sondheimer (2) showed, employing a variational method for solving the Boltzmann equation (Eq.(II.2)), that for $T \ll \theta$ the T^2-term is reduced by a factor of 0.75. Later Klemens (3) pointed out that an exact solution of the Bloch integral equation gives rise to a correction factor of 0.67. Ehrlich (4) found that the T^4-term is also modified, by a factor of 0.71.

In the original derivation of Eqs.(II.19) and (II.20) it was assumed that the electron-phonon scattering occurs through N-processes;electrons interact with longitudinally polarized phonons only. This means that the θ in these expressions should be the Debye temperature for the longitudinal modes θ_ℓ and furthermore that $C = C_\ell = 2\varepsilon_F/3$. Comparison of Eqs.(II.19) and (II.20) with experiment shows large discrepancies, which is not surprising in view of the various simplifying assumptions of the Bloch theory. The major cause for the failure of the Bloch theory has been known for a long time, viz., the neglect of U-processes, which, because they involve large momentum transfer, markedly affect the transport of heat and charge. We first consider the case of a monovalent metal with a spherical FS which does not touch the zone boundaries. The Bloch theory considers only transitions through angles $< \arcsin (q_D/2k_F) \approx 78^0$. The matrix element $M(\vec{k},\vec{k}')$ for electron-phonon scattering is simply a constant, independent of the scattering angle for $|\vec{k}-\vec{k}'| < 2^{1/3} k_F$ and vanishes for larger values of $|\vec{k}-\vec{k}'|$. Bardeen (5)

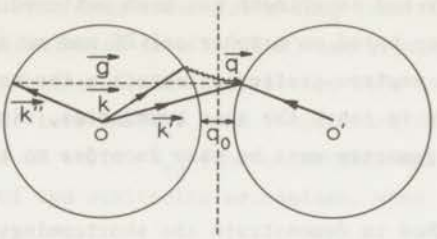

Fig.II.5. An electron-phonon Umklapp process. The interaction of an electron with wave-vector $\vec{k}$ with a phonon with wave-vector $\vec{q}$ yields a final wave-vector $\vec{k}'$, which lies across the zone boundary. The electron state $\vec{k}'$ is, however, equivalent to $\vec{k}''$ and hence the direction of motion of the electron in state $\vec{k}$ is drastically changed.

pointed out that transitions through angles > 78^0 can occur through U-processes if the phonons have wave-vectors larger than the minimum separation q_0 of the FS in neighbouring zones. The geometry of such a transition is shown in Fig.II.5. In particular at high temperatures, where phonons with large wave-vectors are available, these processes are important. Within this simple model one sees that in a certain temperature region U-processes will be frozen out if the wave-vector becomes smaller than q_0. In this temperature region the resistivity decreases rapidly towards a value given by Eqs(II.19) and (II.20) with $\theta = \theta_\ell$. The effect will be more pronounced for the electrical resistivity than for the thermal resistivity, since the former is more sensitive to the occurrence of large angle scattering.

Since the matrix element $M(\vec{k},\vec{k}')$ contains a polarization factor $(\vec{k}-\vec{k}').\vec{\varepsilon}$, where $\vec{\varepsilon}$ is the polarization vector, the transverse modes take part in the interaction through U-processes. Hence $C_t \neq 0$.

As yet we have considered the oversimplified case of a spherical FS. It is obvious that distortions of the FS near the zone boundaries greatly enhance the effect of U-processes. Finally, when the FS touches the zone boundaries, the distinction between N- and U-processes becomes entirely artificial and large momentum transitions occur down to the lowest temperatures.

An adequate theory, which correctly describes the transport properties of metals, demands a precise knowledge of the shape of the FS in order to properly include U-processes. Moreover, a realistic phonon spectrum must be employed. Because of the anisotropy of the crystal, the phonons are purely longitudinally and transversally polarized only in a few directions of high symmetry.

The present state of affairs tells us that only for potassium satisfactory

agreement between theory and experiment has been achieved. The calculations (6) for this alkali metal are based on a spherical FS and on a realistic phonon spectrum, obtained from neutron scattering data. In the case of the noble metals, the FS of which is known to touch the zone boundaries, simplifying assumptions with respect to the FS geometry must be made in order to keep the calculations tractable.

An appropriate method to demonstrate the shortcomings of the Bloch theory is to intercompare Eqs.(II.19) and (II.20), thereby eliminating C. This can be done in several ways, such as a comparision of the low temperature expressions of ρ_{id} and W_{id} (Eq.(II.22)) or by comparing the low and high temperature form of W_{id} (7):

$$\frac{W_{id}}{W_{id}(\infty)} = 63.6\ (\frac{T}{\theta})^2 N_a^{-2/3} \qquad \text{(II.23)}$$

The Sondheimer-Klemens correction, viz., $W_{id}(W_{id} \gg W_0) = 0.67\ W_{id}(W_{id} \ll W_0)$, has been taken into account in Eq.(II.23). The same correction must be applied to Eq.(II.22), where the numerical factor now becomes 7.79. Although there is some ambiguity in the choice of θ, the discrepancy between these two expressions and experiment turns out to be significant.

Klemens and Jackson (8) treated the scattering of the electrons by phonons at low temperatures as a diffusion process on the FS. The Boltzmann equation is then reduced to a diffusion equation. Employing a FS model, which is applicable to the noble metals, they pointed out that U-processes are responsible for an enhancement of the coefficient of the T^5-term of ρ_{id} by a factor of 3 (θ is now some average Debye temperature), thereby reducing the discrepancy between the observed and calculated L_{id} by approximately the same factor. Extension of this theory (9) by including impurity scattering showed that the temperature dependence of ρ_{id} also changes. Similar results were obtained for aluminium (10), which of all polyvalent metals is the most free electron like.

II.3.a.2. Alloys

A discussion of the electrical and thermal resistivity of alloys should start with an examination of Matthiessen's Rule (MR), which can be expressed in the following form: The total resistivity of an alloy is the sum of the resistivity of the pure metal and a temperature independent resistivity term arising from the scattering of the electrons by the added impurities (We consider only nonmagnetic impurities; for a discussion of the validity of MR in dilute magnetic alloys we

refer to Chapter IV). It has been known for a long time that this rule is seldom obeyed. An example of a deviation from MR (DMR) was already discussed in Section II.3.a.1, namely the Sondheimer-Klemens correction term to the thermal resistivity. In the limit $W_0 >> W_{id}$ this term has the same temperature dependence as W_{id}: $W = W_0 + W_{id} + \Delta W$, where $\Delta W = 0.49\ W_{id}$ (The corresponding term in ρ, which result from the superposition of two scattering mechanisms, when solving the Boltzmann equation is very small).

DMR have been mainly studied in the electrical resistivity. An extensive review on this subject has been given by Bass (11). We will give a brief outline of this phenomenon, with emphasis on those aspects which are thought to be important for the electronic thermal resistivity of alloys.

The principal mechanisms, which have been proposed to explain the DMR are:
a) changes in the electronic structure and in the phonon spectrum upon alloying,
b) different anisotropies in electron-impurity and electron-phonon scattering,
c) additional scattering processes, associated with the added impurities.

One of the most difficult problems, which arise when examining the phenomenon of DMR is how to determine the relative magnitude of the contributions resulting from the sources listed above. In relation to the electrical resistivity of dilute alloys (solute concentration less than a few percent), it is generally assumed that the contributions from source a) are negligible compared to those associated with the other mechanisms. In most metals category b) is thought to be the most important source for the occurrence of DMR. The anisotropy in the low temperature electron scattering probability results from a strong orientational dependence of the electron-phonon scattering. The sources for this directional dependence are: b.1) anisotropy of the FS, b.2) anisotropy in the phonon spectrum, b.3) U-processes.

It turns out that elastic (nearly) isotropic electron-impurity scattering can produce a significant change in ρ_{id}, simply by reducing the anisotropy of the scattering time. This effect of 'washing out' the anisotropy of the electron-phonon scattering through the addition of impurities has received much attention recently (12).

The most simple way to deal with anisotropic scattering is by means of the so-called 'two-band' model (13), originally introduced to describe the transport properties of a metal containing two conduction electron bands. The same formalism can, however, be applied to a conduction band containing different groups of electrons, which can be treated independently from each other. In this case, the total conductivity equals the sum of the conductivities of the different bands or groups of electrons. The total resistivity is larger than the sum of the resistivi-

ties of each group or band (in each band MR is assumed to hold). The deviation Δ turns out to be proportional to ρ_{id} if $\rho_0 >> \rho_{id}$. DMR in noble metals have been frequently discussed in terms of this model (14), where electrons in regions of the FS near the zone boundaries ('neck' electrons) and electrons on the other parts of the FS ('belly' electrons) are treated independently.

The correct way to treat DMR arising from sources mentioned in category b) is to include the anisotropy in the electron distribution function and to solve the Boltzmann equation with a variational method using an anisotropic trial function. This has been done for potassium (15) where the spherical geometry of the FS considerably facilitates the calculations. The more simple relaxation time approximation (12), where an anisotropic electron-phonon scattering time is combined with an isotropic impurity scattering time shows DMR which are in good agreement with those obtained from a variational solution of the Boltzmann equation (15).

There have been several attempts to explain DMR in terms of additional scattering mechanisms associated with the added impurities (category c)). We mention inelastic impurity scattering (16) and momentum-non-conservation scattering processes (17). Both mechanisms lack a sound theoretical basis and are subject to criticism. The former process (Koshino effect) arises from the scattering of the electrons by the impurity lattice potential, which is deformed by the lattice vibrations. Damon et al. (18) claimed to have observed a resistivity component $\sim T^4$ caused by this effect in Au-alloys. The latter mechanism results from the fact that in the presence of strong impurity scattering ('dirty' limit) the uncertainty in the electron momentum has become so large, that phonons of any wave-vector q can scatter electrons through large angles. The resulting resistivity term differs from the ideal resistivity in that the large angle factor $(1-\cos\phi)\sim T^2$ is replaced by 1, leading to a T^3-behaviour.

Turning now to the thermal resistivity (W), it must be mentioned that experimental information about DMR in W is strongly limited and not very reliable. Conditions necessary to observe DMR are: a) a small lattice conductivity and b) a relatively large ideal thermal resistivity. Some of the polyvalent metals, notably Al, In, Sn and Pb appear to be the best candidates. The observed DMR in these metals are usually described in terms of an increase of the coefficient of the T^2-term. Possible changes of the temperature dependence of $(W_{id})_{alloy}$ have not been observed due to the poor accuracy of the thermal conductivity measurements.

At first sight one expects the DMR in W arising from anisotropy in the electron scattering to be less pronounced than in ρ, because of the dominant contribution of N-processes to the low temperature thermal resistivity. The anisotropy in N-processes can only result from an anisotropic phonon spectrum and FS and is not expected to be

very large. Hence, the combination of two nearly isotropic processes should not produce large DMR (apart from the Sondheimer-Klemens term (Section II.3.a.1)). However, it has been shown by Schotte and Schotte (19) that the anisotropy due to U-processes, in which transverse phonons take part also, can account for a significant enhancement of W_{id} (a factor of 2 in Al).

Explanations of observed DMR in the thermal resistivity in terms of additional scattering mechanisms (category c)) have also been put forward, but are not very convincing. Campbell (20) suggests that momentum-non-conservation processes give rise to a deviation $\Delta W = \Delta\rho/(0.161 L_0 T)$. Since $\Delta\rho \sim T^3$, ΔW has the same temperature dependence as W_{id}.

II.3.b. Lattice thermal conductivity

As was already mentioned in the preceding section, knowledge of the lattice thermal conductivity λ_g of metals and alloys is essential to obtain information about the DMR in the electronic thermal resistivity. Moreover, it turns out that a study of the phonon conductivity provides additional information about the nature of the electron-phonon interaction. The lattice component of the thermal conductivity can be written as:

$$\lambda_g = \frac{1}{3} \frac{k_B^4 T^3}{2\pi^2 \hbar^3} \sum_j \int_0^{\theta_j/T} \frac{\tau_j}{v_j} \frac{x^4 e^x}{(e^x-1)^2} \, dx \qquad \text{(II.24)}$$

where the summation is over the three phonon modes, $x = \hbar\omega/k_B T$, ω is the phonon frequency, v is the phonon velocity and k_B, $\hbar$ and θ_j are defined as usual. The total relaxation time τ_j is for different scattering processes (i) given by: $\tau_j^{-1} = \sum_i \tau_{ji}^{-1}$.

It should be emphasized that a separation of λ_g in λ_ℓ and λ_t can only be made in isotropic media, where the phonons are either purely longitudinal or purely transverse. However, the complications which arise by taking into account anisotropy usually do not alter the general features of the phonon conductivity.

II.3.b.1. Phonon-phonon processes

An essential point in the discussion of λ_g is the coupling between phonons of different polarization modes. This coupling can be described in terms of phonon-phonon scattering processes, in which two phonons are destroyed, creating a new phonon. As in the electron-phonon interaction, it is convenient to distinquish

between N and U-processes. The former processes do not produce resistance because of momentum conservation, but must be taken into account for their influence in establishing equilibrium. The latter processes can be treated as one of the many phonon scattering processes, that limit λ_g.

From general considerations it can be shown that the only types of 3-phonon processes allowed are: (1) $\ell + t \leftrightarrows \ell$ and (2) $t + t \leftrightarrows \ell$, where ℓ represents a longitudinal phonon and t a transverse phonon. In anisotropic media other types of processes may occur, such as $t_s + t_f \leftrightarrows t_f$ where t_s and t_f are slow and fast transverse phonons, respectively.

Following Callaway (21) and Holland (22) we may account for the effect of N-processes on λ_g in the following way, writing

$$\lambda_g = \lambda_1 + \lambda_2 \tag{II.25}$$

where λ_1 is Eq.(II.24) with $\tau_j^{-1} = \sum_i \tau_{ji}^{-1} + \tau_{jN}^{-1}$. The relaxation time of N-processes is τ_{jN} and τ_{ji} is the relaxation time of those processes which do not conserve momentum. The correction term λ_2 results from the non-resistive nature of N-processes and is given by:

$$\lambda_2 = \frac{1}{3} \frac{k_B^4 T^3}{2\pi^2 \hbar^3} \frac{\left[\sum_j \int_0^{\theta_j/T} \frac{1}{v_j^3} \frac{\tau_{jN}^{-1}}{\tau_j^{-1}} \frac{x^4 e^x}{(e^x - 1)^2} dx\right]^2}{\sum_j \int_0^{\theta_j/T} \frac{1}{v_j^5} \frac{\tau_{jN}^{-1}(\tau_j^{-1} - \tau_{jN}^{-1})}{\tau_j^{-1}} \frac{x^4 e^x}{(e^x - 1)} dx} \tag{II.26}$$

The relaxation times τ_N for transverse and longitudinal phonons at low temperatures are (23):

$$\tau_{tN}^{-1} \approx \frac{60\, \gamma^2 k_B T^4}{M v^2 \theta^3} \omega \tag{II.27}$$

$$\tau_{\ell N}^{-1} \approx \frac{10\, \gamma^2 k_B a^3 T}{M v^2 v_\ell^3} \omega^4 \tag{II.28}$$

where γ is the Grüneisen constant, M is the atomic mass, a^3 is the atomic volume,

v_ℓ is the longitudinal phonon velocity, θ is the Debye temperature and v is some average phonon velocity.

For anisotropic media Herring (24) derived a more general form of τ_N for all low frequency modes: $\tau_N^{-1} \sim \omega^n T^{5-n}$.

Three-phonon U-processes turn out to be the dominant mechanism in limiting λ_g at high temperatures ($T \gtrsim \theta_D$) and give $\lambda_g \sim T^{-1}$. At low temperatures, the thermal resistivity due to U-processes decreases exponentially with temperature as the number of phonons needed for these processes fall off exponentially.

II.3.b.2. Electron-phonon scattering

The most important phonon scattering mechanism, which limits λ_g at low temperatures is the electron-phonon scattering. This interaction is responsible for the fact that the lattice conductivity of metals and alloys is considerably smaller than the conductivity of insulators. The first extensive treatment of the influence of this interaction on λ_g was given by Makinson in 1938 (25). Within the framework of the free electron model he obtained the following expression for the relaxation time

$$\tau_j^{-1} = \frac{C_j^2 m^2 a^3}{2\pi M \hbar^3 v_j} \omega \qquad \text{(II.29)}$$

where C_j is a parameter of dimension energy, characterizing the strength of the electron-phonon interaction. The lattice conductivity at low temperatures ($T \ll \theta_j$) can then be written as

$$\lambda_g = \frac{1}{3} \frac{k_B^3 M T^2 \hbar}{\pi m^2 a^3} J_3\left(\frac{\theta}{T}\right) \sum_j \frac{1}{C_j^2} \qquad \text{(II.30)}$$

where $J_3(\theta/T)$ is given by Eq.(II.21).

Within the free electron approximation electrons interact only with longitudinal phonons, the interaction constant being $C_\ell = 2\varepsilon_F/3$. If however $C_t = 0$, then λ_g would become comparable to the phonon conductivity of insulators, in contrast to what has been observed. Makinson therefore assumed $C_t = C_\ell$ in real metals. A justification for this assumption was later given by Klemens (26), who pointed out that the coupling between the transverse and longitudinal phonons (Section II.3.b.1) would tend to make the effective relaxation time of both branches equal. Furthermore, electrons also inter-

act directly with transverse waves, making C_t non-zero (Section II.3.a.1).

Calculations of the coupling constant C become highly complicated in real metals, because they require the knowledge of the geometry of the FS and the inclusion of real phonons. Klemens (7) therefore compared the low temperature expressions of λ_g and W_{id} (Eq.(II.20)) with each other, in order to eliminate C. Taking into account the polarization of the lattice waves one obtains for isotropic media from Eqs. (II.30) and (II.20)

$$\lambda_g W_{id} = 35(C_\ell^2 + 2\,C_t^2)\left(\frac{1}{C_\ell^2} + \frac{2}{C_t^2}\right)\left(\frac{T}{\theta}\right)^4 N_a^{-4/3} \qquad \text{(II.31)}$$

where the characteristic temperature θ depends on the relative magnitude of C_ℓ and C_t. If $C_t \ll C_\ell$ then $\theta \approx \theta_\ell$, the Debye temperature of the longitudinal phonons; if $C_t = C_\ell$ than $\theta = \theta_D$ and Eq.(II.31) becomes:

$$\lambda_g W_{id} = 315\left(\frac{T}{\theta_D}\right)^4 N_a^{-4/3} \qquad \text{(II.32)}$$

Comparison of the experimentally determined λ_g and W_{id} with Eqs.(II.31) and (II.32) can therefore provide information about the nature of the coupling between the conduction electrons and the phonons.

Since λ_g cannot be measured in pure metals, because of the large electronic contribution to the thermal conductivity, values of the lattice conductivity must be extracted from thermal conductivity data on dilute alloys. Unfortunately, it has been observed that λ_g is strongly dependent on impurity content in the dilute regime. Although the cause of this variation has been controversial for quite some time, it has been gradually accepted that this phenomenon was related with the fact that the introduction of impurities affects the electron-phonon interaction, resulting in a correlation between the strength of the electron-phonon interaction and the residual resistivity or the electron mean free path. This aspect of the electron-phonon interaction was already contained in a theory of ultrasonic attenuation of sound waves in metals developed by Pippard in 1955 (27). He showed that the attenuation of sound waves due to the interaction with the conduction electrons depends on a parameter $q\ell$, where q is the wave-vector of the sound wave and ℓ is the mean free path of the electrons. His results for the case of a free electron metal can be summarized in the following expressions for the attenuation coefficients α of the longitudinal and transverse waves:

$$\alpha_\ell = \frac{Nm}{dv_\ell \tau_0} F(q\ell) \qquad \text{(II.33)}$$

where

$$F(q\ell) = \frac{(q\ell)^2}{3} \frac{\tan^{-1}(q\ell)}{q\ell - \tan^{-1}(q\ell)} - 1 \quad F(q\ell) = \frac{4}{15}(q\ell)^2 \quad q\ell \ll 1 \qquad \text{(II.34.a)}$$

$$F(q\ell) = \frac{\pi}{6} q\ell \quad q\ell \gg 1 \qquad \text{(II.34.b)}$$

$$\alpha_t = \frac{Nm}{dv_t \tau_0} \begin{cases} \frac{1}{5}(q\ell)^2 & q\ell \ll 1 \qquad \text{(II.35.a)} \\ 1 + \frac{4}{3\pi} \frac{q\ell}{1 + (q\delta)^6} & q\ell \gg 1 \qquad \text{(II.35.b)} \end{cases}$$

where N is the number of free electrons per unit volume, d is the density of the metal, $\tau_0 = \ell/v_F$ (v_F is the Fermi velocity of the electrons) and δ is the characteristic length of the anomalous skin effect ($\delta \sim q^{-1/3}$).

An important aspect of this theory is that two regions can be distinquished, separated by the condition $q\ell \simeq 1$, in which the attenuation coefficients have a different character. In the region where $q\ell \gg 1$ it is interesting to note that, if α_ℓ is interpreted as the reciprocal of the mean free path of the longitudinal phonons, this attenuation coefficient is exactly the same as the one derived from the quantum mechanical treatment of the electron-phonon interaction. This is illustrated by comparing $\tau = \Lambda_{ph}/v_\ell = (\alpha_\ell v_\ell)^{-1}$ with the Makinson expression Eq. (II.29), where $C = 2\varepsilon_F/3$. In the region $q\ell \ll 1$ the adiabatic principle breaks down (28). that is, the interaction between electrons and sound waves cannot be given in terms of well defined quantum states anymore.

The consequences of the above mentioned interpretation of α in terms of a phonon mean free path are rather interesting for the thermal conductivity as first pointed out by Pippard (29). The thermal waves in a metal may be considered as a collection of sound waves travelling in all directions and having a wide band of frequencies. In applying Pippard's theory for ultrasonic waves to thermal phonon frequencies, it should be noted that, whilst in ultrasonic experiments the region $q\delta \gg 1$ has not been reached, in alloys the condition $q\delta \gg 1$ usually holds. This has important consequences for the attenuation of the transverse waves. The relaxation time for scattering of transverse phonons by conduction electrons when $q\ell \gg 1$ is obtained from Eq. (II.35.b):

$$\tau_t^{-1} = \frac{Nmv_F}{d\ell} \qquad (II.36)$$

leading to a cubic dependence on temperature of λ_g (Eq.(II.24))

$$\lambda_t = \frac{4\pi^2}{45} \frac{k_B^4 \, d\ell}{\hbar^3 v_t Nmv_F} T^3 \qquad (II.37)$$

This shows that even within the free electron model there is an interaction between transverse phonons and electrons, a result, which is not contained in the quantum mechanical treatment of the electron-phonon interaction.

For a non spherical FS it can be shown that the attenuation coefficients for both polarization modes are very similar (30). In the limit $q\ell \ll 1$ α still varies as $q^2\ell$, whereas in the region where $q\ell \gg 1$ α is proportional to q and independent of ℓ for both longitudinal and transverse waves. The dependence of α_t on the electron mean free path in the free electron model in the latter limit (Eq.(II.35. b)) does not exist in the non-ideal case. Because of the sensitivity of the electron phonon interaction to the detailed shape of the FS, in particular for the transverse phonons, theory can so far only give a qualitative description of λ_g. The lattice conductivity will probably vary as T^2 in the dilute regime ($q\ell \gg 1$) at low temperatures. However, the correct magnitude cannot be predicted yet.

Another phenomenon which usually complicates transport calculations is the anisotropy of the phonon spectrum. It has been shown, however, that the use of a realistic phonon spectrum in the calculations does not produce a significant modification in both the temperature dependence and magnitude of λ_g (31).

II.3.b.3. Other phonon scattering processes

Although the phonon-electron scattering, discussed in the preceding section, dominates in alloys at low temperatures, other phonon scattering processes must be taken into account in a complete analysis of λ_g. The theory of these mechanisms has been developed in connection with the thermal conductivity of insulators, but can also be applied to metals (26).

Scattering by sample boundaries is in principle important only in nonmetals and superconductors. In normal metals boundary scattering becomes dominant only at extremely low temperatures ($T \ll 1K$). If the phonon mean free path equals the shortest linear dimension of the crystal (L), the lattice conductivity exhibits a

cubic dependence on temperature (32), provided that the effect of other scattering processes is negligible

$$\lambda_g = \frac{16\pi^5}{15} \frac{k_B^4}{\hbar^3 v^2} LT^3 \qquad \text{(II.38)}$$

In polycrystalline samples λ_g is reduced below the value given by Eq.(II.38) due to phonon scattering by grain boundaries.

The scattering of phonons by point defects has been discussed extensively by Klemens. For isotropic media he derived the following expression for τ_p (26,33):

$$\tau_p^{-1} = \frac{3a^3 n_p}{\pi v^3} \{\frac{1}{12} (\frac{\Delta M}{M})^2 + [\frac{1}{\sqrt{6}} (\frac{\Delta F}{F}) - 3.4\gamma (\frac{\Delta R}{R})]^2\}\omega^4 \qquad \text{(II.39)}$$

where n_p is the defect concentration, γ is the Grüneisen constant, F is the force constant of a linkage, R is the interatomic distance and ΔM, ΔF and ΔR are the changes in M, F and R at the site of the defect. Point defect scattering can affect the lattice conductivity down to very low temperatures, because, in particular, high frequency waves are strongly scattered by point defects. The only well known quantity in Eq.(II.39) is ΔM. The other factors ΔF and ΔR cannot be obtained from first principles. Furthermore, the numerical factors in Eq(II.39) are not very well established. ΔR is usually taken from the difference between the atomic radii of the foreign and host atoms. The change in force constants can in some cases be deduced from elastic constants data.

Dislocation scattering is described by a relaxation time given by:

$$\tau_D^{-1} = 3 \times 10^{-2} N_d b^2 \gamma^2 \omega \qquad \text{(II.40)}$$

where N_d is the number of dislocation lines per unit area, b is the Burgers vector and γ is the Grüneisen constant. It is interesting to note that the strong dependence of the magnitude of λ_g on the presence of solute atoms (Section II.3.b.2) was originally attributed to this scattering mechanism. The extremely high dislocation densities ($N_d \approx 10^{11}/cm^2$), necessary to account for the variation of T^2/λ_g in dilute alloys, were explained by assuming that dislocations are locked in by impurities. However, thermal conductivity measurements on superconducting alloys have shown that dislocation scattering is unimportant in well annealed alloys.

Additional electron-phonon scattering associated with solute atoms, which is

thought to give rise to DMR in the electronic thermal resistivity (Koshino effect, Section II.3.a.2) may also affect the phonon conductivity. The enhanced scattering of phonons by electrons is according to Klemens (16) described by a relaxation time τ_K such that

$$\tau_K^{-1} = \frac{A}{\tau_0} \frac{\hbar^2}{Mv^2\epsilon_F} \omega^2 \qquad \text{(II.41)}$$

where τ_0 is the electron relaxation time corresponding to the residual resistivity ρ_0 and A is a constant whose magnitude depends on the model used.

A final remark regarding the phonon scattering mechanisms discussed above is in order. Equations (II.38) - (II.41) are obtained under sometimes extremely simplified conditions. Although it is not to be expected that correct calculations of the different relaxation times would change the qualitative aspects of the theory, it must be noted that the numerical factors in these expressions are not very reliable. Hence, any conclusion drawn from a comparison of the theory with experimental data must be regarded as rather tentative.

II.3.c. Thermopower

The main contribution to the thermopower of a metal at low temperatures comes from the conduction electrons. This 'diffusion thermopower' may be written as

$$S_e = \frac{W_0}{W_0 + W_{id}} S_{imp} + \frac{W_{id}}{W_0 + W_{id}} S_{id} \qquad \text{(II.42)}$$

where W_0 and W_{id} are the impurity and ideal thermal resistivity, respectively and S_{imp} and S_{id} are the contributions to S_e from electron-impurity and electron-phonon scattering. If the alloy contains more than one type of impurity, we may write S_{imp} as:

$$S_{imp} = \frac{1}{W_0} \sum_i W_0^i S_{imp}^i \qquad \text{(II.43)}$$

where $W_0 = \sum_i W_0^i$.

Within the free electron model S_{id} is given by (Eqs.(II.11) and (II.14)):

$$S_{id} = \frac{\pi^2 k_B^2}{3e\epsilon_F} T \quad (T \ll \theta) \qquad \text{(II.44)}$$

Because of the sign of e, S_{id} is negative.

The thermopower arising from electron-impurity scattering may be written as

$$S_{imp} = \frac{\pi^2 k_B^2 T}{3e} \left[\frac{1}{\sigma(\varepsilon)} \frac{d\sigma(\varepsilon)}{d\varepsilon}\right] \quad \varepsilon = \varepsilon_F \qquad \text{(II.45)}$$

where

$$\sigma(\varepsilon) = \frac{2e^2}{(2\pi)^3} \int \frac{\tau(\varepsilon)\, v^2}{|\vec{\nabla}_{\vec{k}}\, \varepsilon|} dS \qquad \text{(II.46)}$$

The thermopower depends much more sensitively on the details of the electron scattering processes than do the electrical and thermal resistivity. This is because S_{imp} depends on the energy derivative of the impurity relaxation time. In the case of ordinary impurity scattering $\tau(\varepsilon)$ is a slowly varying function of energy and S_{imp} is of the same order of magnitude as S_{id}. If, however, $\tau(\varepsilon)$ varies strongly with energy in the vicinity of ε_F, S may become anomalously large (see also Section II.2.a. and Chapter IV).

II.4. Experimental details

II.4.a. Alloy preparation

The alloys were prepared from master alloys of Cu containing 0.1 at.% Ge, Sn, Fe, Cr or Mn and were melted in an Edwards radiation furnace in high vacuum ($< 10^{-5}$ Torr) during 15 minutes. Rods were obtained by pressing the melt into a quartz tube of 3 mm diameter using argon gas. Two strips, 1 mm thick and of the same material as the rod were welded to the rod, about 6 cm apart. After etching and annealing in vacuo at 700^0 C for three hours, the specimens were slowly cooled to room temperature. Some sample characteristics are given in Table II.1. The electrical resistivity values are those at the lowest temperatures of the measurements (T = 1.3K) and are equal to $\rho(T = 0)$ for the Cu-Ge and Cu-Sn alloys only. The concentration of some alloys was determined spectrographically. Two Cu-Mn alloys were analysed chemically.

II.4.b. Sample mounting

The measurements of the electrical and thermal conductivity and the thermopower of the specimens were performed in a brass vacuum can. The rods were screwed into a teflon holder, which was placed on an Electrovac metal-glass seal, soldered with

Table II.1

Sample characteristics

Alloy	nominal concentration (ppm)	analysed concentration (ppm)	ρ(T=1.3K) (nΩcm)	ρ/c (μΩcm/at.%)
Cu-I	-	0.5 ppm Fe	1.02	
Cu-II	-	0.5 ppm Fe ≈2 ppm Mn	1.20	
Cu-Ge	60	30	11.7	3.9
	50	-	15.1	3.0
	80	-	27.4	3.4
	100	-	39.8	4.0
	150	150	54.3	3.6
	300	-	101	3.4
	1000	-	349	3.5
Cu-Sn	500	430	98.3	2.3
	1000	-	275	2.8
Cu-Fe	20	12	15.1	12.6
	20	15	18.5	12.3
	30	20	23.1	11.6
	75	-	81.5	10.9
	100	-	110	11.0
Cu-Cr	10	-	16.2	16.2
	30	-	56.3	18.8
Cu-Mn	30	26	12.5	4.8
	60	-	25.1	4.2
	300	270	113	3.8
	1000	-	330	3.3

The metals used were pure Asarco copper (99.999 + at.%), Ge from Johson and Matthey (no. 4066 and S 8614), Sn (Billiton 99.99995 at.%), Fe (J.M. no. 2262 and 27967), Cr (J.M. no. 4898), Mn (J.M. no. S 6759). The resistivity values given in the last two columns are obtained by subtracting the resistivity of Cu-I from the measured resistivity.

Wood's metal to the bottom of the vacuum can. In this way electrical insulation was ensured. Two home-made carbon resistance thermometers (34) and two potential leads for the electrical resistivity measurements were soldered to the strips. At both ends of the rod a current lead was fixed and also a heater, consisting of a 30 micron constantan wire of approximately 800Ω, wound on an insulated copper wire of 1 mm diameter. All leads were niobium wires, except for one copper current wire which served as a heat leak to the bath. Thin platinum wires were spot welded to the niobium wires in order to allow soldering of the leads to the strips, rod and feed-throughs.

II.4.c. Experimental set-up and measuring procedure

The experimental aspects of the measurements of the electrical and thermal conductivity and the thermopower at low temperatures have been extensively discussed in previous publications (35, 36). We mention briefly some features relevant to the present measurements.

The temperature differences were applied with the heater at the top of the rod. The lower heater was used to raise the average temperature of the sample with respect to that of the bath. The thermometer resistances were measured in a double Wheatstone bridge described elsewhere (35). The calibration procedure of the thermometers has also been discussed previously (34).

The resistance of the samples was small ($10^{-7}\Omega$ for Cu, $10^{-5}\Omega$ for Cu-Fe 100 ppm). In order to attain a precision of 0.1 % in the electrical resistivity measurements, it was necessary to detect voltages of the order of 10^{-11} V. Therefore, a superconducting modulator, as discussed by de Vroomen and van Baarle (36) was used. The apparatus served as a null-detector by introducing a compensation resistor (Cu-Zn 1 at.%, $\rho_0 = 1.879 \times 10^{-5}\Omega$) in the circuit, the value of which changed by less than 0.1% over a period of 4 years. Selective amplification of the a.c. signal was achieved in a lock-in amplifier (PAR model HR 8). The current values used did not exceed 50 mA with an exception for Cu: 200 mA. The current supply was built by the 'Laboratorium voor Instrumentele Electronica', Amsterdam. Its stability was better than 10 ppm.

The measuring current causes a temperature gradient to occur along the sample rod, due to Joule heating and to the Peltier effect. This results in a thermoelectric voltage, for which the total voltage in the resistivity measurements should be corrected. The effect of Joule heating was negligible for the present samples. The correction for the Peltier effect in the electrical resistivity is $\Delta\rho/\rho = S^2/L$ (L is the Lorenz number (Eq.(I.1)) and $S = \pi/T$, where π is the Peltier coefficient

and S is the thermoelectric power), which for Cu-Fe is of the order of 1% at 9K. The thermopower of all other alloys is so small that the Peltier correction can be neglected. Values for the thermopower of the alloys are of the order of 10^{-7}V/K except for Cu-Fe and Cu-Mn where S is an order of magnitude larger. Therefore, with a typical value of $\Delta T \approx 0.1$K the same technique as in the resistivity measurements was employed to detect the voltages.

The precision of the thermal conductivity data is mainly determined by the calibration of the thermometers and is estimated to be about 0.5 %. The largest errors in the absolute values of the electrical and thermal conductivity are caused by the error in the determination of the geometrical shape factor, which is about 3 %. However, this does not affect the Lorenz number since the electrical as well as the thermal conductivities are measured on the same specimen. In view of the error in the electrical conductivity measurements (0.1%), we, therefore, estimate the error in the determination of the Lorenz number to be about 0.5%.

References

1. See for example:
   a. A.H. Wilson, The Theory of Metals. (Cambridge University Press, 1953)
   b. J.M. Ziman, Electrons and Phonons (Oxford University Press, 1960).
2. E.H. Sondheimer, Proc. Roy. Soc. A 203 (1950) 75.
3. P.G. Klemens, Aust. J. Phys. 7 (1954) 64.
4. A.C. Ehrlich, Phys. Rev. B 8 (1973) 3610.
5. J. Bardeen, Phys. Rev. 52 (1937) 688.
6. A large number of papers have recently been published discussing the low temperature transport properties of potassium. See for example:
   J.W. Ekin and B.W. Maxfield, Phys. Rev. B 4 (197]) 4215.
   J.W. Ekin, Phys. Rev. B 6 (1972) 371.
   M. Kaveh and N. Wiser, Phys. Rev. Lett. 29 (1972) 1374.
   R.S. Newrock and B.W. Maxfield, Phys. Rev. B 7 (1973) 1283.
7. P.G. Klemens, Handbuch der Physik, ed. S. Flugge (Springer Verlag, Berlin, 1956), Vol. 14, p. 198.
8. P.G. Klemens and J.L. Jackson, Physica 30 (1964) 2031.
9. A.C. Ehrlich, Phys. Rev. B 1 (1970) 4537.
10. D. Schotte and U. Schotte, Solid State Comm. 10 (1972) 131.
11. J. Bass, Adv. in Phys. 21 (1972) 431.
12. See for instance: F.W. Kos and J.P. Carbotte, J. Phys. F 3 (1973) 1828.

13. E.G. Sondheimer and A.H. Wilson, Proc. Roy. Soc. A 190 (1947) 435.
14. J.S. Dugdale and Z.S. Basinsky, Phys. Rev. 157 (1967) 552.
15. J.W. Ekin and A. Bringer, Phys. Rev. B 7 (1973) 4468.
16. a. S. Koshino, Progr. Theor. Phys. 24 (1960) 484, 1049.
b. P.L. Taylor, Proc. Phys. Soc. A 80 (1962) 755, Phys. Rev. 135 (1964) A 1333.
c. P.G. Klemens, J. Phys. Soc. Japan 18, Suppl. II (1963) 77.
17. I.A. Campbell, A.D. Caplin and C. Rizzuto, Phys. Rev. Lett. 26 (1971) 239.
18. D.H. Damon, M.P. Mathur and P.G. Klemens, Phys. Rev. 176 (1968) 876.
19. D. Schotte and U. Schotte, J. Phys. F 4 (1974) 429.
20. I.A. Campbell, Solid State Comm. 9 (1971) 1513.
21. J. Callaway, Phys. Rev. 113 (1959) 1046.
22. M.G. Holland, Phys. Rev. 132 (1963) 2461.
23. P.G. Klemens, in Thermal Conductivity, ed. R.P. Tye (Academic Press, London and New York, 1969), Vol. 1, p.1.
24. C. Herring, Phys. Rev. 95 (1954) 954.
25. R.E.B. Makinson, Proc. Camb. Phil. Soc. 34 (1938) 474.
26. P.G. Klemens, Solid State Physics, ed. F. Seitz and D. Turnbull (Academic Press, New York), Vol. 7 (1958) 1.
27. A.B. Pippard, Phil. Mag. 46 (1955) 1104.
28. Reference 1.b, p. 212.
29. A.B. Pippard, J. Phys. Chem. Sol. 3 (1957) 175.
30. A.B. Pippard, Proc. Roy. Soc. A 257 (1960) 165.
31. C. Feldmann, Phys. Rev. 139 (1965) A 211.
32. H.B.G. Casimir, Physica 5 (1938) 495 (Comm. Kamerlingh Onnes Lab., Leiden, Suppl. 85b).
33. P.G. Klemens, Proc. Phys. Soc. (London) A 68 (1955) 1113.
34. W.M. Star, J.E. van Dam and C. van Baarle, J. Phys. E 2 (1969) 257, Comm. Kamerlingh Onnes Lab., Leiden, No. 375 d.
35. A.R. de Vroomen, C. van Baarle and A.J. Cuelenare, Physica 26 (1960) 19, Comm. Kamerlingh Onnes Lab., Leiden, No. 319 d.
36. A.R. de Vroomen and C. van Baarle, Physica 23 (1957) 785, Comm. Kamerlingh Onnes Lab., Leiden, No. 309 a.

CHAPTER III

LOW TEMPERATURE TRANSPORT PROPERTIES OF COPPER AND SOME DILUTE NONMAGNETIC COPPER ALLOYS

Abstract

The electrical and thermal conductivity and the thermopower of two copper samples and some dilute Cu-Ge and Cu-Sn alloys ($c < 0.1$ at.%) have been measured from 1.3 to 30 K. The first part of this chapter deals with the low temperature transport properties of Cu. The two samples examined, contained small traces of Fe and Mn impurities, responsible for the occurrence of weak anomalies in the transport properties. Combining the electrical resistivity and thermopower data the effect of Fe and Mn could be eliminated. The temperature dependence and the magnitude of the ideal thermal resistivity depart from the predictions of the Bloch theory. These deviations can be accounted for by Deviations from Matthiessen's Rule (DMR), in the sense as have been discussed by Sondheimer and Klemens, and the participation of transverse phonons in the electron-phonon interaction as a consequence of the fact that Cu cannot be described with the free electron model.

The second part of this chapter deals with the thermal conductivity of dilute Cu-Ge and Cu-Sn alloys. A careful analysis of the experimental results permits a separation of the thermal conductivity into an electronic and lattice component. The present results yield for the first time reliable estimates of DMR in the electronic thermal resistivity of noble metal alloys. These DMR appear to be comparable in magnitude to those observed in polyvalent metals. The lattice conductivity at the lowest temperatures of our measurements is discussed in the light of Pippard's theory of ultrasonic attenuation in metals. The present results extend the knowledge about the influence of the electron-phonon interaction on the behaviour of the lattice thermal conductivity to alloys with $c < 0.1$ at. % and indicate that heat is mainly carried by the transverse phonons. The data at higher temperatures are analysed in terms of point defect scattering and show a large contribution from lattice distortion scattering.

III.1. Copper

III.1.a. Introduction

The low temperature transport properties of copper are not expected to behave

according to the predictions of the Bloch theory, because of the intrinsic shortcomings of this theory and because of the fact that copper is far from being a free electron metal. Nevertheless, this theory forms a useful guide for a qualitative discussion of the experimental results and will therefore be employed frequently in the following sections.

We have measured the electrical and thermal conductivity and the thermopower of two copper samples between 1.3 and 12 K. Unfortunately, a straightforward comparison between theory and experiment is not possible, since both specimens show weak anomalies in their transport properties. These anomalies arise from conduction electron scattering by transition metal impurities (Kondo effect). A chemical analysis indicate the presence of about 0.5 ppm Fe in Cu-I and about 2 ppm Mn in addition to 0.5 ppm Fe in Cu-II (the latter specimen resulted from an unsuccesful attempt to prepare a Cu-Mn alloy (Chapter IV)).

Before proceeding with a discussion of the ordinary (nonmagnetic) behaviour of the various transport properties of Cu, it is therefore necessary to account for these anomalies. Hence, it is inevitable to use some experimental results obtained for the Cu-Fe and Cu-Mn alloy systems. For a detailed discussion of the experimental and theoretical features of the Kondo effect in these alloys we refer to Chapter IV. For our present purpose we briefly outline those aspects, which are important for the analysis of the experimental results of the Cu samples.

The strongly energy dependent scattering of the electrons by magnetic impurities manifests itself in the transport quantities through a temperature dependent component in the electrical and thermal resistivity, a large thermopower and a Lorenz number, L_{mag} which exceeds the theoretical value L_0. The last two quantities have been briefly discussed in a qualitative way in Section II.2.a. The Kondo effect is most clearly visible in the electrical resistivity and the thermopower. In the thermal resistivity it is sometimes overshadowed by a relatively large electron-phonon resistivity.

The observed differences of the anomalies in the two alloy systems under consideration reflect the different nature of the Fe and Mn impurities in the Cu host. Within a specific alloy system the following aspects may be noted. To a good approcimation S, L_{mag}, $\rho(T_1)/\rho(T_2)$ and $W(T_1)/W(T_2)$ are concentration independent in the very dilute regime. This important result can be used to separate the magnetic terms in the different transport properties from the nonmagnetic components, the procedure for which we now present.

If we write the electrical resistivity as a sum of a temperature dependent term ρ_{mag} and a temperature independent term ρ_{pot}, arising from scattering by

nonmagnetic impurities and structural lattice defects, the following equality should hold in the temperature range where ρ_{id} is negligibly small:

$$\frac{(\rho_{meas} - \rho_{pot})_{T = T_1}}{(\rho_{meas} - \rho_{pot})_{T = T_2}} = \frac{\rho(T = T_1)}{\rho(T = T_2)} \qquad \text{(III.1)}$$

('pure' copper) (Cu-Fe or Cu-Mn)

With Eq.(III.1), ρ_{pot} and hence ρ_{mag} ($=\rho_{meas} - \rho_{pot}$) of Cu-I and Cu-II may be obtained. From the relation $L_0 = \rho_{pot}/W_{pot}T$ and the characteristic concentration independent L_{mag} ($= \rho_{mag}/W_{mag}T$) the impurity term of the thermal resistivity $W_{imp} = W_{pot} + W_{mag}$ is obtained, which enables us to determine the ideal thermal resistivity. A second method to determine the impurity thermal resistivity is the application of Eqs.(II.42) and (II.43) to the thermopower data. As the characteristic thermopower of Fe and Mn in Cu is some orders of magnitude larger than the thermopower resulting from nonmagnetic impurities or from scattering by phonons, the reduced form of Eq.(II.42), viz., $W_{mag}S_{mag} = W_{meas}S_{meas}$ should yield a reliable estimate of W_{mag}.

III.1.b. Electrical resistivity, thermopower and Lorenz number of Cu

The electrical resistivity as a function of temperature of the Cu-I and Cu-II rods is shown in Fig. III.1. Due to some experimental problems ρ (Cu-II) was measured only up to $T \simeq 5K$. Note the strong temperature dependence of ρ (Cu-II) due to Mn impurities. The small impurity resistivity causes the ideal electrical resistivity to become important already at $T \simeq 6K$. In order to obtain reliable values for ρ_{id}, the electrical resistivity of a wire, drawn from the same material from which the Cu-I rod was obtained, was measured up to $T \simeq 40K$ (Fig. III.2). The differences in magnitude of the electrical resistivity of the Cu-I rod and Cu-I wire at low temperatures can be attributed to size effects. It is believed that size effects do not significantly affect the magnitude of ρ_{id} (1). Between 15 and 35 K the ideal electrical resistivity may be represented by: $\rho_{id} = 8.0 \times 10^{-16} T^{4.65} \Omega cm$.

Having subtracted the phonon induced resistivity, the electrical resistivity of Cu-I is now easily separated into the two terms ρ_{pot} and ρ_{mag} using Eq.(III.1) and the electrical resistivity data of Cu-Fe, to be found in Chapter IV. We obtain $\rho_{pot} = (0.48 \pm 0.03) \times 10^{-9} \Omega cm$). From the characteristic incremental resistivity of

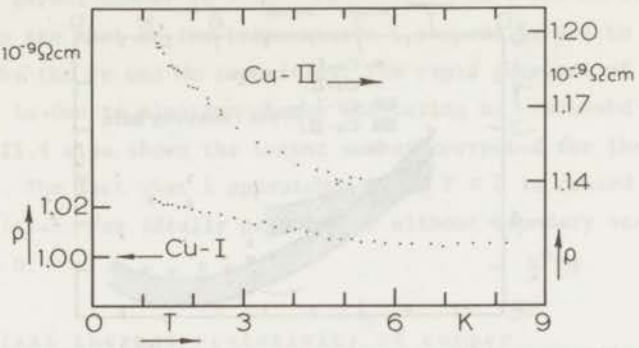

Fig.III.1. The electrical resistivity of the Cu rods versus T.

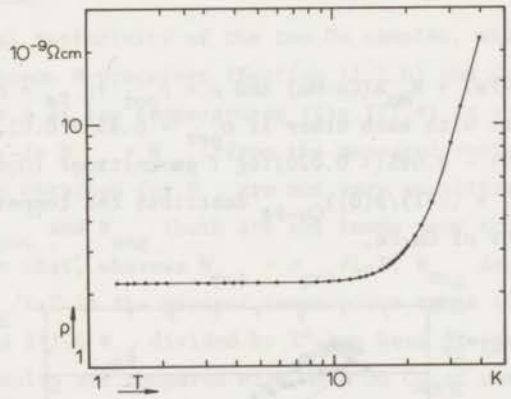

Fig.III.2. The electrical resistivity of a Cu-I wire as a function of temperature.

Fe in Cu: $(\Delta\rho/c)_{T=0} \simeq 11\mu\Omega$ cm/at.% (Chapter IV) the Fe concentration in Cu-I is estimated to be 0.4 ppm in fair agreement with the estimate from chemical analysis.

The thermopower data (Fig.III.3) should be compared with the characteristic thermopower of Fe and Mn in Cu (Fig. IV.5 and IV.6). The second procedure, outlined in the preceding section, to determine the magnetic contribution to the resistivity from thermopower measurements is consistent with the first method. This is demonstrated for Cu-I by calculating W_{mag} from $W_{mag} = (\rho_{meas} - \rho_{pot})/L_{mag}T$ where L_{mag} is the characteristic Lorenz number of the Cu-Fe system (Chapter IV). Fig.III.3 shows that the calculated thermopower $S = W_{mag}S(Cu\text{-}Fe)/W_{meas}$ is in good agreement with the measured S.

The situation is somewhat more complicated in Cu-II, since both Fe and Mn are present in the Cu host. Nevertheless, the same procedure may be followed with

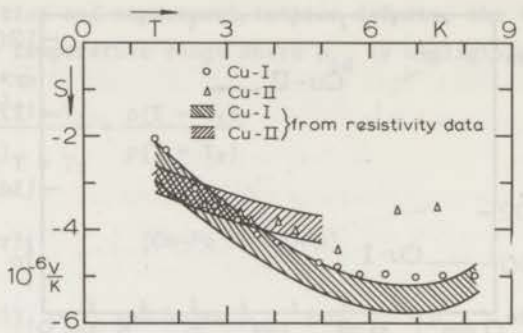

Fig.III.3. The thermopower of the Cu specimens versus T. The thermopower calculated from the resistivity data is represented by bands, which reflect the uncertainty in the determination of the resistivity contributions from the Fe and Mn impurities.

$W_{meas}S_{meas} = W_{Fe}S(Cu\text{-}Fe) + W_{Mn}S(Cu\text{-}Mn)$ and $\rho = \rho_{pot} + \rho_{Fe} + \rho_{Mn}$. The two methods can be made consistent with each other if $\rho_{pot} = 0.45 \pm 0.03$, $\rho_{Fe} = (0.25 \pm 0.05)f(T)$ and $\rho_{Mn} = 0.50(\pm 0.05) - 0.085(\pm 0.020)\log T$ in units of $10^{-9}\Omega$cm (T is expressed in K). The function $f(T) = (\rho(T)/\rho(0))_{Cu\text{-}Fe}$ describes the temperature variation of the electrical resistivity of Cu-Fe.

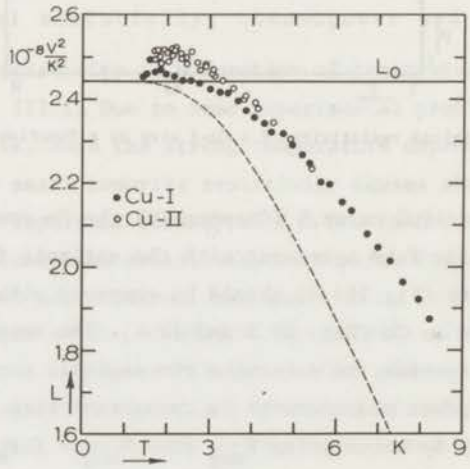

Fig.III.4. The Lorenz number of Cu as a function of temperature. The symbols represent the measured Lorenz numbers of Cu-I and Cu-II. The Lorenz number of Cu-I arising from ordinary (nonmagnetic) impurity scattering ($\rho_{pot} = 0.48 \times 10^{-9}\Omega$cm) and electron-phonon scattering is indicated by the dashed curve.

The measured Lorenz number ($L = \rho_{meas}/W_{meas}T$) of Cu-I and Cu-II is shown in Fig.III.4. One can see that at low temperatures L exceeds L_0 due to the scattering of the electrons by the Fe and Mn impurities. The rapid decrease of L, as the temperature increases, is due to electron-phonon scattering as discussed in Section II.2 (Fig.II.4). Fig.III.4 also shows the Lorenz number corrected for the magnetic resistivity terms. The fact that L approaches L_0 at T = 0 is caused by residual nonmagnetic impurities. For ideally pure copper without boundary scattering L should go to zero as $T \to 0$.

III.1.c. The ideal thermal resistivity of copper

III.1.c.1. Bloch theory

The ideal thermal resistivity of the two Cu samples, which is caused by inelastic electron-phonon N-processes (Section II.2.b) and is responsible for the rapid decrease of L at low temperatures (Fig.III.4) is obtained by subtracting the impurity term W_{imp} (= W_{pot} + W_{mag}) from the measured resistivity. It should be noted that the values obtained for W_{id} are not very sensitive to the precise relative values of W_{pot} and W_{mag} (both are not known very accurately). This results from the fact that, whereas $W_{pot} = \rho_{pot}/L_0T$, W_{mag} departs only up to a few percent from ρ_{mag}/L_0T in the present temperature range (Chapter IV).

In Fig.III.5 and III.6 W_{id} divided by T^2 has been plotted against T. In the latter figure our results are compared with data on Cu of comparable purity taken

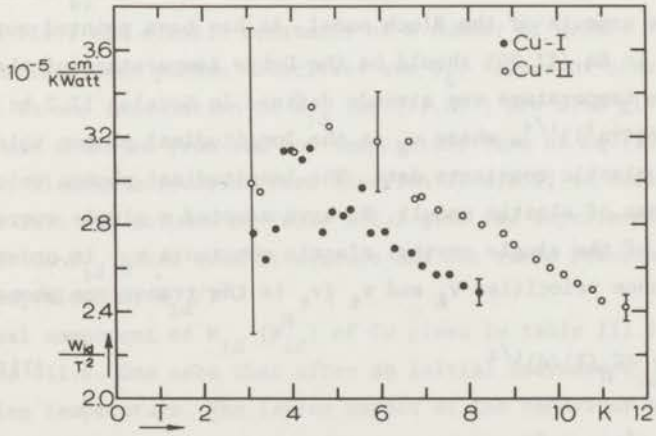

Fig.III.5. The coefficient of the T^2 term of the ideal thermal resistivity as a function of temperature for Cu-I and Cu-II.

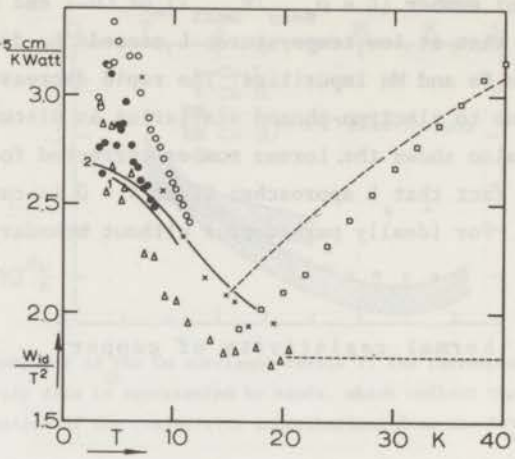

Fig.III.6. W_{id}/T^2 versus T up to 40K for some Cu specimens.
● Cu-I; 0 Cu-II; Δ Schriempf (3), $\rho_0 = 0.579 \times 10^{-9}\Omega cm$; x Schriempf (3), $\rho_0 = 1.12 \times 10^{-9}\Omega cm$; □ Powell et al. (4), $\rho_0 = 1.01 \times 10^{-9}\Omega cm$; – – – White (2), $\rho_0 \approx 5 \times 10^{-9}\Omega cm$.
The short dashed line indicates the value of W_{id}^N/T^2 obtained by subtracting ρ_{id}/L_0T^3 from W_{id}/T^2 (see text). The solid lines represent $W_{id}^N/T^2 + \Delta/T^3$ (Cu-I: curve 1; Cu-II: curve 2), where Δ corresponds to DMR in WT as calculated by Ehrlich (31).

from various sources (2,3,4). According to the Bloch theory the quantity W_{id}/T^2 is approximately independent of temperature at $T \ll \theta$ (Eq.II.20). In order to account for the observed departures from a T^2 behaviour of W_{id} we examine some of the quantitative aspects of the Bloch model. As has been pointed out in Section II.3.a.1, the θ in Eq.(II.20) should be the Debye temperature of the longitudinal modes. The Debye temperature was already defined in Section II.2.b: $\theta_\ell = (2\pi\hbar/k_B)v_\ell(3/(4\pi a^3))^{1/3}$, where v_ℓ is the longitudinal phonon velocity and may be calculated from elastic constants data. The longitudinal phonon velocity can be expressed in terms of elastic moduli. We have adopted a simple averaging scheme, due to Anderson (5) of the single crystal elastic constants c_{ij} in order to obtain values for the mean phonon velocities v_ℓ and v_t (v_t is the transverse phonon velocity).

$$v_\ell = ((K_H + 4G_H/3)/d)^{1/2} \qquad \text{(III.2)}$$

$$v_t = (G_H/d)^{1/2} \qquad \text{(III.3)}$$

where $G_H = (G_V + G_R)/2$ and $K_H = (K_V + K_R)/2$. K_V and K_R are the Voigt bulk modulus and the Reuss bulk modulus, respectively; G_V and G_R are the Voigt shear modulus and Reuss shear modulus. These moduli can be expressed in terms of single crystal constants by:

$$9\,K_V = (c_{11} + c_{22} + c_{33}) + 2(c_{12} + c_{23} + c_{31}) \qquad \text{(III.4)}$$

$$15\,G_V = (c_{11} + c_{22} + c_{33}) - (c_{12} + c_{23} + c_{31}) + 3(c_{44} + c_{55} + c_{66}) \qquad \text{(III.5)}$$

$$1/K_R = (s_{11} + s_{22} + s_{33}) + 2(s_{12} + s_{23} + s_{31}) \qquad \text{(III.6)}$$

$$15/G_R = 4(s_{11} + s_{22} + s_{33}) - 4(s_{12} + s_{23} + s_{31}) + 3(s_{44} + s_{55} + s_{66}) \qquad \text{(III.7)}$$

where c_{ij} and s_{ij} are the elastic stiffness and compliance, respectively. For cubic systems Eqs.(III.4) - (III.7) reduce to:

$$K_V = K_R = (c_{11} + 2c_{12})/3 \qquad \text{(III.8)}$$

$$G_V = (c_{11} - c_{12} + 3c_{44})/5 \qquad \text{(III.9)}$$

$$G_R = \frac{5c_{44}(c_{11} - c_{12})}{4c_{44} + 3(c_{11} - c_{12})} \qquad \text{(III.10)}$$

In table III.1 the elastic constants of a number of metals are listed, together with the calculated mean phonon velocities and θ_ℓ. Values of some physical quantities relevant to the calculation of W_{id} (Eq.(II.20)) are also given. Values for $(W_{id}/T^2)_{calc}$ are obtained from the low temperature form of Eq.(II.20) with $\theta = \theta_\ell$. The Sondheimer-Klemens correction term (Section II.3.a.1) is included in this quantity. The last two columns of Table III.1 give the experimental values of the T^2 coefficient of W_{id} taken from literature and the ratio between the experimental and calculated values of W_{id}/T^2.

The normal component of W_{id} (W_{id}^N) of Cu given in table III.1 was obtained from Fig. III.5 and III.6. One sees that after an initial decrease W_{id}/T^2 starts to rise with increasing temperature. The latter aspect of the behaviour of W_{id} is not contained in the Bloch theory. The coefficient of the T^4 term in Eq.(II.20) is negative up to $T \simeq \theta/6$. The explanation of this discrepancy has already been put

Table III.1

The observed and calculated W_{id}^N/T^2 and some parameters used in the calculations for various metals

	c_{11}	c_{12}	c_{44}	K_H	G_H	d	v_ℓ	v_t	a^3	θ_ℓ	$\frac{W_{id}^N}{T^2}$ calc.	$\frac{W_{id}^N}{T^2}$ obs.	$\frac{W_{id}^N \text{ obs.}}{W_{id}^N \text{ calc.}}$	references
	$10^{10}\ \frac{\text{dyne}}{\text{cm}}$					$\frac{\text{g}}{\text{cm}}$	10^5 cm s^{-1}	10^5 cm s^{-1}	10^{-24} cm^3	K	$\frac{10^{-5}\ \text{cm}}{\text{K Watt}}$	$\frac{10^{-5}\ \text{cm}}{\text{K Watt}}$		
Cu	176.2	124.9	81.8	142.0	51.2	9.02	4.83	2.38	11.70	630	0.55	1.8	3	present measurements
Ag	131.5	97.3	51.8	108.7	32.8	10.64	3.79	1.76	16.84	440	1.2	3.0	2.5	14,15,16
Au	201.6	169.7	45.3	180.3	29.8	19.49	3.36	1.24	16.78	390	1.1	16	≈15	17,18,19
K	4.16	3.41	2.86	3.66	1.27	0.91	2.42	1.18	71.3	170	92	150	1.5	20
Na	8.7	7.3	6.2	7.8	2.7	1.01	3.36	1.6	37.75	300	20	35	1.5	21
Rb	3.42	2.88	2.21	3.06	0.95	1.62	1.64	0.77	87.63	110	220	930	4	21
Cs	2.57	2.13	1.65	2.28	0.74	2.028	1.28	0.60	108.8	80	480	3000	6	21
Li	15.5	13.1	11.0	13.9	4.7	0.546	6.05	2.93	21.09	650	3.7	16	5	21
Pb	55.5	45.4	19.4	48.8	11.3	11.6	2.35	0.99	29.65	230	7.0	200	>10	22
Al	114.3	61.9	31.6	79.4	29.3	2.733	6.58	3.27	16.39	770	0.52	2	4	23
In				46.3	7.3	7.47	2.74	0.99	25.5	280	6.0	100	>10	24
Sn				57.9	24.4	7.3	3.50	1.82	26.6	350	2.3	40	>10	25
Mg				36.9	19.8	1.76	5.99	3.35	22.9	630	1.2	80	>10	26

The elastic constants data have been taken from Kittel (6): Cu, Ag, Au, K, Pb, Al; Diederich (7): Na; Gutman (8): Rb; Nash (9): Li; Kollarits (10): Cs.
The moduli of the non-cubic metals Sn, In, Mg were calculated by means of Equations (III.4) - (III.7). The six elastic constants for these metals are not listed but can be found in Rayne (11): Sn; Chandrasekhar (12): In; Slutsky (13): Mg.

forward in Section II.3.a.1, viz., the neglect of U-processes. These processes are particularly important in the electrical resistivity. Since the J_5T^4 term in Eq. (II.20) arises from the same scattering mechanism as ρ_{id}, it may be argued that U-processes enhance this term to the same extent as ρ_{id} is increased above its Bloch value. Because U-processes are large angle scattering processes, the WFL law holds. If we then substract ρ_{id}/L_0T^3 (= W_{id}^U/T^2) from the measured W_{id}/T^2, we find that W_{id}^N/T^2 is approximately constant between 15 and 40 K. Here we have used the experimantally determined ρ_{id} of Cu-I (Section III.1.b), which is in reasonable agreement with other data found in literature (27). The value obtained for W_{id}^N/T^2, viz., 1.8×10^{-5} cm/K Watt., is larger than the value predicted by the Bloch expression by a factor of about 3. Taking into account phonon dispersion, which effectively lowers θ_ℓ, this factor is slightly reduced. The observed discrepancy can be accounted for by a significant contribution to W_{id}^N from the interaction between the elec-

trons and transverse phonons, because of elastic anisotropy and a nonspherical FS. The values given in the last column of Table III.1 show that in the case of monovalent metals the discrepancy between experiment and theory is never larger than about a factor of 4 with a rather puzzling exception for Au. In the most free electron like metals Na and K the discrepancy has the smallest value ($\simeq$ 1.5). Up to now calculations of W_{id} including a realistic phonon spectrum and a wave-vector dependent electron-phonon interaction have been performed only for K (28). For all model potentials employed, good agreement is achieved with experimental data.

In the case of multivalent metals the discrepancy is a factor of order 10 (except for Al, which is more or less free electron like), illustrating the failure of the Bloch theory.

It should be noted that the experimental values of the T^2 term of W_{id} are often not very reliable, either because of insufficiently experimental accuracy or because they are obtained from insufficiently pure samples (for example Au (17,18,19), where W_{id} was measured on samples with $\rho_0 \simeq 5 \times 10^{-9}\Omega$cm), so that DMR can give too large values for W_{id}. Hence, the numbers given in the last column of Table III.1 have only some qualitative meaning, in the sense that the Bloch theory gives an increasingly poorer description of the real situation, when the metal behaves less free electron like, which is after all not surprising.

III.1.c.2. Deviations from Matthiessen's Rule

The low temperature behaviour of W_{id}/T^2 of Cu is characterized by an increase of this quantity as T decreases below T $\simeq$ 15 K (Fig.III.5 and III.6). At these temperatures $W_{id} \simeq W_{imp}$, so that DMR as have been discussed by Sondheimer (29) and Klemens (30) are expected to occur. Ehrlich (31) has extended the treatment of DMR by calculating the thermal resistivity for any ratio of phonon to impurity scattering. At high temperatures $(WT/(WT)_0 > 10$, where WT is the experimentally determined thermal resistivity times temperature and $(WT)_0 = \lim(WT)$ as $T \to 0$) the deviation from Matthiessen's Rule in WT ($\Delta = WT - (WT)_0 - (W_{id}T)_{\rho_0 = 0}$, where the latter quantity is the ideal thermal resistivity times temperature in the absence of impurity scattering) becomes $\Delta = 0.47\ (WT)_0$. At low temperatures $(0 < (WT - (WT)_0)/(WT)_0 \lesssim 0.3)$, $\Delta \simeq 0.3\ (WT - (WT)_0)$, which gives $\Delta \simeq 0.42\ (W_{id}T)_{\rho_0 = 0}$. Thus Δ/T exhibits the same temperature dependence ($\sim T^2$) as W_{id} in the absence of impurity scattering. The latter result agrees within 5 % with that of Klemens (30).

In Fig.III.6 these DMR are accounted for by adding Δ/T^3 to W_{id}^N/T^2 using $(WT)_0 =$

0.040 for Cu-I and $(WT)_0$= 0.046 for Cu-II in units of cm K^2/Watt and W_{id}^N/T^2= 1.8×10^{-5}cm/K Watt. The solid lines in Fig.III.6 represent the quantity $(W_{id}^N + \Delta/T)/T^2$.

An increase of W_{id}/T^2 similar to the present case has been observed in Ag by van Baarle et al. (15). Kos (32) attributed this to the occurrence of an additional scattering mechanism, namely phonon assisted impurity scattering (Section II.3.a.2), but his arguments are not very convincing. The additional resistivity should be approximately independent of temperature contrary to the theoretical predictions. Moreover, even in the electrical resistivity a contribution from this mechanism is not very well established. Our results show that the Sondheimer-Klemens correction in the sense as has been calculated by Ehrlich must be taken into account in order to explain the observed behaviour of W_{id}^N/T^2 as a function of temperature and gives apparently the largest contribution to the DMR in the thermal resistivity of pure metals at low temperatures.

III.2. Cu-Ge and Cu-Sn

III.2.a. Introduction

The problems encountered when analyzing the thermal conductivity data of very dilute nonmagnetic alloys (c < 0.1 at.%) arise from the fact that even at low temperatures the electronic contribution λ_e to the total thermal conductivity of these alloys is not simply related to the residual electrical resistivity ρ_0 by means of the WFL law: $\lambda_e = L_0T/\rho_0$. The presence of a non-negligible phonon induced term in the electronic thermal resistivity can account for this aspect. This contribution is expected to be enhanced due to the occurrence of positive DMR similar to the electrical resistivity case.

We have measured the electrical and thermal conductivity and the thermopower of seven Cu-Ge alloys with Ge concentrations ranging from 30 to 1000 ppm and two Cu-Sn alloys (c = 500 and 1000 ppm) from 1.3 to 9 K. The thermal conductivity measurements on Cu-Ge (80, 300 and 1000 ppm) and Cu-Sn (1000 ppm) were extended up to T ≃ 30 K.

The electrical resistivity was measured in order to test the validity of the WFL law at low temperatures and in order to obtain an accurate value for the impurity term W_{imp} of the electronic thermal resistivity.

The thermopower was measured primarily for experimental reasons, as discussed in Section II.4. The magnitude of the thermopower of the alloys turns out to be an order of magnitude smaller than the thermopower of the 'pure' Cu samples. The

contribution of the magnetic impurities as discussed in the preceding section is now quenched by the nonmagnetic solutes.

The main emphasis was placed on the thermal conductivity measurements, not in the last place because some of the experimental results of the nonmagnetic Cu alloys are needed to analyse the transport properties of the Kondo alloys in Chapter IV. As was noted before, the analysis of the low temperature thermal conductivity offers specific problems due to the occurrence of an extra conductivity term λ_g arising from the transport of heat by the lattice, which competes with a decrease of λ_e caused by an enhanced ideal thermal resistivity.

III.2.b. Electrical resistivity and Lorenz number

The results of the electrical resistivity measurements are shown in Fig.III.7, where $\rho_{alloy} - \rho_{Cu}$ is plotted against the concentration of the Ge and Sn impurities. In the temperature range of our measurements the electrical resistivity is constant within the experimental accuracy ($\approx$ 0.1%), apart from a small upturn ($\approx$ 0.2%) in the most dilute alloys, which must be attributed to the presence of Fe. The characteristic incremental resistivity for Ge in Cu is 3.6μ Ωcm/at.% and 2.7 $\mu\Omega$/at.% for Sn in Cu in agreement with other reported values (33, 34, 35).

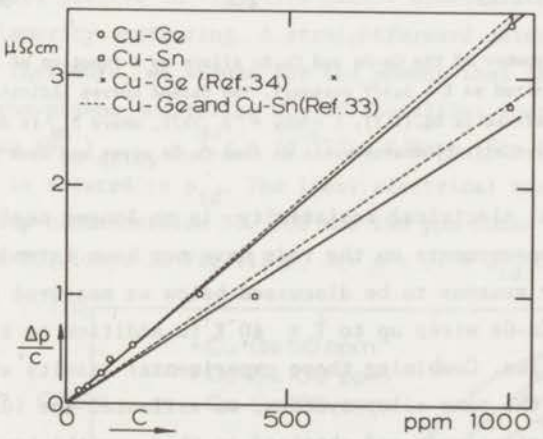

Fig.III.7. The residual resistivity versus impurity concentration for Cu-Ge and Cu-Sn alloys.

In Fig.III.8 the Lorenz number $L = \rho_0\lambda/T$ of the Cu-Ge and Cu-Sn alloys is plotted as a function of temperature. It should be noted that the plotted L represents the Lorenz number as defined in Eq.(I.1) only up to $T \simeq 10$ K. At higher

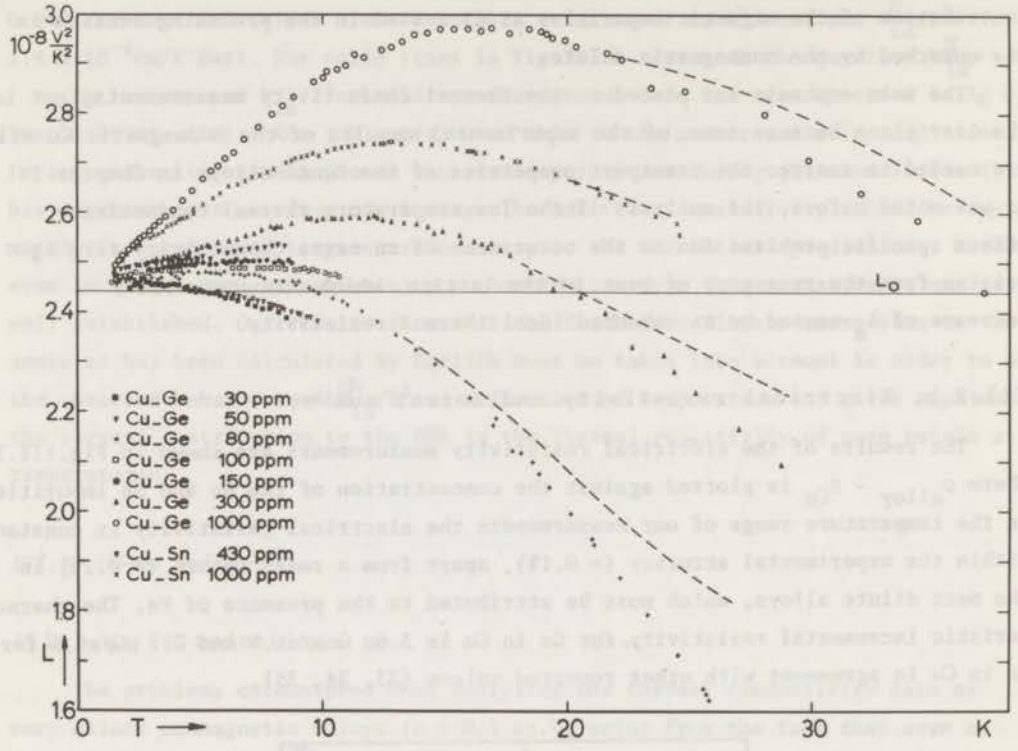

Fig.III.8. The Lorenz number of the Cu-Ge and Cu-Sn alloys as a function of temperature. The data are plotted as $L = \rho_0\lambda/T$ versus T. The dashed curves indicate the Lorenz number as defined in Eq.(I.1), $L = (\rho_0 + \rho_{id})\lambda/T$, where ρ_{id} is determined from electrical resistivity measurements on some Cu-Ge wires and from ref. 33.

temperatures the ideal electrical resistivity is no longer negligible. The electrical resistivity measurements on the rods have not been extended to these temperatures. However, for reasons to be discussed below we measured the electrical resistivity of some Cu-Ge wires up to $T \approx 40$ K in addition to a Cu-I wire mentioned in the preceding section. Combining these experimental results with data of Dugdale and Basinski (33) on the same alloy systems, we estimated the ideal electrical resistivity of the various rods and obtained in this way the Lorenz numbers according to Eq.(I.1), which are represented by broken lines in Fig.III.8.

The reason why we plotted our data as $\rho_0\lambda/T$ versus T is that Fig.III.8 reflects the behaviour of the thermal conductivity as a function of temperature. One can see that at the lowest temperatures of our measurements L closely approaches L_0. For the very dilute alloys ($c \lesssim 50$ ppm) L remains approximately constant and close to

L_0 at liquid He-temperatures, indicating that the dominant contribution to λ comes from the electrons. The downward trend in L as T increases for these alloys may be attributed to the appearance of the ideal thermal resistivity..

As more impurities are added to the Cu host, the electronic component of the thermal conductivity is reduced by a factor proportional to ρ_0. The ideal thermal resistivity is overshadowed by the impurity term since, as was discussed in Section II.3.a.2, W_{id} is not strongly affected by the addition of impurities, that is, the DMR vary less than linearly with ρ_0. Simultaneously the Lorenz number of the more concentrated alloys exceeds L_0, indicating that the lattice conductivity is less reduced than λ_e when ρ_0 increases. The downward trend in L of these alloys at higher temperatures is a result of several competing factors, such as the reduction of λ_g through phonon scattering processes, which are apparently unimportant at low temperatures, and the reduction of λ_e caused by scattering of electrons by phonons.

III.2.c. Lattice conductivity

III.2.c.1. Introduction

In order to extract the lattice conductivity from the measured thermal conductivity, λ_e (= $(W_{imp} + W_{id})^{-1}$) must be known. W_{imp} can determined from ρ_0 by means of the WFL law. The data plotted in Fig.III.8 nicely demonstrate the validity of this law for electron-impurity scattering. A straightforward determination of W_{id} is not possible,however. Therefore, we assume for the moment that the resistivity arising from Normal electron-phonon scattering W^N_{id} of the alloys equals W^N_{id}(Cu-I, II). Since $W_{imp} >> W_{id}$ we take $(W^N_{id})_{alloy} = 3.2 \times 10^{-5} T^2$cm K/Watt (Fig.III.5). The Umklapp resistivity (W^U_{id}) is related to ρ_{id}. The ideal electrical resistivity of three Cu-Ge alloys with impurity concentration 50, 100 and 150 ppm turns out to be larger than ρ_{id}(Cu-I) (Section III.1.b). In Fig.III.9, Δ(= $\rho - \rho_0 - \rho_{id}$(Cu)) divided by ρ_0

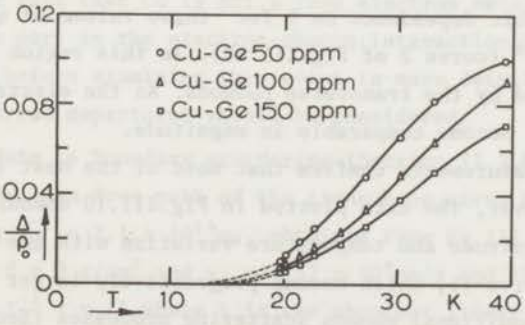

Fig.III.9. Δ/ρ_0 versus T for three Cu-Ge wires, where $\Delta = \rho - \rho_0 - \rho_{id}$(Cu).

(residual resistivity) is plotted against T. The results are in reasonable agreement with data from Dugdale and Basinski (33), that is, as good as can be expected, since Δ very sensitive to the magnitude of $\rho_{id}(Cu)$. Below T $\approx$ 25 K Δ exhibits approximately the same temperature variation as $\rho_{id}(Cu)$, supporting on explanation of the observed DMR in terms of a two-band model (Section II.3.a.2).

Using the results from Fig.III.9 and data on more concentrated alloys (33), $(W^U_{id})_{alloy} = W^U_{id}(Cu) + \Delta/L_0T$ can be determined. Finally, values for the lattice conductivity are obtained by subtracting $\lambda_e = (\rho_0/L_0T + W_{id}(Cu) + \Delta/L_0T)^{-1}$ from the measured thermal conductivity.

III.2.c.2. Some general remarks on the behaviour of the lattice thermal conductivity

Since the low temperature lattice conductivity of metallic alloys is dominated by the electron-phonon interaction, it is convenient to compare our results with the predictions of Pippard's theory (36) of the electron-phonon interaction (Section II.3.b.2). This theory suggests that, within the free electron approximation, the phonon mean free path and hence λ_g is a function of the parameter $q\ell$ or T/ρ_0, where q is the phonon wave-vector and ℓ is the electron mean free path. We have therefore plotted in Fig.III.10 the quantity $\lambda_g/T\rho_0$ against T/ρ_0 for those alloys, for which the lattice conductivity could be determined with reasonable accuracy. Curve 1 and 2 are obtained from Eqs.(II.37) and (II.33) substituted in Eq.(II.24), respectively, with $\rho_0\ell = 6.5 \times 10^{-12}\ \Omega cm^2$ (37). For the present measurements the parameter $q\ell$ ranges from about about 30 to 6000 for transverse phonons and from about 15 to 3000 for longitudinal phonons. Here q has been taken to be the wave-vector of the dominant phonons: $q \approx 1.6\ kT/\hbar v$ (Section II.2.b). To our knowledge the measurements, presented here, provide the first thermal conductivity data in the range where $q\ell > 10^2$.

As was noted before, the thermal conductivity of the transverse modes (λ_t) should exhibit a cubic dependence on T for these values of $q\ell$ (curve 1 in Fig. III. 10), whereas $\lambda_\ell \sim T^2$ (curve 2 of Fig.III.10). In this region the heat is almost entirely transported by the transverse phonons. As the electron mean free path decreases λ_ℓ and λ_t become comparable in magnitude.

The present measurements confirm that most of the heat is carried by the transverse phonons. However, the data plotted in Fig.III.10 demonstrate large discrepancies both in magnitude and temperature variation with the predictions of the free electron theory (curve 1), which become progressively larger as T/ρ_0 increases. At high temperatures additional phonon scattering processes (Section II.3.b.3) become important, giving rise to a complicated temperature variation of λ_g as will be

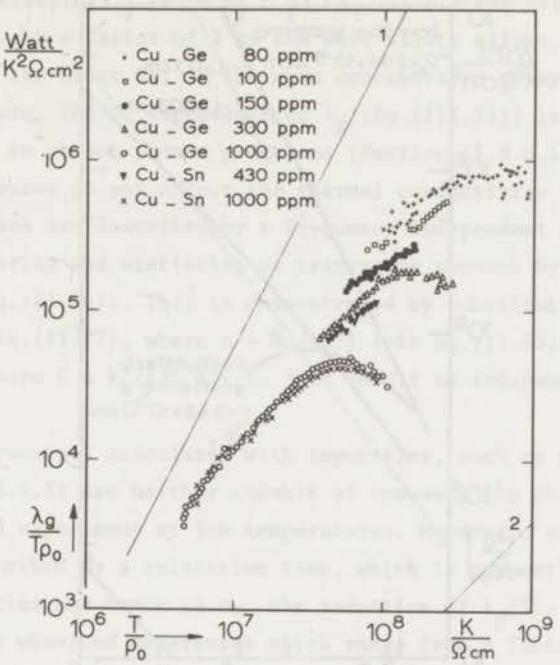

Fig.III.10. Values for $\lambda_g/T\rho_0$ versus T for some Cu-Ge and Cu-Sn alloys. The data of Cu-Ge 30 and 50 ppm are not shown. The free electron curves for the transverse and longitudinal modes as given by the Pippard theory are indicated by the solid lines denoted by 1 and 2, respectively. The lattice thermal conductivity (λ_g) was obtained by subtracting the electronic thermal conductivity (λ_e) from the measured thermal conductivity, where $\lambda_e = (\rho_0/L_0T + W_{id}(Cu) + \Delta/L_0T)^{-1}$.

discussed below. At lower temperatures electron-phonon scattering should be dominant. At first sight it can therefore be argued that the observed discrepancies are accounted for by the fact that Cu is not a free electron metal. In that case transverse waves can take part in the electron-phonon interaction both through N and U-processes. However, before examining this point in more detail, other possible reasons for the observed departures should be considered.

A likely candidate is boundary scattering (Section II.3.b.3), which should become important if the mean free path of the transverse waves becomes large with increasing ℓ. Taking $\tau_t^{-1} = 2.1 \times 10^{14}\rho_0$, obtained from Eq.(II.36) with $N = 8.5 \times 10^{22}cm^{-3}$, $d = 9\ g/cm^3$ and $v_F = 1.57 \times 10^8 cm/s$ and the relaxation rate for boundary scattering $\tau_B^{-1} = v_t/L$ where L is the shortest linear dimension of the sample, the lattice conductivity of the transverse modes divided by $T\rho_0$ becomes (Eq.(II.24)):

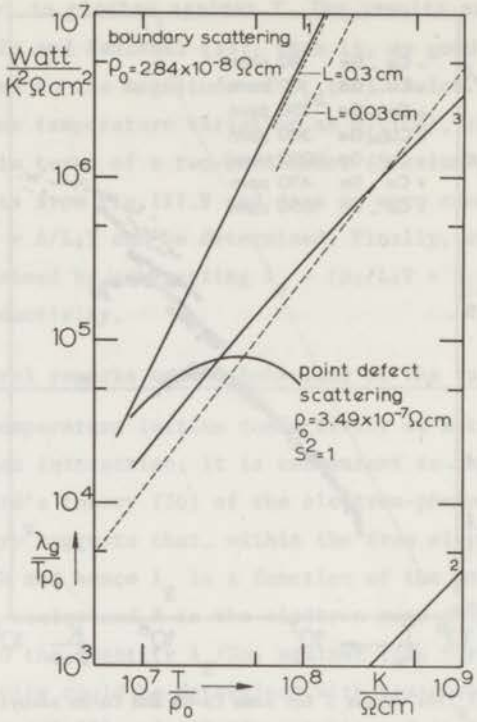

Fig.III.11. Schematic representation of the influence of some phonon scattering mechanisms on the lattice conductivity. The solid lines 1 and 2 are the theoretical $\lambda_g/T\rho_0$ vs T/ρ_0 curves for the transverse and longitudinal modes, respectively. The dashed line is $\lambda_g/T\rho_0 = 9.2 \times 10^{-6}(T/\rho_0)^{1.3}$ and represents a fit to the low temperature lattice thermal conductivity data of Cu-Ge and Cu-Sn as described in the text. The solid line 3 is obtained with the assumption that the interaction between the electrons and the transverse phonons, arising from the departures from the free electron model, is described by $(\tau_t')^{-1} = 10^7 Tx$, where $x = \hbar\omega/k_B T$.

$$\frac{\lambda g}{T\rho_0} = 5.7 \times 10^{-10} \left(\frac{T}{\rho_0}\right)^2 \frac{1}{1 + \frac{1.1 \times 10^{-9}}{\rho_0 L}} \qquad \text{(III.11)}$$

In the present case L = 0.3 cm. In the most dilute alloys ($\rho_0 \simeq 2 \times 10^{-8}\Omega cm$) external boundary scattering gives rise to a reduction of λ_g by only $\approx 20\%$ (Fig.III.11). In polycrystalline samples it is often observed (38) that L or the mean free path of the phonons is smaller than the size of the specimen, indicating the presence of

grain boundary scattering. A value of 0.03 cm, which seems not unreasonable, would reduce $\lambda_g/T\rho_0$ only by a factor of 2 in the most dilute alloys, whereas the observed discrepancy is of the order 50. In the more concentrated alloys the effect is even smaller. Furthermore, the T^3 dependence of λ_g (Eq.(III.11)) is not observed.

With respect to phonon-phonon processes (Section II.3.b.1) it can readily be shown that N-processes do not affect the thermal conductivity if the resistive phonon scattering processes are described by a frequency independent relaxation time, such as boundary scattering and scattering of transverse phonons by electrons in the free electron model (Eq.(II.36)). This is demonstrated by substituting $\tau^{-1} = a$ and $\tau_N^{-1} = BT^5x$ (see Eq.(II.27), where $x = \hbar\omega/k_BT$) into Eq.(II.25). One obtains $\lambda_g = CT^3J_4(x)/a$ where $C = k_B^4/(3\pi^2\hbar^2v_t)$. This result is independent of the nature or magnitude of τ_N.

Scattering processes associated with impurities, such as point defect scattering (Section II.3.b.3) are neither capable of removing the observed discrepancy between theory and experiment at low temperatures. Moreover, since these types of processes are described by a relaxation time, which is proportional to the concentration of impurities and hence to ρ_0, the reduction of $\lambda_g/T\rho_0$ is independent of ρ_0 contrary to the observed departures which range from a factor of 5 in the 0.1% alloys to about 50 in the 80 ppm alloy. The effect of point defect scattering on λ_g is shown in Fig.III.11 for the 0.1% alloy. Values for λ_g have been calculated from Eq.(II.24) with $\tau_t^{-1} = 2.1 \times 10^{14}\rho_0$ and τ_p^{-1} given by Eq.(II.39). The term in braces is given the large value of 1, in order to demonstrate once more that these types of scattering mechanisms cannot account for the departures from the theoretical curve.

For the sake of completeness we mention three other effects. As the temperature increases, the mean free path ℓ of the conduction electrons is shortened through scattering by the phonons. Hence, in Eqs.(II.33) - (II.37) ℓ should be taken to be temperature dependent. However, in the temperature range of the measurements and considering the electrical resistivity of the present alloys one can see that this effect is not very important.

The neglect of DMR in the electronic thermal resistivity introduces an error in the determination of λ_g only at the highest temperatures of our measurements. One can see, by comparing the values of $W_0 (= \rho_0/L_0T)$ and $W_{id}(Cu)$, that, even if the ideal thermal resistivity of the alloys is larger than the pure Cu resistivity by a factor of 3, our results will not be measurably affected at the lowest temperatures ($T \lesssim 5K$).

Finally, it has been shown (39) that the inclusion of an anisotropic phonon

spectrum has a minor effect on the lattice conductivity as described by curve 1 in Fig. III.11.

III.2.c.3. The lattice thermal conductivity at low temperatures. Electron-phonon interaction

In the light of the discussion given in the preceding section we are led to the conclusion that the inadequacy of the free electron model as applied to Cu must account for the discrepancies shown in Fig. III.10. Unfortunately, we have now also reached the point, at which a quantitative comparison between experiment and theory has become impossible, since as yet no proper calculation of λ_g of a non-free electron metal has been presented.

We can account in a qualitative way for the interaction of the transverse phonons with the electrons by adding the reciprocal of a relaxation time of the form $(\tau_t')^{-1} = ATx$ to the reciprocal of the free electron relaxation time Eq.(II.36). The similarity of τ_t' and the longitudinal phonon relaxation time (Eq.(II.29)) has already been mentioned in Section II.3.b.2.

Curve 3 in Fig.III.11 is computed from:

$$\frac{\lambda_g}{T\rho_0} = 2.2 \times 10^{-11}\left(\frac{T}{\rho_0}\right)^2 \int \frac{x^4 e^x \, dx}{(e^x - 1)^2\left(1 + 4.8 \times 10^{-6}\left(\frac{T}{\rho_0}\right)x\right)} \qquad \text{(III.12)}$$

Eq.(III.12) can be obtained from Eq.(II.24) by substituting the appropriate values for the physical constants and by taking $\tau_t^{-1} = 2.1 \times 10^{14}\rho_0 \ s^{-1}$ and $(\tau_t')^{-1} = 10^7 Tx \ s^{-1}$. This latter value should be compared with $\tau_\ell^{-1} = 2 \times 10^8 Tx \ s^{-1}$ obtained from Eq.(II.29) or from Eqs.(II.33) and (II.34.b) with $v_\ell = 4.8 \times 10^5$cm/s. In view of the fact that the experimental results on the ideal thermal resistivity (Section III.1.c.1) suggest $C_t \approx 0.1 \ C_\ell$ (see also Eq.(II.20)) the value of $(\tau_t')^{-1}$ seems not unreasonable.

Because of the sensitivity of the electron-phonon interaction to the detailed shape of the FS, in particular for the transverse modes, departures from the free electron predictions can be expected to occur in most metals. This is shown in Fig.III.12, where a number of lattice thermal conductivity data of alloys with different solvents, collected from various sources, has been plotted using a scaling procedure first employed by Lindenfeld and Pennebaker (34). The scaling factors are $N_a^{2/3}/M\theta$ for the variable $\lambda_g/T\rho_0$ and $(N_a^{2/3}N^{1/3}\theta)^{-1}$ for T/ρ_0, which follows from the fact that in the Pippard theory the phonon mean free path is a universal function of $q\ell$, where $\ell \sim (\rho_0 N_a^{4/3})^{-1}$.

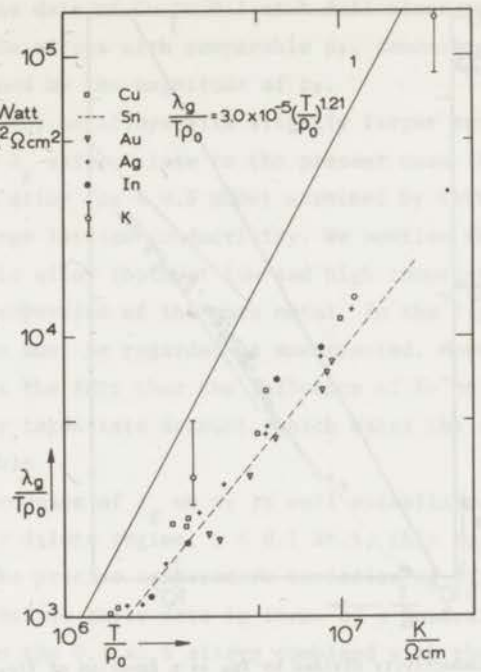

Fig.III.12. Values for $\lambda_g/T\rho_0$ versus T/ρ_0 for a number of alloys with different solvents, scaled as described in the text. The lattice conductivity has been taken at T = 3 K except for K, where the values at T = 0.6 K were used. The solutes are not mentioned. Data are obtained from various sources. Cu alloys: Lindenfeld (34), Tainsh (40); Ag alloys: van Baarle (41), Tainsh (40), Klemens (42); Au alloys: Garbarino (19), Birch (43); Sn alloys: Gueths (44); In alloys: Lindenfeld (45), Sladek (46); K-Cs: Archibald (47). The solid line 1 is the theoretical curve for $\lambda_g/T\rho_0$ vs T/ρ_0 of the transverse modes in the free electron model.

Although the different data show appreciable scatter, one sees that the departures from theory follow the same pattern for all types of alloys except for the data on potassium alloys (47), which seem to be in better agreement with the Pippard theory. This confirms our remark that the observed discrepancies are due to FS effects. On the other hand, the striking similarity of these departures for a wide variety of alloys seems to contradict this statement. However, the small range of values of $q\ell$ (or T/ρ_0) and the large scatter of the points in Fig.III.12 can easily mask the differences of the scaled $\lambda_g/T\rho_0$ vs. T/ρ_0 curves of the various alloy systems. In fact, it is likely that lattice conductivity measurements on more dilute alloys, such as present Cu-alloys, will reveal differences between the various curves, since in this region FS effects become increasingly important.

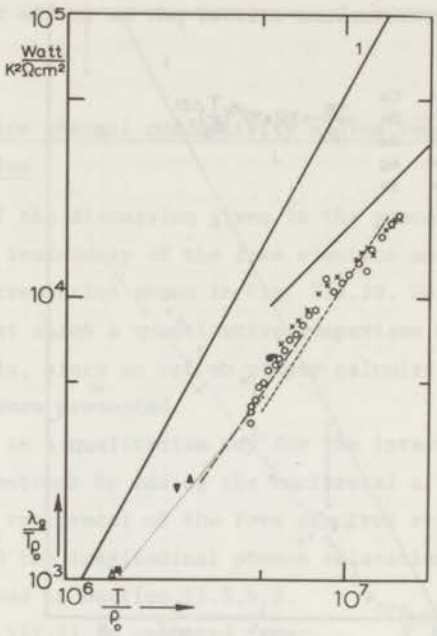

Fig.III.13. The lattice conductivity divided by $T\rho_0$ as a function of T/ρ_0 for a number of Cu alloys collected from literature.

Tainsh (40): ● Cu-Zn 2 at.% (ρ_0 = 0.56 μΩcm), ▼ Cu-Zn 5 at.% (ρ_0 = 1.20 μΩcm), ■ Cu-Zn 10 at.% (ρ_0 = 1.94 μΩcm), ▲ Cu-Pt 0.5 at.% (ρ_0 = 1.07 μΩcm), Δ Cu-Pt 0.9 at.% (ρ_0 = 2.04 μΩcm). The values of λ_g at T = 3 K have been used.

Lindenfeld (34): ----- Cu-Ge 0.06 at.% (ρ_0 = 0.301 μΩcm), — — — Cu-Ge 0.125 at.% (ρ_0 = 0.600 μΩcm), ·····Cu-Ge 0.25 at.% (ρ_0 = 1.08 μΩcm).

White (48): —— Cu-Fe 0.056 at.% ($\rho_0 \simeq$ 0.53 μΩcm).

Included are the low temperature data of Cu-Ge 0.1 at.% (0), ρ_0 = 0.349 μΩcm and Cu-Sn 0.1 at.% (x), ρ_0 = 0.276 μΩcm. The theoretical $\lambda_g/T\rho_0$ vs T/ρ_0 curve for the transverse modes is denoted by 1.

We will now discuss in more detail the experimental results shown in Fig.III.10. Firstly, we note the excellent agreement between the experimental data of our Cu-Ge 0.1 at.% alloy and the most dilute one (c ≃ 600 ppm) of Lindenfeld and Pennebaker (34) (Fig.III.13). This emphasizes the unimportance of dislocation scattering (Section II.3.b.3) because these alloys received rather different heat treatments. Since dislocation scattering has more or less the same frequency dependence as phonon-electron scattering, it is always difficult to separate their contribution to the lattice resistivity.

The fact that the data of Cu-Sn 0.1 at.% fall close to the $\lambda_g/T\rho_0$ vs. T/ρ_0 curve of the two Cu-Ge alloys with comparable ρ_0, demonstrates that the magnitude of λ_g is mainly determined by the magnitude of ρ_0.

Older data (40, 48) on alloys with slightly larger residual resistivities ($\rho_0 \approx 0.5$ μΩcm) give λ_g values close to the present ones (Fig.III.13). A notable exception is a Cu-Fe alloy ($\rho_0 \approx 0.5$ μΩcm) examined by White and Woods (48), which exhibits a rather large lattice conductivity. We mention these measurements because the properties of this alloy (both at low and high temperatures) are often considered to be close to the properties of the pure metal. In the light of the present measurements this conclusion must be regarded as unwarranted. Moreover, a more serious problem in this alloy is the fact that the influence of Fe on the transport properties has not been properly taken into account, which makes the determination of λ_g at low temperatures unreliable.

Whereas the dependence of λ_g on ρ_0 is well established (the present measurements show that in the very dilute regime, $c < 0.1$ at.%, this correlation between λ_g and ρ_0 is still present), the precise temperature variation of λ_g is still open for discussion. Most authors analyse their data in terms of a quadratic temperature dependence of λ_g. Our results on the 0.1 at.% alloys combined with the data of Lindenfeld and Pennebaker (34) seem to favour a somewhat stronger temperature variation. In the more dilute alloys λ_g has become too small, so that a possible variation stronger than quadratic in T cannot be extracted from the data.

Until a more complete theory of the electron-phonon interaction is available, which correctly takes FS effects into account, both the expressions $\lambda_g/T\rho_0 = C(T/\rho_0)^n$ and $\lambda_g/T\rho_0 = C'T/(\rho_0)^n$, where $n > 1$, may be used to describe the temperature dependence and magnitude of λ_g of well annealed dilute alloys at low temperatures.

The present results as shown in Fig.III.10 and III.13 can be very well represented in the low temperature range by means of a universal curve of the form:

$$\frac{\lambda_g}{T\rho_0} = 9.2 \times 10^{-6} \left(\frac{T}{\rho_0}\right)^{1.3} \qquad \text{(III.13)}$$

in units of Watt/K^2cm$^2\Omega$. The alternative description of the experimental results can be put in the form:

$$\lambda_g = 6.6 \times 10^{-6} \frac{T^2}{(\rho_0)^{0.35}} \qquad \text{(III.14)}$$

in units of Watt/Kcm.

A remark concerning Eq.(III.14) is in order. A T^2 behaviour of λ_g is often related with the electronic thermal resistivity by means of Eqs.(II.31) and (II.32). In particular, the application of Eq.(II.32), derived under the assumption $C_t = C_\ell$, to the experimentally determined W_{id} of the pure metal and λ_g of its most dilute alloy available, seems to give consistent results in many cases (38). The data presented here, together with theoretical objections discussed previously, show that the observed agreement is fortuitous.

III.2.c.4. The lattice thermal conductivity at higher temperatures (T > 10 K)

As the temperature is increased, phonon scattering processes other than the mechanism discussed in the previous section will become important and eventually dominate phonon-electron scattering. Their effect on λ_g is enhanced through the presence of N-processes (Section II.3.b.1). These phonon-phonon processes do not produce resistance by themselves, but transfer energy and momentum from the low frequency modes, not scattered very strongly, to higher frequency modes, where the scattering is more effective.

The scattering process, which is most likely responsible for the fact that λ_g departs from its initial T^2 or $T^{2.3}$ behaviour as T increases, is point defect scattering. It has been observed that λ_g goes through a maximum at $T \approx 0.2\theta$. Above this temperature region the lattice conductivity is thought to be mainly governed by phonon U-processes leading to $\lambda_g \sim T^{-1}$ at $T \gtrsim \theta$. These U-processes disappear exponentially with falling temperature in the vicinity of the maximum of λ_g. Because of the lack of a good quantitative theory, it is difficult to decide if these processes are still important in the temperature range of our measurements ($T < 0.1\theta$).

For reasons discussed below, we will consider only phonon-electron scattering, point defect scattering and N-processes. Noting that most of the heat is carried by the transverse modes, the lattice conductivity may be written, using Eqs.(II.25), (II.26), (II.27) and (II.39), as:

$$\lambda_g = \frac{2}{3}\frac{k_B^4 T^3}{2\pi^2\hbar^3 v_t}\left[\int \frac{x^4 e^x}{(e^x-1)^2}\frac{dx}{AT^n x^n + BT^4x^4 + CT^5x} + \right.$$

$$\left. + \frac{\left(\int \frac{x^4e^x}{(e^x-1)^2}\frac{CT^5x\,dx}{AT^nx^n + BT^4x^4 + CT^5x}\right)^2}{\int \frac{x^4e^x}{(e^x-1)^2}\frac{(ACT^{5+n}x^{5+n} + BCT^9x^5)\,dx}{AT^nx^n + BT^4x^4 + CT^5x}}\right] \qquad \text{(III.15)}$$

where $B = (3a^3k_B^4n_pS^2)/(\pi v_t^3\hbar^4)$. The scattering parameter S^2 in this expression is the term in braces in Eq.(II.39), C is given by Eq.(II.27) and the reciprocal of the relaxation time for phonon-electron scattering $\tau_t^{-1} = AT^nx^n$ is obtained from Eq.(II.13) or Eq.(III.14). In the free electron case n = 0 and τ_t^{-1} is given by Eq.(II.36). The results presented above show that τ_t^{-1} is frequency dependent, although the precise value of n cannot be determined. This uncertainty in the relaxation time for phonon-electron scattering is reflected in the scatter of the values of B and therefore of S^2 obtained by fitting Eq.(III.15) to the data, as will be shown below. Moreover, the form of τ_N^{-1} (Eq.(II.27)) can be questioned. In nonmetals it has been observed (49) in some cases that a relaxation time of the form $\tau_N^{-1} = C'T^4x$ can just as well account for the behaviour of λ_g. A further complication, which is typical for metallic alloys, is the lack of a precise knowledge of λ_e at elevated temperatures. As was noted before, the values of λ_g plotted in Fig.III.10 are obtained under the assumption that W_{id}^N(Cu) remains unchanged when impurities are added to the Cu host. At low temperatures the neglect of DMR has little effect. However, a possible change in W_{id}^N could significantly alter the temperature dependence and magnitude of λ_g at higher temperatures.

We have attempted to account for DMR in the electronic thermal resistivity in the following way. From Eq.(III.13) the scattering rate for phonon-electron scattering in Cu-Ge 0.1 at.% is calculated to be $\tau_t^{-1} = 5.7 \times 10^7T^{0.7}x^{0.7}$ s^{-1}. The experimentally determined λ_g as shown in Fig.III.10 (obtained with $(W_{id}^N)_{alloy} = (W_{id}^N)_{Cu} = 3.2 \times 10^{-5}T^2$cm K/Watt) was fitted to Eq.(III.15) using the following parameters: $B = 2.5 \times 10^5n_pS^2$ in units of $K^{-4}s^{-1}$ (Eq.(II.39), where $a^3 = 11.7 \times 10^{-24}$cm^3 and $v_t = 2.38 \times 10^5$cm s^{-1}), $n_p = 10^{-3}$ and C ranging from 0 to 20 $K^{-5}s^{-1}$. In this way a rough estimate of the point defect scattering parameter S^2 was obtained. These values together with $n_p = 3 \times 10^{-4}$ and $\tau_t^{-1} = 2.7 \times 10^7T^{0.7}x^{0.7}$ s^{-1} (obtained from Eq.(III.13) with $\rho_0 = 1.016 \times 10^{-7}\Omega$cm) were substituted in Eq.(III.15) in order to calculate λ_g (Cu-Ge 300 ppm). The calculated lattice conductivity was then compared with the λ_g values plotted in Fig.III.10 for the 300 ppm alloy. The observed discrepancies were attributed to an incorrect choice of the electronic component of the thermal conductivity in the date plotted in Fig.III.10, and W_{id}^N(Cu-Ge 300 ppm) was determined. This value was now used to fix λ_e(Cu-Ge 0.1 at.%). Here the assumption has been made that W_{id}^N of the two alloys under consideration are not very much different, which is a very reasonable assumption in view of the fact that DMR in ρ and W in other metals are observed to depend rather weakly on ρ_0.

The values of λ_g obtained in this way ($\lambda_g = \lambda_{meas} - \lambda_e$) yielded new values for S^2 of the 0.1 at.% alloy. This procedure was repeated several times until consistent

results for the two alloys were obtained. The same method of analysis was also applied to the alloys using a phonon-electron relaxation time derived from Eq.(III.14). The values obtained for S^2 and C, which gave the best fits to the data of the 300 and 1000 ppm alloys were used to determine the DMR in Cu-Ge 80 ppm, since the small size of λ_g in this alloy made it impossible to determine S^2 and C directly.

The results for both types of phonon-electron scattering rates are listed in Table III.2 and shown in Fig.III.14. One can see that $(W_{id}^N)_{alloy}$ is similar for both relaxation times, but the values of S^2 are rather sensitive to the form assumed for τ_t^{-1}. It should also be noted that consistent results could only be obtained with $C < 10\ K^{-5}s^{-1}$. The value of C calculated from Eq.(II.27) is approximately 15 $K^{-5}s^{-1}$. This value is subject to considerable uncertainty, however, since Eq.(II.27) was derived with several oversimplified assumptions. Also, as was noted before, the frequency dependence of τ_N might be different from that given m Eq.(II.27).

The analysis described above may of course be questioned. In the first place it should be noted that the values obtained for S^2 are quite large. Usually, point defect scattering is interpreted in a first approximation as mass defect scattering

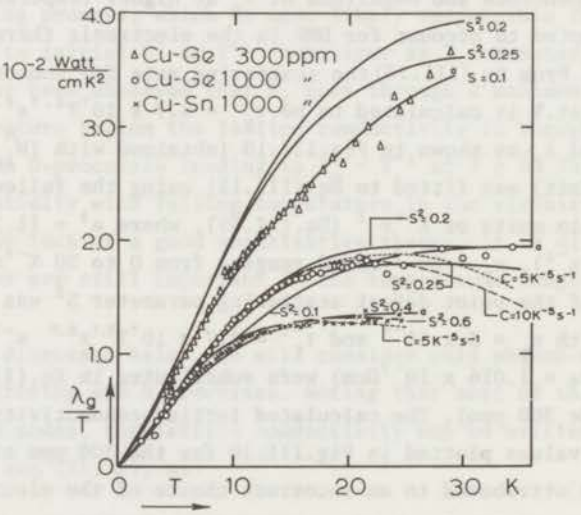

Fig.III.14. The lattice conductivity divided by T as a function of temperature for Cu-Ge 300 and 1000 ppm and Cu-Sn 1000 ppm between 2 and 35 K. The data are obtained with $W_{id}^N/T^2 = 6 \times 10^{-5}$ cm/K Watt for Cu-Ge 300 ppm, $W_{id}^N/T^2 = 8 \times 10^{-5}$ cm/K Watt for Cu-Ge 1000 ppm and $W_{id}^N/T^2 = 7 \times 10^{-5}$ cm/K Watt for Cu-Sn 1000 ppm. The solid lines are calculated from Eq.(III.15) with C = 0, n = 0.7 and values of S^2 as given in the figure. The dashed curves are obtained with non-vanishing N-scattering. The curves denoted by a are calculated assuming $\lambda_g \sim T^2$ at low temperatures (Eq.(III.14)).

Table III.2

Analysis of the lattice conductivity of some Cu alloys by means of Eq.(III.15) as shown in Fig.III.14.

alloy	$\tau_t^{-1}(s^{-1})$ phonon-electron scattering	W_{id}^N/T^2 (10^{-5}cm/K Watt)	C ($s^{-1}K^{-5}$)	S^2
Cu-Ge 300 ppm	$3.9 \times 10^7 T^{0.7} x^{0.7}$ $1.9 \times 10^7 Tx$	5.5 - 6.5	< 10	0.20 - 0.25 ≈ 0.10
Cu-Ge 1000 ppm	$5.7 \times 10^7 T^{0.7} x^{0.7}$ $2.7 \times 10^7 Tx$	6 - 10	< 10	0.20 - 0.25 ≈ 0.10
Cu-Sn 1000 ppm	$5.3 \times 10^7 T^{0.7} x^{0.7}$ $2.7 \times 10^7 Tx$	6 - 9	< 10	0.55 - 0.65 ≈ 0.4
Cu-Ge 80 ppm		4.5 - 5.5		

with $S_M^2 = (\Delta M/M)^2/12$, which is 1.6×10^{-3} for Cu-Ge. However, it has been observed in many cases that lattice strain scattering dominates mass defect effects (38), and this is apparently also the case in the present alloys. In order to check this, we measured the lattice thermal conductivity of a Cu-Sn 0.1 at.% alloy. The mass defect parameter is larger than S_M^2(Cu-Ge) namely 0.063, but still much too small to account for the observed behaviour of λ_g. We find that $S^2 = 0.6$ gives a reasonable fit to the data (see Fig.III.14), indicating a larger lattice distortion scattering. As was mentioned in Section II.3.b.3, it is difficult to obtain an accurate theoretical estimate of the magnitude of this scattering mechanism. It is, however, directly related to the relative change in the atomic volume.

Klemens (50) calculated the distortion term using a model, in which the impurity atom was taken to be a sphere forced into a spherical hole of slightly different size in an elastic medium. He obtained $S^2 = 3\gamma^2(\Delta R/R)^2$, where $\Delta R/R$ is the fractional change of the atomic radius. If we identify $\Delta R/R$ with $\Delta a/a$, the fractional change in the lattice parameter, we obtain S^2(Cu-Ge) ≈ 0.1 and S^2(Cu-Sn) ≈ 0.6, where the values of $\Delta a/a$ have been taken from Pearson (51).

The agreement between these calculated values and the values listed in Table III.2 must be considered as fortuitous, in view of the simplicity of the model used

and also, because the introduction of Ge and Sn in Cu causes electronic changes in the lattice. Nevertheless, the experimental results are not inconsistent with the theory of point defect scattering.

A more serious objection against the method of analysis employed above, namely the neglect of phonon scattering processes, different from those discussed above, can now also be removed. The different behaviour of λ_g of Cu-Ge and Cu-Sn at elevated temperatures indicates that λ_g is governed by scattering processes which depend critically on the type of impurities. This implies that, to a large extent, scattering processes such as phonon assisted impurity scattering, whose magnitude is determined by the electron mean free path and hence by ρ_0, and U-processes may be excluded from a discussion of the behaviour of λ_g at these temperatures.

Another result, obtained, which gives us confidence in the procedure employed is the magnitude of the DMR in the electronic thermal resistivity as shown in Fig. III.15. The enhancement of the coefficient of the T^2 term of W_{id} by a factor of 2-3 in Cu-Ge 0.1 at.% relative to the pure Cu value is very similar to what has been observed in other metals, notably Al, In, Sn.

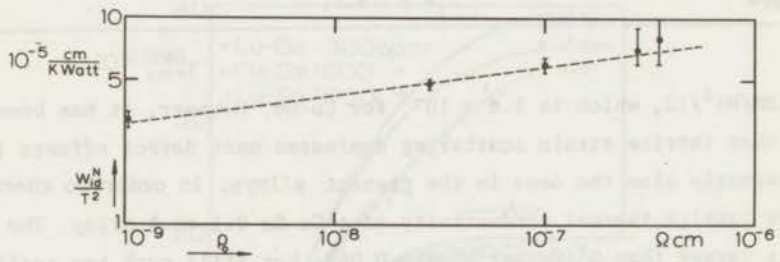

Fig.III.15. W_{id}^N/T^2 as a function of ρ_0.

III.2.c.5. Concluding remarks

To our knowledge the present results are the first more or less reliable estimates of DMR in the thermal resistivity of noble metal alloys. The fact, that White (2) observed DMR in Cu has only some qualitative meaning, since no corrections for the lattice conductivity were made. Moreover, his samples contained Fe, which was not corrected for. The same objections can be put forward with regard to the measurements of W_{id} in deformed Cu by Holzhauser (52), who determined the correlation between the coefficient of the T^2 term of W_{id} and ρ_0 of the deformed specimens.

The values of the point defect scattering parameter S^2 listed in Tabel III.2 are sensitive to the form assumed for τ_t^{-1} (Eqs.(III.13) and (III.14)). Hence, until a

more complete theory of electron-phonon scattering is available, which takes into account the nonspherical shape of the FS and real phonons, the behaviour of the lattice conductivity of metallic alloys at elevated temperatures can only be discussed in a very qualitative way. For the present alloy systems we have shown that lattice distortion scattering dominates mass defect scattering. The fact that S^2(Cu-Sn) > S^2 (Cu-Ge) is not inconsistent with what is to be expected from the difference in atomic volume and solubility of Ge and Sn in Cu.

Finally, in Fig.III.16 we have plotted $\lambda_g/T\rho_0$ against T/ρ_0 for the measured alloys. The lattice thermal conductivity data of the 300 and 1000 ppm alloys are the same as those plotted in Fig.III.14. The values for the other alloys are obtained by taking into account the DMR in the electronic thermal resistivity (Fig.III.15) and using the appropriate values of S^2 listed in Table III.2. Fig.III.16 should be compared with Fig.III.10, the points of which have not been corrected for by changes of W^N_{id} upon alloying.

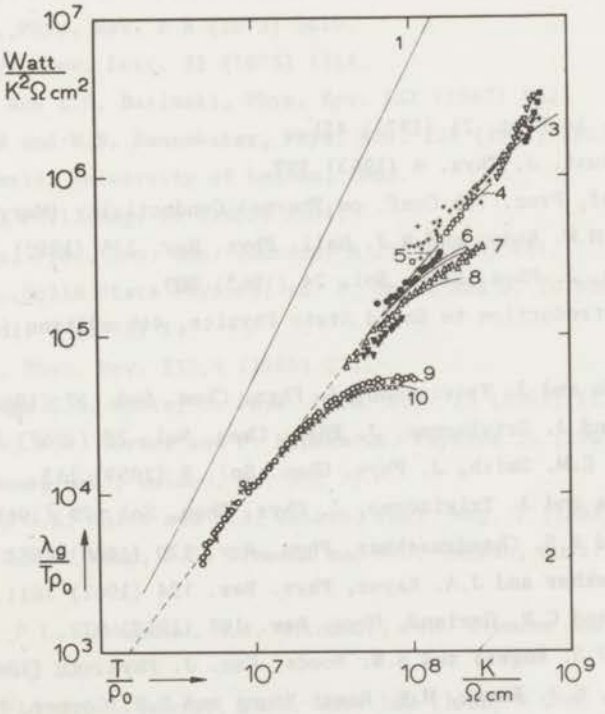

Fig.III.16. Values of $\lambda_g/T\rho_0$ vs T/ρ_0 for the measured Cu alloys. The values of λ_g have been corrected for DMR in the electronic thermal resistivity and are obtained by subtracting λ_e from the measured thermal conductivity where the electronic thermal

conductivity $\lambda_e = (\rho_0/L_0T + (W^N_{id})_{alloy} + W^U_{id}(Cu) + \Delta/L_0T)^{-1}$. The following values of $(W^N_{id}/T^2)_{alloy}$ in units of cm/K Watt have been used: Cu-Ge 30 ppm (■), 4.2 x 10^{-5}; Cu-Ge 50 ppm (▽), 4.5 x 10^{-5}: Cu-Ge 80 ppm (+), 4.8 x 10^{-5}; Cu-Ge 100 ppm (□), 5.5 x 10^{-5};Cu-Ge 150 ppm (●), 5.5 x 10^{-5}; Cu-Ge 300 ppm (Δ), 6.0 x 10^{-5}; Cu-Ge 1000 ppm (0), 8 x 10^{-5}; Cu-Sn 430 ppm (▼), 6 x 10^{-5}; Cu-Sn 1000 ppm (x), 7 x 10^{-5}. This figure should be compared with Fig.III.10 where the values of $\lambda_g/T\rho_0$ were obtained with $(W^N_{id})_{alloy} = W^N_{id}(Cu) = 3.2 \times 10^{-5} T^2$cm K/ Watt. The solid lines 1 and 2 are the theoretical curves of the transverse and longitudinal modes, respectively, in the free electron model. The dashed curve is Eq.(III.13). The curves 3 - 10 have been obtained by taking into account point defect scattering but neglecting phonon N-processes (Eq.(III.15)). Curve 3 refers to Cu-Ge 80 ppm with $S^2 = 0.2$. Curve 4 and 5 represent the calculated values for $\lambda_g/T\rho_0$ of Cu-Ge 100 and 150 ppm with $S^2 = 0.2$. Curve 6 and 7 apply to Cu-Ge 300 ppm with $S^2 = 0.20$ and 0.25, respectively (see also Fig.III.14). Curve 8 indicates the calculated $\lambda_g/T\rho_0$ values for Cu-Sn 430 ppm with $S^2 = 0.6$ whereas curve 9 and 10 are for the Cu-Ge 1000 ppm and Cu-Sn 1000 ppm alloy with $S^2 = 0.25$ and 0.6, respectively.

References

1. J. Bass, Adv. in Phys. 21 (1972) 431.
2. G.K. White, Aust. J. Phys. 6 (1953) 397.
3. J.T. Schriempf, Proc. 7th Conf. on Thermal Conductivity (Maryland, 1968), p. 249.
4. R.L. Powell, H.M. Roder and W.J. Hall, Phys. Rev. 115 (1959) 314.
5. O.L. Anderson, J. Phys. Chem. Sol. 24 (1963) 909.
6. C. Kittel, Introduction to Solid State Physics, 4th edition (John Wiley, 1971), p. 149.
7. M.E. Diederich and J. Trivisonno, J. Phys. Chem. Sol. 27 (1966) 637.
8. E.J. Gutman and J. Trivisonno, J. Phys. Chem. Sol. 28 (1967) 805.
9. H.C. Nash and C.M. Smith, J. Phys. Chem. Sol. 9 (1959) 113.
10. F.J. Kollarits and J. Trivisonno, J. Phys. Chem. Sol. 29 (1968) 2133.
11. J.A. Rayne and B.S. Chandrasekhar, Phys. Rev. 120 (1960) 1658.
12. B.S. Chandrasekhar and J.A. Rayne, Phys. Rev. 124 (1961) 1011.
13. L.J. Slutsky and C.W. Garland, Phys. Rev. 107 (1957) 972.
14. E.W. Fenton, J.S. Rogers and S.B. Woods, Can. J. Phys. 41 (1963) 2026.
15. C. van Baarle, G.J. Roest, M.K. Roest-Young and F.W. Gorter, Physica 32 (1966) 1700 (Commun. Kamerlingh Onnes Lab., Leiden, No. 350 a).
16. A.C. Ehrlich and J.T. Schriempf, Solid State Comm. 14 (1974) 469.
17. H.M. Rosenberg, Phil. Trans. Roy. Soc. London, A 247 (1955) 441.

18. G.K. White, Proc. Phys. Soc. (London) A 66 (1953) 559.
19. P.L. Garbarino and C.A. Reynolds, Phys. Rev. B 4 (1971) 167.
20. R.S. Newrock and B.W. Maxfield, Phys. Rev. B 7 (1973) 1283.
21. D.K.C. MacDonald, G.K. White and S.B. Woods, Proc. Roy. Soc. (London) A 235 (1956) 358.
22. H.M. Rosenberg, Phil. Trans. Roy. Soc. London, A 247 (1955) 441.
23. P. Seeberg and T. Olsen. Phys. Norv. 2 (1967) 197.
24. I.A. Campbell, Solid State Comm. 9 (1971) 1513.
25. J.E. Gueths, N.N. Clark, D. Markowitz, F.V. Burckbuchler and C.A. Reynolds, Phys. Rev. 163 (1967) 364.
26. G.K. White, Proc. Roy. Soc. (London) A 66 (1953) 1077.
27. G.K. White and S.B. Woods, Phil. Trans. Roy. Soc. A 251 (1959) 273.
28. J.W. Ekin, Phys. Rev. B 6 (1972) 371.
29. E.H. Sondheimer, Proc. Roy. Soc. (London) A 203 (1950) 75.
30. P.G. Klemens, Aust. J. Phys. 7 (1954) 64.
31. A.C. Ehrlich, Phys. Rev. B 8 (1973) 3610.
32. J.F. Kos, Phys. Rev. Lett. 31 (1973) 1314.
33. J.S. Dugdale and Z.S. Basinski, Phys. Rev. 157 (1967) 552.
34. P. Lindenfeld and W.B. Pennebaker, Phys. Rev. 127 (1962) 1881.
35. B. Knook, Thesis, University of Leiden, 1962.
36. A.B. Pippard, Phil. Mag. 46 (1955) 1104.
37. R.G. Chambers, Proc. Roy. Soc. (London) A 215 (1952) 481.
38. P.G. Klemens, Solid State Physics, ed. F. Seitz and D. Turnbull (Academic Press, New York), Vol. 7 (1958) 1.
39. C. Feldmann, Phys. Rev. 139 A (1965) 211.
40. R.J. Tainsh and G.K. White, J. Phys. Chem. Sol. 23 (1962) 1329.
41. C. van Baarle, F.W. Gorter and P. Winsemius, Physica 35 (1967) 223 (Commun. Kamerlingh Onnes Lab., Leiden, No. 350 c).
42. P.G. Klemens, G.K. White and R.J. Tainsh, Phil. Mag. 7 (1962) 1323.
43. J.A. Birch, W.R.G. Kemp, P.G. Klemens and R.J. Tainsh, Aust. J. Phys. 12 (1959) 455.
44. J.E. Gueths, P.L. Garbarino, M.A. Mitchell, P.G. Klemens and C.A. Reynolds, Phys. Rev. 178 (1969) 1009.
45. P.L. Lindenfeld and H. Rohrer, Phys. Rev. 139 (1965) A 206.
46. R.J. Sladek, Phys. Rev. 91 (1953) 1280.
47. M.A. Archibald, J.E. Dunick and M.H. Jericho, Phys. Rev. 153 (1967) 786.

48. G.K. White and S.B. Woods, Can. J. Phys. 33 (1955) 58.

49. See for example:
R. Berman, C.L. Bounds and S.J. Rogers, Proc. Roy. Soc. A 289 (1965) 46, 66.
C.C. Ackerman and R.A. Guyer, Ann. Phys. 50 (1968) 128.

50. P.G. Klemens, Phys. Rev. 169 (1968) 229.
See also: P. Carruthers, Rev. Mod. Phys. 33 (1961) 92.

51. W.B. Pearson, A Handbook of Lattice Spacings and Structures of Metals and Alloys (Pergamon Press, 1958).

52. W. Holzhauser, Cryogenics 7 (1967) 18.

CHAPTER IV

LOW TEMPERATURE TRANSPORT PROPERTIES OF DILUTE CU-FE, CU-CR AND CU-MN ALLOYS

Abstract

This chapter deals with the transport properties of dilute magnetic alloys, notably, Cu-Fe, Cu-Cr and Cu-Mn. The electrical and thermal conductivity and thermopower of these alloy systems have been measured from 1.3 to 9 K. The alloys have been chosen such that the measurements cover the temperature range from $T < T_K$ (Cu-Fe) via $T \approx T_K$ (Cu-Cr) to $T >> T_K$ (Cu-Mn) where T_K is the Kondo temperature. The Lorenz number for impurity scattering is determined from the measured electrical and thermal conductivity. Values for the lattice thermal conductivity and the ideal thermal resistivity are obtained from data on nonmagnetic alloys as discussed in Chapter III. The present Lorenz number data yield the first experimental observation of the theoretically predicted maximum in the Lorenz number for electron-impurity scattering in dilute magnetic alloys at $T \approx T_K$. The Lorenz number of Cu-Mn is a few percent higher than L_0 in the present temperature region ($T >> T_K$) and is comparable to that of dilute Au-Fe and Ag-Mn alloys. The magnitude of L (Cu-Mn) decreases with increasing manganese concentration due to the quenching of the Kondo effect by impurity interactions. The Lorenz number data of Cu-Fe and Cu-Cr, which, for the first time give an impression of the behaviour of L as a function of temperature for $T \leq T_K$, can be interpreted in terms of a resonance in the scattering amplitude for electron-impurity scattering at the Fermi energy. An alternative interpretation within the framework of the localized spin fluctuation model results in a Lorenz number for electron-electron scattering of $(0.32 \pm 0.05)\ L_0$ for Cu-Fe at the lowest temperature of our measurements. This result should be compared with the value obtained for Pd-Ni: $L_{e\text{-}e} \approx 0.45\ L_0$.

IV.1. Theoretical aspects of the dilute magnetic alloy problem

IV.1.a. Virtual bound state; Anderson model

The problem of transition metal impurities dissolved in a simple host metal has traditionally been considered as having two distinct aspects, viz., the question of magnetic moment formation on the impurity, which in fact should be viewed as the problem of moment survival (1), and the influence of a local moment on the physical properties of the alloy. The latter aspect is the subject of the present chapter.

The problem of moment formation has been treated in a phenomenological way by Friedel and co-workers (2) in terms of a description of the impurity state or virtual bound state (vbs) by resonance scattering theory. The vbs is a non-localized state with energy width Δ, built up by resonance between the energy levels of the impurity and the conduction electron states. The magnitude of the intra-atomic exchange interaction and Δ determine the conditions for which the vbs is magnetized. These conditions are more quantitatively treated in the Anderson model (3), which describes the transition metal impurity as an extra d-orbital placed in the conduction band of the host metal, having energy ε_d. The interaction between the conduction electron states and the impurity d-states leads to a broadening of the impurity level corresponding to the vbs in the Friedel picture. The Hartree-Fock (HF) approximation of the Anderson model provides a criterion for the occurrence of a localized moment. It leads to a sharp boundary between two regimes, the nonmagnetic regime (spin up and spin down vbs having the same energy) and the magnetic regime (two vbs split in energy). The condition for the occurrence of magnetism in the non-degenerate case is $U\rho_d(0) = 1$, where U is the Coulomb interaction between two electrons with opposite spin and $\rho_d(0)$ is the d-electron density of states at the Fermi level:

$$\rho_d(\omega) = \frac{1}{\pi} \frac{\Delta}{(\omega - \varepsilon_d)^2 + \Delta^2} \qquad \text{(IV.1)}$$

where Δ is the half width of the vbs, $\omega = \varepsilon - \varepsilon_F$ and ε_d is measured relative to the Fermi energy. In the orbitally degenerate case this condition is relaxed due to the exchange interaction I: $(U + 4I)\rho_d(0) = 1$. The neglect of d-d correlations in the HF treatment leads to difficulties in the magnetic regime ($U >> \Delta$). It appears that orbital degeneracy must be taken into account, since correlation effects reduce the Coulomb interaction. This reduction severely restricts the condition for the occurence of magnetism. In fact, in the non-degenerate case the renormalization of U implies that the magnetic regime is never reached at T = 0 (4). Attemps to improve the HF treatment have only been partly succesful and a proper treatment of correlations in the degenerate Anderson model has yet to be given.

The historical meaning of the HF theory was the distinction between two classes of alloy systems, nonmagnetic and magnetic, separated by the condition $U\rho_d(0) = 1$. The latter class of systems can be treated within the context of a model of somewhat older age than the Anderson model, the s-d exchange model (5). This model assumes the existence of a well-defined impurity spin and has become very popular since the appearance of Kondo's paper (6) in 1964 (see below). The link between the s-d model

and the Anderson model in the strongly magnetic limit was established some years later (7). The understanding of the so-called 'border-line' cases ($U\rho_d(0) \approx 1$) waited for further developments and is still subject to discussion.

IV.1.b. The s-d model - Kondo effect

The s-d model has played an important role in clarifying the second aspect of the problem of transition metal atoms in a simple metal. It assumes a Heisenberg type of interaction between the conduction electrons and the impurity

$$H = - J \vec{s}.\vec{S} \qquad (IV.2)$$

where J is the s-d exchange integral, s is the conduction electron spin and S is the impurity spin. After numerous fruitless attempts, it was Kondo (6) who explained in principle, on the basis of the s-d exchange interaction, the 'minimum in the electrical resistivity', a phenomenon known for more than 30 years (8). This minimum occurs as a consequence of a decreasing term in the electrical resistivity with increasing temperature combined with the phonon induced resistivity ($\sim T^5$). Kondo calculated the scattering of the conduction electrons by the impurity in second Born approximation (up to order J^3) and found a logaritmic term in the electrical resistivity, which for antiferromagnetic coupling ($J < 0$) leads to a divergence at $T = 0$. It is this logarithmic dependence on T, which also occurs in other physical properties, that is usually called the Kondo effect. In the years following 1964 the main emphasis was placed on attempts to remove the divergence. It turned out that inclusion of higher order terms in the pertubation calculations (9) led for $J < 0$ to a shift of the divergence of the scattering amplitude at ε_F from $T = 0$ to a characteristic temperature, which is now called the Kondo temperature T_K. This temperature has turned out to be the key parameter in the dilute magnetic alloy problem.

Subsequent theoretical efforts, based on nonpertubative approaches to the Kondo problem (10) led to the removal of the unphysical divergences and revealed that some kind of bound state was formed below T_K. The decrease of the moment of the impurity system as $T \to 0$ was thought to arise from correlations in the electron gas, building up a negative polarization which compensates the impurity spin, leading to a nonmagnetic state at $T = 0$. This interpretation was given in view of the fact that in the s-d model the impurity moment cannot disappear.

Experimentalists (see, e.g., (11)) noticed, however, that these theories were incapable of describing correctly the observed behaviour of the various physical properties at $T < T_K$. The idea was gradually put forward that the properties of

magnetic alloys exhibit Fermi gas characteristics at $T \ll T_K$, that is, the temperature dependences are of the 'simple power law' type (12). The discrepancies between theory and experiment were attributed to the insufficiency of the approximations, employed. This has generated new methods (13, 14) of handling the Kondo problem (path integral methods, renormalization group theory). The question whether the theoretical low temperature behaviour is totally non-singular or whether there are still traces of singular behaviour at low temperatures remained controversial for some time. The final answer seems to be given by Wilson (15) who showed, using renormalization group considerations, that the Kondo impurity looks like a nonmagnetic scattering resonance at $T = 0$, as was already suggested by Anderson (13). This paper should provide a link to a different approach of the dilute alloy problem, the localized spin fluctuation model, which has become very popular especially among experimentalists. We, therefore, return to the years around 1968.

IV.1.c. Back to the Andersom model - localized spin fluctuations

The unsatisfactory situation with repect to the s-d model and the theoretical low temperature behaviour ($T < T_K$) of dilute magnetic alloys induced some authors to return to the more fundamental Anderson model. The fact that, around that time a weak resistance minimum was observed in Al-Mn (16), a system which was thought to belong to the nonmagnetic regime of the Anderson model, stimulated this approach.

The HF solution of the Anderson model leads to an unphysically sharp transition between the magnetic and nonmagnetic regime. Furthermore, it cannot explain, why a particular alloy looks 'magnetic' at high temperatures and 'nonmagnetic' at low temperatures. The neglect of correlation effects in the HF approximation is rather unimportant if $U \ll \Delta$. However, if $U \gtrsim \Delta$ lifetime arguments become important. The Coulomb repulsion U tries to prevent the simultaneous occupation of the d-state by two electrons of opposite spin (in the non-degenerate case) or, equivalently, it tries to couple an electron and hole of opposite spin and preserve the memory of the spin for a longer time than the lifetime of the vbs $\hbar/\Delta$. This electron-hole coupling is called a localized spin fluctuation (lsf).

The lsf were first treated by Lederer and Mills (17) employing the linearized time dependent HF approximation (RPA). Rivier and co-workers (18, 19) proposed the idea that the appearance of magnetism is simply a competition between the thermal fluctuations and the fluctuations of the moment, the lifetime of which is given by

$$\tau_{sf} = \frac{\pi\rho_d(0)}{1 - U\rho_d(0)} \qquad \text{(IV.3)}$$

At $T < T_{sf} = \hbar/k_B\tau_{sf}$ the alloy looks nonmagnetic with additional spin fluctuation effects, whereas at $T > T_{sf}$ the alloy looks magnetic, that is, the spin fluctuations become slower than the thermal fluctuations of the moment that they describe. This attractive picture raises mathematical problems, however, in that the RPA description of the lsf breaks down at the HF instability point where τ_{sf} diverges. Although a fully renormalized theory has yet to be written, it is generally believed that the gross features sketched above will not be significantly modified in a complete theory.

IV.1.d. Some concluding remarks

The problem of magnetic impurities in a nonmagnetic host has been tackled from two, at first sight, contradictory points of view, the s-d model and the lsf picture. At present we should establish the fact that both models have their merits in a limited range of Anderson parameters (ε_d, U, Δ) and temperature (the most recent approaches to the Kondo problem within the context of the s-d model (13 - 15) have in principle provided a solution, but as yet no numerical results have been produced for verification). Experimental evidence suggests that these models form two aspects of an unified theory with one key parameter T_K or T_{sf}. In this respect we note the similarity in the behaviour of the physical properties of alloys such as Al-Mn and Cu-Fe as a function of T/T_{sf} or T/T_K, respectively.

From the discussion presented above it has become obvious that a comparison between experiment and theory should only be made, while keeping in mind the limitations of the various models proposed. Even when working within a particular model, the approximations employed give such a comparison at present only some qualitative meaning.

IV.2. Transport properties of dilute magnetic alloys

IV.2.a. Introduction

This section deals with the second aspect of the dilute magnetic alloy problem, namely the effect of a local moment on the physical properties of the alloy. We will discuss the behaviour of the electrical and thermal resistivity and the thermopower as predicted by the models mentioned in the preceding section.

The electrical resistivity (ρ) has played a dominant role in the history of the dilute magnetic alloy problem. Friedel (2) compared his model with the experimentally determined high temperature electrical resistivity. The structure of the vbs and its location relative to ε_F are reflected in the behaviour of the scattering amplitude

and, therefore, of the electrical resistivity as a function of the parameters U, Δ and ε_d. Spinflip scattering was treated within the s-d model by Kondo (6) to explain the minimum in the electrical resistivity at low temperatures, whereas the behaviour of ρ as $T \to 0$ ($\sim T^2$) induced the conception of the lsf model.

The thermopower (S) is also drastically affected by the presence of magnetic impurities. The extreme sensitivity of the thermopower to the type of solute and to the presence of spurious impurities makes this quantity more difficult to handle.

The thermal resistivity (W) is usually considered in connection with the Lorenz number and can provide information regarding inelastic scattering processes.

IV.2.b. The s-d model

IV.2.b.1. Electrical resistivity

The calculation of the scattering of electrons by magnetic impurities via the s-d exchange interaction (Eq.(IV.2)) in second Born approximation results in the following expression for the spin dependent term of the electrical resistivity (6):

$$\rho_K = c\rho_m(1 + 4\, J\rho_s \ln \frac{k_B T}{D}) \qquad \text{(IV.4)}$$

where

$$\rho_m = \frac{4\pi\hbar}{N_a e^2 k_F} (J\rho_s)^2 \pi^2 S(S+1) \qquad \text{(IV.5)}$$

N_a is the number of conduction electrons per atom, S is the impurity spin, ρ_s is the host density of states and D is the half width of the conduction band. One-third of the temperature independent resistivity term ρ_m is contributed by non-spin flip scattering and two-thirds by spin flip scattering. When Eq.(IV.4) is combined with the phonon resistivity a minimum in the resistivity results for $J < 0$. Nowadays, it is known that the validity of Eq.(IV.4) is rather restricted, but the essential feature emerging from this expression, viz., the logaritmic behaviour, is characteristic for the problem under discussion. Extension of this calculation by summing up the most divergent terms results for antiferromagnetic coupling in a removal of the divergence of the scattering amplitude at ε_F from $T = 0$ (Eq.(IV.4)) to $T = T_K = (D/k_B)e^{1/2J\rho_s}$. The expression for the electrical resistivity obtained by Abrokosov (9) reads:

$$\rho = c\rho_m(1 - 2J\rho_s \ln \frac{k_B T}{D})^{-2} \qquad \text{(IV.6)}$$

The nonpertubative treatments of the Kondo problem removed the divergence and produced the logaritmic terms (Eqs.(IV.4) and (IV.6)) at $T >> T_K$. Suhl and Wong (20) employed S-matrix theory and calculated numerically the transport properties taking both exchange (J) and potential scattering (V) into account. At this point the importance of potential scattering, in discussing transport phenomena in connection with the Kondo effect, should be emphasized. Apart from its straightforward relevance to the thermopower, potential scattering markedly affects the temperature dependent electrical and thermal resistivity component. The combination of a strongly energy dependent relaxation time and a relaxation time which varies weakly with energy leads to significant DMR. We will examine this point in more detail, when discussing our experimental results. For the moment it is sufficient to note that, in comparing theory with experiment, potential scattering should always be taken into account and a simple subtraction procedure: $\rho_{mag} = \rho_{meas} - \rho_{pot}$ is only allowed when $\rho_{mag} >> \rho_{pot}$ or $\rho_{mag} << \rho_{pot}$.

The calculations by Suhl and Wong show a smoothly increasing electrical resistivity with decreasing temperature and a flattening off as a function of logT as $T \to 0$. At $T = 0$, ρ has attained the unitarity limit value. The manner in which this limit is approached depends on the magnitude of the screened Coulomb potential V.

A different nonpertubative approach, i.e., the equation of motion method (21, 22, 23) yielded equivalent results. An analytical expresseion for the electrical resistivity was obtained by Hamann (22):

$$\rho = \frac{\rho_u}{2}\left[1 - \frac{\ln(T/T_K)}{[(\ln(T/T_K))^2 + \pi^2 S(S+1)]^{1/2}}\right] \qquad \text{(IV.7)}$$

where ρ_u is the unitarity limit value ($\rho_u = 4\pi\hbar c/(N_a e^2 k_F)$). Inclusion of potential scattering gives (24):

$$\rho = \frac{\rho_u}{2}\left[1 - \frac{\cos 2\delta_V \ln(T/\bar{T}_K)}{[(\ln(T/\bar{T}_K))^2 + \pi^2 S(S+1)]^{1/2}}\right] \qquad \text{(IV.8)}$$

where δ_v is the phase shift due to potential scattering and $\bar{T}_K = (D/k_B)e^{1/2\bar{J}\rho_s}$ with $\bar{J} = J\cos^2\delta_v$. The general features emerging from Eqs.(IV.7) and (IV.8) turn out to be correct, but the precise shape of ρ as given by these expressions disagrees with experiment at $T < T_K$. For sufficiently high temperatures ($\ln(T/T_K) >> \pi[S(S+1)]^{1/2}$), it can be readily shown that Eq.(IV.7) returns to the Kondo form (Eq.(IV.4)), indicating that the original Kondo calculation applies only to extremely high temperatures.

IV.2.b.2. Thermopower

Calculations within the s-d model show a broad peak in the thermopower around the Kondo temperature, the general features of which are in agreement with experiment. However, as in the case of the electrical resisitivitym detailed agreement is lacking. In particular, the model is incapable of producing the experimentally observed proportionality to T at low temperatures.

IV.2.b.3. The Lorenz number

Calculations of the thermal resistivity of Kondo alloy are scarce. The thermal resistivity is mostly considered by means of the Lorenz number. The deviations from the WFL law demonstrate the presence of a strongly energy dependent (near ε_F) relaxation time, as was discussed qualitatively in Section II.2.a. The numerical computations by Suhl and Wong (20) show a broad peak of L on a logarithmic temperature scale around T_K, the height and shape of which strongly depend on the magnitude of the potential scattering. An analytical expression for the Lorenz number for combined exchange and potential scattering in the Hamann theory has been given by Fischer (24) and Nam and Fullenbaum (25) for large values of $|\ \ln(T/\bar{T}_K)\ |$:

$$L = L_0\left(1 + \frac{2}{3}\left(\frac{\rho_u}{2\rho} - 1\right)\frac{\pi^2 S(S+1)}{\ln(T/\bar{T}_K)\left[(\ln(T/\bar{T}_K))^2 + \pi^2 S(S+1)\right]}\right) \qquad \text{(IV.9)}$$

where ρ is given by Eq.(IV.8). In the limit $T \to 0$

$$L = L_0\left(1 + \frac{2}{3}\frac{\cos 2\delta_v}{1 + \cos 2\delta_v}\ \frac{\pi^2 S(S+1)}{|\ \ln(T/\bar{T}_K)\ |^3}\right) \qquad \text{(IV.10)}$$

At high temperatures, where the Kondo term ρ_K (Eq.(IV.4)) is dominant, L is approximately temperature independent. If the potential term $\rho_{pot} >> \rho_K$ and if Matthiessen's rule holds, one obtains:

$$L = L_0\left(1 - \frac{2}{3}\frac{1}{\rho}\frac{d\rho}{d(\ln(k_B T/D))}\right) \qquad \text{(IV.11)}$$

IV.2.b.4. Some comments

As has been mentioned several times before, calculations on the basis of the s-d model cannot describe the observed behaviour of transport properties correctly at

$T < T_K$. However, problems arise also at higher temperatures. The expressions given in the preceding sections suggest a dependence of the transport properties on the spin value S, which is not in agreement with experimental observations. Furthermore, the neglect of non-logaritmic terms in the calculations could lead to serious errors, in particular for the transport properties.

The logaritmic terms which govern the temperature dependence of the transport properties severely restrict the value of a quantitative comparison between theory and experiment in a limited temperature interval. The presence of nonmagnetic terms in the resistivity and thermopower hampers the examination of the Kondo effect within a particular alloy system in a temperature region, which extends over several decades. An extension of the measuring range is sometimes obtained by studying several alloy systems having different values of T_K. The similar behaviour of the transport properties as a function of T/T_K for different alloy systems is then utilized to construct 'universal curves'. However, the value of this procedure for the resistivity may be questioned in view of the fact that the presence of different nonmagnetic contributions in the alloy systems under consideration leads to different DMR.

IV.2.c. Localized spin fluctuations

IV.2.c.1. Introduction

The essential quantity in the lsf approach is the lifetime of the moment. A smooth transition between a nonmagnetic behaviour and the appearance of a well defined moment with increasing temperature occurs as a result of the competition between the intrinsic fluctuations of the moment and the thermal fluctuations. These lifetime arguments lead in a natural way to the experimentally observed non-singular behaviour as a function of temperature of the physical properties at low temperatures. Although the mathematics of the lsf approach can be questioned, there is a general feeling that a renormalized theory will not significantly modify its predictions.

The lsf theory was originally applied to systems belonging to the nonmagnetic regime of the Anderson model. The similar behaviour as a function of temperature of the transport properties of alloys belonging to the magnetic and nonmagnetic regime suggests that a correct lsf theory should provide a meaningful description of both classes of systems.

IV.2.c.2. Electrical resistivity

The main features of the temperature dependence of the electrical resistivity

have been discussed by Rivier and Zlatic (26). They considered a vbs undergoing spin fluctuations. The conduction electrons scatter into the extra d-orbital state before seeing the lsf. Since the electrons at the vbs are at the unitarity limit, the scattering by the lsf leads to a decrease of the resistivity (this is opposite to what happens in iso-electronic alloys, which do not have a vbs near ϵ_F). The electrical resistivity decreases as T^2 at very low temperatures ($T << T_{sf}$). The temperature dependence becomes linear at $T \approx T_{sf}/6$ and gradually approaches a log T behaviour at $T > T_{sf}$. The calculations seem to be consistent with the experimental results on Al-Mn, the most thoroughly investigated system from the nonmagnetic regime. Rivier and Zlatic (27) suggest that the electrical resistivity of alloys such as Al-Mn is in fact the mirror image of the electrical resistivity of iso-electronic alloys like Pd-Ni and Rh-Fe, viz., $\tilde{\rho}(\text{Pd-Ni}) = 1 - \tilde{\rho}(\text{Al-Mn})$, where $\tilde{\rho}(\text{Al-Mn})$ is the resisitivity normalized to its value at $T = 0$ and $\tilde{\rho}(\text{Pd-Ni})$ is the resistivity normalized to its value at $T \to \infty$.

IV.2.c.3. The Lorenz number

A maximum in L is expected to occur at $T \approx T_{sf}$, if both resonance scattering and scattering by the lsf are taken into account (28). Following the suggestion of Rivier and Zlatic (27) concerning the relation between the electrical resistivity of alloys, described by the Anderson model, and iso-electronic alloys, a similar 'mirror equation' may be set up for the thermal resistivity, based on the observation that the dynamics of the scattering (lsf) is the same in both cases. Hence, the quantity $(\rho(T = 0) - \rho(T))/(WT(T = 0) - W(T)T)$ for Al-Mn types of alloys should be equal to the Lorenz number arising from spin fluctuation scattering in Pd-Ni types of alloys. This Lorenz number, L_{e-e} (where e-e stands for electron-electron scattering) has been subject to some interest in recent years with regard to the iso-electronic alloys (29-32). We have already introduced such a Lorenz number in Section II.2.c. and discussed its features in a qualitative way. Delaying a discussion of L_{e-e} with respect to our experimental results to a later stage, we note that within the framework of the lsf model a comparison between the temperature dependent terms of ρ and of WT by means of a Lorenz number, which we call L_{e-e}, analogously to the nomenclature in the iso-electronic alloys may contribute to the knowledge of the nature of the lsf in alloys described by the Anderson model.

IV.2.d. Concluding remarks

The discussion of the lsf model in connection with the transport properties in

the preceding section has been restricted to Al-Mn types of alloys as a consequence of the fact that lsf theories have as yet not been properly extended to more magnetic systems. A quantitative comparison of our experimental results on Cu-Fe, Cu-Cr and Cu-Mn with calculations from the lsf model is therefore out of the question. Similar remarks have been made with respect to the s-d model. Consequently, we have arrived at the unsatisfactory situation (from an experimental point of view) that the interpretation of our data will be rather phenomenological. We note in this respect that our results are consistent with the general opinion that the lsf and s-d model are two aspects of a single model, which seems to be on the verge of being conceived (15, 33).

In the preceding sections two parameters, characterizing the nonmagnetic-magnetic transition, have been introduced, namely the Kondo temperature T_K, determined by s-d correlations and the spin fluctuation temperature T_{sf}, determined by d-d correlations. The relation between these parameters is as yet unclear, but should be established by an universal theory. In what follows we will mainly use the notation 'Kondo temperature' (partly for historical reasons).

The three alloy systems, which have been studied, display a large variation in the value of T_K (Cu-Fe, $T_K \approx 10^1$K; Cu-Cr, $T_K \approx 10^0$K; Cu-Mn, $T_K \approx 10^{-2}$K). If we take for granted the statement that T_K is the key parameter in the dilute magnetic alloy problem then, from an experimental point of view, a combined study of these alloys is a promising method to replace a study of a specific alloy system in the temperature range $T \ll T_K$ to $T \gg T_K$, which, in practice, is impossible to perform. However, constructions of universal curves should be performed with caution (Section IV.2.b.4).

IV.3. Previous experimental results

Since the experimental results on the electrical resistivity and thermopower have been extensively reviewed by various authors (8, 34, 35) we will restrict ourselves by summing up the previous experiments on the Lorenz number of Kondo alloys. Lorenz number data are scarce due to the limited experimental accuracy of thermal conductivity measurements and because of the complicated structure of λ, which hampers the interpretation of the data.

The experimental results, published so far, were mainly restricted to alloys with a very low T_K ($\ll$ 1K). The only exceptions are a preliminary report on our measurements on some Cu-Fe alloys (36), which will be discussed in the next sections and recently published data on Cu-Fe and Cu-Cr (37, 38). The latter results do not permit a meaningful discussion, however, in view of the poor experimental accuracy of the measurements and an incorrect procedure for eliminating the ideal thermal

resistivity and the lattice thermal conductivity. Older data on Mg alloys (39) and on Ag-Mn (40, 41) suffer from the same shortcomings. The remaining data are those on Au-Fe (42) and Ag-Mn (43). Both systems have been studied below T ≈ 4K. The electrical resistivity of the most dilute alloys of these systems can be adequately fitted to Eq.(IV.4). The Lorenz number is temperature independent and approximately 3% higher than L_0 (see Section IV.4.c.4).

IV.4. Experimental results on Cu-Fe, Cu-Cr and Cu-Mn alloys

In this section we present our measurements on the electrical and thermal conductivity and the thermopower of some dilute Cu-Fe, Cu-Cr and Cu-Mn alloys. The electrical resistivity of these alloy systems has been frequently discussed in the literature (34, 35) in connection with sometimes extremely accurate measurements, in particular on Cu-Fe (44, 45), the key system in the history of the Kondo effect. The limited accuracy (0.1%) of the present electrical resistivity measurements on the rods does not permit a detailed quantitative discussion as has been done before. In fact, this remark also applies to the thermal resistivity. However, in this case the present measurements fill a gap, since the thermal conductivity and the Lorenz number of Kondo alloys have not received much attention in the past (Section IV.3). In the present section we restrict ourselves to some comments on the observed behaviour of the three transport properties and postpone a more quantitative discussion of the Lorenz number, which involves the electrical resistivity and the thermopower as well, to a subsequent section.

We have studied five Cu-Fe alloys with concentrations 12, 15, 20, 75 and 100 ppm, two Cu-Cr alloys (10 and 30 ppm) and four Cu-Mn alloys (26, 60, 270 and 1000 ppm) between 1.3 and 9K. The latter two Cu-Mn alloys will be discussed separately, since in these alloys the Kondo effect is quenched by impurity-impurity interactions.

IV.4.a. Electrical resistivity

IV.4.a.1. Cu-Fe

The electrical resistivity of two Cu-Fe alloys, corrected for the pure copper resistivity is plotted in Fig.IV.1. The resistivity of each of the alloys could be scaled to the others within 0.2%, indicating that the Kondo effect is not significantly influenced by impurity-impurity interactions in the present concentration range. The average value for the incremental resistivity of Fe in Cu at T = 1.3 K is 11.7μΩcm/

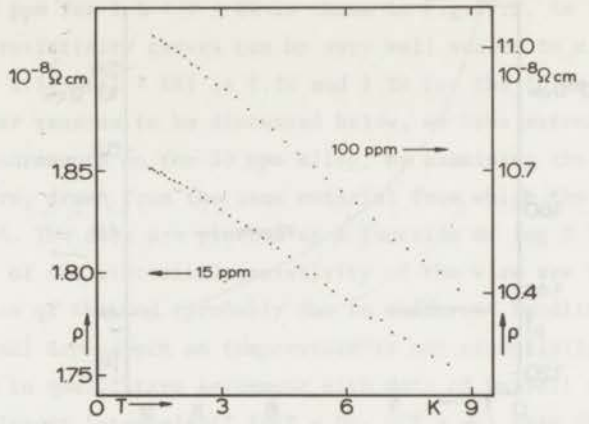

Fig.IV.1. The electrical resistivity as a function of temperature for two Cu-Fe alloys. The pure Cu resistivity has been subtracted.

at.%. A detailed analysis of the electrical resistivity of Cu-Fe, performed by Star (44, 45), revealed a quadratic temperature dependence of ρ below T = 1.5K (which is outside our measuring range);

$$\rho = \rho_0(1 - (\frac{T}{\theta})^2) \qquad \text{(IV.12)}$$

where the characteristic temperature $\theta(\approx 20K)$ is usually defined as the Kondo temperature. An inflection point is observed around T = 6K. In this temperature region the resistivity varies approximately linearly with T, which is sometimes identified (46) with the linear behaviour of the impurity resistivity as predicted by spin fluctuation theories (Section IV.2.c.2). The behaviour as a function of temperature of the electrical resistivity of the Cu-Fe alloys is similar to what has been observed in Al-Mn types of alloys, if the temperature is scaled according to the characteristic temperature θ. We note that a detailed comparison is not possible due to the different contributions from potential scattering. It turns out that DMR can be significant especially at $T \approx \theta$ (Section IV.5). The T^2 term is not affected, however (see also (44)), so that a simple subtraction procedure in order to obtain the magnetic term ($\rho_{mag} = \rho_{meas} - \rho_{pot}$) can only be applied at $T \ll \theta$.

IV.4.a.2. Cu-Cr

The incremental electrical resistivity as a function of temperature of

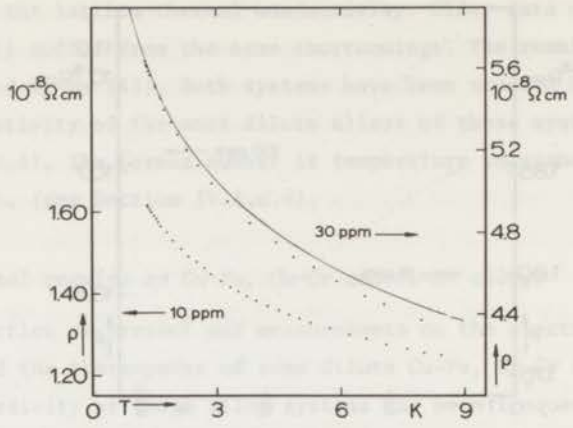

Fig.IV.2. The electrical resistivity of Cu-Cr 10 and 30 ppm as a function of temperature. The pure Cu resistivity has been subtracted. The solid line represents the electrical resistivity of a Cu-Cr 30 ppm wire. The resistivity data of the wire were shifted by 0.20 x $10^{-8}\Omega$cm in order to match with the results on the 30 ppm rod at T = 1.5K.

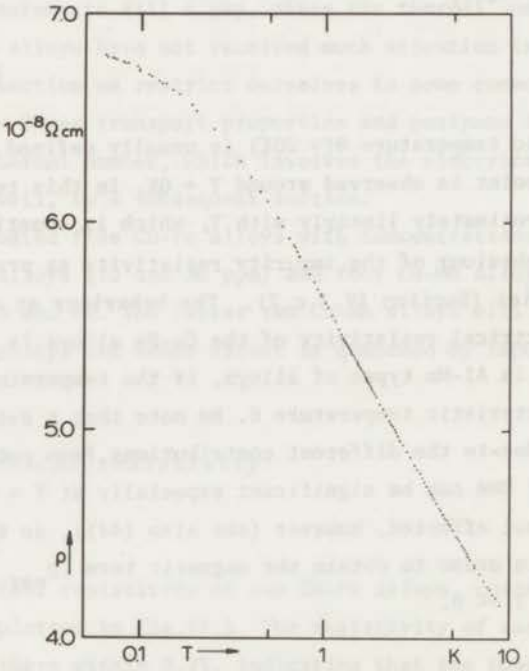

Fig.IV.3. The electrical resistivity of Cu-Cr 30 ppm (wire) between 0.06 and 9K. The electrical resistivity of Cu has been subtracted.

Cu-Cr 10 and 30 ppm for $1.3 < T < 9K$ is shown in Fig.IV.2. As in the case of Cu-Fe, the two resistivity curves can be very well scaled to a single curve. We find that $\rho(T = 1.3K)/\rho(T = 8K)$ is 1.26 and 1.24 for the 10 and 30 ppm alloy, respectively. For reasons to be discussed below, we have extended the electrical resistivity measurements on the 30 ppm alloy, by examining the resistivity of a Cu-Cr 30 ppm wire, drawn from the same material from which the rod was obtained, down to T =0.06K. The data are plotted as a function of log T in Fig.IV.3. The absolute values of the electrical resistivity of the wire are somewhat smaller ($\approx$ 4%) than those of the rod (probably due to different handling of the samples), but the functional dependence on temperature is not essentially changed (Fig.IV.2). Our results are in qualitative agreement with data of Daybell and Steyert (47) and display a much larger 'stepheight' ($\rho(T = 0) - \rho(T \rightarrow \infty)$) than the resistivity of Cu-Fe.

An attempt to interpret the data within the framework of the s-d model leads to a comparison with the Hamann expression (Eq.(IV.8)). Taking the potential scattering contribution, the spin value and the Kondo temperature as adjustable parameters, we can fit our results quite well for $T \gtrsim 1K$, using $S = 0.5$, $\cos 2\delta_v = 0.39$ and $T_K = 2.5K$. These values are in good agreement with those obtained for a 15 and 30 ppm alloy (48). If the measured value of the high temperature spin is used ($S = \frac{3}{2}$), the r.m.s. of the fit increases by an order of magnitude, illustrating the fact that the Hamann theory applies only to $S = \frac{1}{2}$. Upon decreasing the temperature below 1K the disagreement between the experimental and calculated values of ρ becomes increasingly larger, demonstrating the shortcomings of the present theories, based on the s-d model, at $T < T_K$.

Regarding the functional dependence on T at these temperatures, we note that the T^2 term of ρ is apparently outside the range of our measurements ($T < 0.06K$). Between 0.06 and 0.25K the resistivity is approximately a linear function of T: $\rho = a(1 - T/\theta_1)$ with $a = 6.92 \times 10^{-8} \Omega cm$ and $\theta_1 = 3.6K$. The characteristic temperature θ_1 is, according to calculations, within the lsf model, by Rivier and Zlatic (26), roughly twice θ(Eq.(IV.12)). Hence, neglecting the effect of potential scattering and assuming that these calculations may also be applied to alloys from the magnetic regime of the Anderson model (in this case, the relation between θ, θ_1 and the Anderson parameters is as yet unknown and should be obtained from a renormalized lsf theory), the quadratic temperature dependence of the electrical resistivity of Cu-Cr is determined by $\theta \approx 1.8K$ which turns out to be close to the Kondo temperature.

IV.4.a.3. Cu-Mn

The electrical resistivity of Cu-Mn 26 and 60 ppm, plotted in Fig.IV.4, can be adequately fitted to an expression of the form:

$$\rho = A - B\ln T \qquad \text{(IV.13)}$$

in the temperature interval T = 1.3 - 9K. The values of A, B and B/A are listed in Table IV.1. The different values of B/A for the slopes of the resistivity

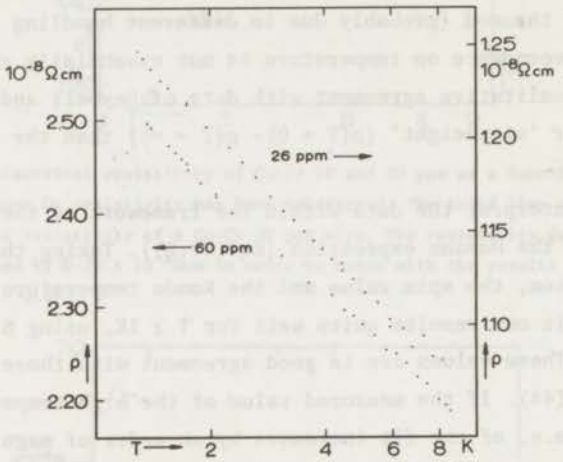

Fig.IV.4. The electrical resistivity as a function of the temperature for the two most dilute Cu-Mn alloys. The resistivity of Cu has been subtracted.

Table IV.1

Resistivity parameters of Cu-Mn

concentration (ppm)	A ($10^{-8}\Omega$cm)	B ($10^{-8}\Omega$cm)	C $(\frac{cm\ K^2}{Watt})$	D $(\frac{cm\ K^2}{Watt})$	$\frac{A}{C}$ $(10^{-8}\frac{V^2}{K^2})$	$\frac{B}{D}$ $(10^{-8}\frac{V^2}{K^2})$	$\frac{B}{A}$	$\frac{D}{C}$
26	1.268	0.092	0.484	0.030	2.62	3.1	0.073	0.062
60	2.542	0.161	0.964	0.056	2.64	3.5	0.063	0.058
270	11.77	0.65	4.59	0.24	2.56	2.7	0.055	0.052

The coefficients A, B, C and D are obtained by filting the resitivity data to Eqs.(IV.13) and (IV.14). The coefficients for the 270 ppm alloy have been obtained from a fit to the high temperature data, in view of the onset of a maximum in ρ (Fig.IV.18).

curves indicate the occurrence of impurity-impurity interactions. We refer, in this respect, to Fig.IV.18 where $d\rho/d\ln T$ of Cu-Mn 270 ppm decreases with decreasing temperature. At the higher temperatures of the measurements the resistivity may be described by Eq.(IV.13). The value of B/A (Table IV.1) is again reduced with respect to the dilute alloy values.

Expressions such as Eq.(IV.13) can be derived from a pertubative approach to the s-d model if ρ is calculated in second Born approximation (ref.(6), Eq.(IV.4)). If the exchange coupling constant J is calculated from the coefficient B of the logarithmic term, one obtains, using Eq.(IV.4), J = -0.60 and -0.55 eV for the 26 and 60 ppm alloy, respectively. These values are not very reliable, however, for the following reasons:

1. The neglect of DMR in the electrical resistivity. A straightforward calculation starting from Eq.(IV.8) shows that the presence of potential scattering leads to a modification of the coefficient of the $\ln(k_B T/D)$ term in Eq.(IV.4) by a factor $\cos 2\delta_v \cos^6 \delta_v$ (49).
2. Eq.(IV.4) is valid only at $\ln(T/T_K) \gg 1$. Since T_K is of the order of 10^{-2}K (50), the resistivity should, in fact, be compared to expressions obtained from non-pertubative treatments of the s-d model (Eq.(IV.8)). However, the limited experimental accuracy and the limited temperature range of our measurements exclude such a comparison.
3. The different slopes of the resistivity curves indicate that impurity-impurity interactions are still important in these dilute alloys.

IV.4.b. Thermopower of Cu-Fe, Cu-Cr and Cu-Mn

The thermopower data for the three alloy systems have been plotted in Fig. IV.5 - IV.7. The thermopower of Cu-Fe and Cu-Mn is larger than the thermopower of nonmagnetic Cu alloys by an order of magnitude. The thermopower of Cu-Cr is comparable to that of nonmagnetic alloys.

The thermopower of Cu-Fe can be represented at the lowest temperatures of our measurements by S = -3.0 T μV/K, suggesting that simple power laws also govern the thermopower at $T \ll T_K$. We observe that in the present concentration range (c < 100 ppm) the thermopower is essentially concentration independent. Again, as for the electrical resistivity, we note the similarity between the thermopower of Cu-Fe and Al-Mn. By matching the initial slopes of S for the two alloy systems, the thermopower can be scaled to a single curve as a function of T/θ (51), where θ is obtained from Eq.(IV.12), and displays a peak at $T \approx \theta$.

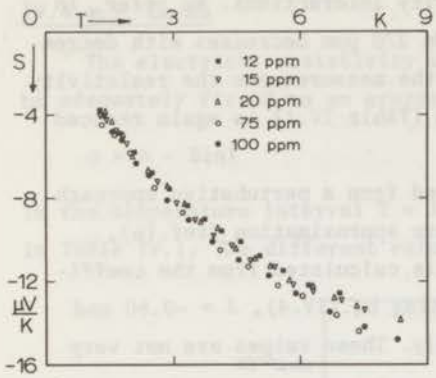

Fig.IV.5

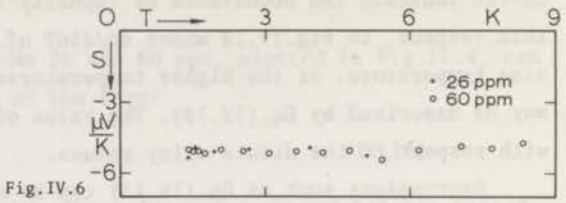

Fig.IV.6

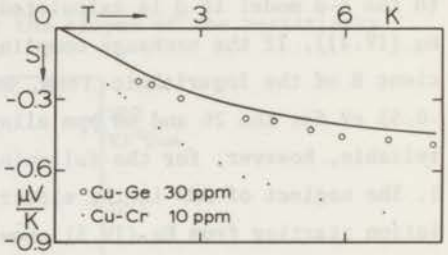

Fig.IV.7

Fig.IV.5. The thermopower of five Cu-Fe alloys as a function of temperature.

Fig.IV.6. The thermopower of Cu-Mn 26 and 60 ppm versus temperature.

Fig.IV.7. The thermopower of Cu-Cr 10 ppm versus T. The thermopower of Cu-Ge 30 ppm (ρ_0 = 1.17 x $10^{-8}\Omega$cm) is shown for comparison. The solid line represents the thermopower of 0.4 ppm Fe in this Cu-Ge alloy calculated with Eq.(II.43).

The thermopower of Cu-Mn is concentration and temperature independent in the present range. A correction for the presence of small traces of Fe, which strongly affects the observed thermopower of 'pure' Cu (Section III.1.b) may slightly modify the values of the thermopower plotted in Fig.IV.6.

The effect of traces of Fe seems to be more pronounced in Cu-Cr. The observed thermopower of Cu-Cr 10 ppm (Fig.IV.7) is an order of magnitude smaller than the thermopower of Cu-Fe and comparable to that of nonmagnetic alloys. For comparison we have plotted in Fig.IV.7 the data of a Cu-Ge 30 ppm alloy which has approximately the same electrical resistivity as Cu-Cr 10 ppm. When we analyse the Cu-Ge 30 ppm data in the same way as has been done for the Cu specimens (Section III.1.b) we observe that the magnitude of the measured thermopower can almost entirely be accounted for by the presence of 0.4 ppm Fe in the Cu host (Fig.IV.7). This impedes a determination of the thermopower of Ge in Cu. It also implies that an accurate determination of the thermopower of Cr in Cu is out of the question, except for the observation that S_{Cr} is not anomalously large. A Fe concentration somewhat higher than 0.4 ppm would even make S_{Cr} positive. This was in fact reported by Read and Guenault (52) who attributed the small thermopower of Cu-Cr alloys to the fact that a negative contribution

of the Fe impurities is almost balanced by a positive thermopower from the Cr solute. However, their conclusions have been criticized by Templeton (53), who suggests that the data should be re-evaluated in terms of a much lower concentration of iron impurities, thereby making S_{Cr} smaller in magnitude or even changing sign, in better agreement with our data.

IV.4.c. The Lorenz number

IV.4.c.1. Introduction

In order to obtain values for the Lorenz number due to electron-impurity scattering (both magnetic and nonmagnetic), the impurity contribution to the electronic thermal resistivity must be extracted from the measured thermal conductivity. This is done by subtracting the lattice thermal conductivity (λ_g) from the measured thermal conductivity, inverting the result and subtracting the ideal thermal resistivity (W_{id}) from the electronic thermal resistivity. Values of λ_g and W_{id} for the magnetic alloys are obtained from the experimental results on nonmagnetic alloys as discussed in Chapter III and they are listed in Table IV.2. We implicitely assume in applying this procedure that the magnitude of λ_g and W_{id} is determined by one parameter, that is, the electrical

Table IV.2

Alloy	concentration (ppm)	ρ_{imp}(T = 1.3K) ($10^{-8}\Omega$cm)	W_{id}/T^2 (10^{-5} $\frac{cm}{K\ Watt}$)
Cu-Fe	12	1.51	4.4
	15	1.85	4.5
	20	2.31	4.7
	75	8.15	5.5
	100	11.0	6
Cu-Cr	10	1.62	4.4
	30	5.63	5.2
Cu-Mn	26	1.25	6.3
	60	2.51	4.7
	270	11.3	6
	1000	33.0	8

The lattice conductivity was calculated from Eq.(III.13). The weak variation of W_{id} and λ_g on ρ_{imp} causes the effect of the temperature dependence of ρ_{imp} to be unimportant for $T \lesssim 10K$.

resistivity and that the functional dependence of λ_g and W_{id} on ρ and T is the same for both nonmagnetic and magnetic alloys. The latter assumption may be questioned in view of the presence of a strongly energy dependent impurity scattering contribution in the magnetic alloys. This aspect has recently been discussed in the literature (54, 55), but the situation is still unclear (56). For the moment we will work with these assumptions and hope for the best.

IV.4.c.2. Cu-Fe

The impurity Lorenz number of the Cu-Fe alloys is shown in Fig.IV.8. The accuracy of L_{imp} at the lowest temperatures is mainly determined by the experimental accuracy in the thermal conductivity measurements whereas at higher temperatures the error introduced by the subtraction procedures dominates.

The low temperature data suggest that L_{imp} attains the value L_0 at T = 0. The breakdown of the WFL law as T increases can be attributed to the presence of an energy dependent scattering mechanism (see also Section II.2.a). The magnitude of L_{imp} for the five Cu-Fe alloys indicates that in the present concentration range, just as in the electrical resistivity, impurity-impurity interactions are unimportant in the thermal resistivity.

An analysis of the Lorenz number on the basis of calculations from the s-d model is at present rather meaningless for $T < T_K$. This is demonstrated by considering the behaviour of L_{imp} in the limit $T \to 0$ as given by Eq.(IV.10). The low temperature slope of the calculated Lorenz number differs drastically from the experimentally determined L_{imp}, viz., $dL_{imp}/dT \to \infty$ versus $dL_{imp}/dT \to 0$ (Section IV.6).

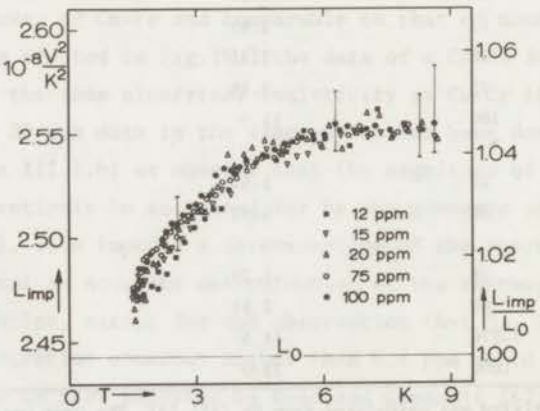

Fig.IV.8. The impurity Lorenz number as a function of temperature for five Cu-Fe alloys.

IV.4.c.3. Cu-Cr

The Lorenz number for electron-impurity scattering of the two Cu-Cr alloys in the temperature range from 1.3 to 9K is shown in Fig.IV.9. The concentration independence of L_{imp} indicates the unimportance of impurity-impurity interactions in the present temperature range. Since the Kondo temperature of Cu-Cr is of the order of 1K (in section IV.4.a.2 we obtained T_K = 2.5K from resistivity data) it is likely that the value of L_{imp} at the lowest temperatures of our measurements (1.10 L_0) is close to the maximum value. The decrease of L_{imp} with increasing temperatures for $T < T_K$ (Fig.IV.9) is consistent with the theoretical predictions (Section IV.2.b.3). A comparison with the impurity Lorenz number of Cu-Fe, which was determined in Section IV.4.c.2 for $T \lesssim 0.5\ T_K$, is hampered by the fact that the magnitude of L_{imp} depends on the magnitude of the resistivity due to potential scattering relative to the term due to exchange scattering. The term due to potential scattering pushes L_{imp} towards L_0. Since the 'stepheight' in the electrical resistivity of Cu-Cr is larger than that of Cu-Fe, we expect the impurity Lorenz number of Cu-Cr to be larger than L_{imp} (Cu-Fe) in the vicinity of T_K (see also Section IV.5).

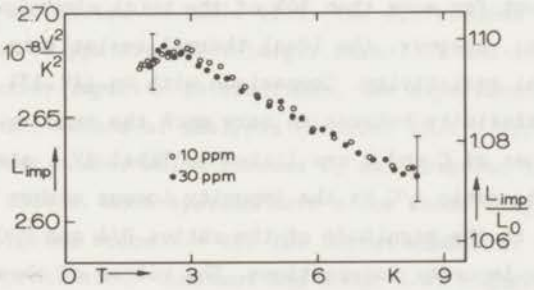

Fig.IV.9. The impurity Lorenz number versus T for Cu-Cr 10 and 30 ppm.

IV.4.c.4. Cu-Mn

The thermal conductivity of the two most dilute alloys with manganese concentration 26 and 60 ppm was measured up to T = 13K. Fig.IV.10 is a plot of $W_{imp}T$ against the logarithm of the temperature (the pure Cu resistivity has been subtracted). Apart from departures at the highest temperatures of our measurements, $W_{imp}T$ can be very well represented by

$$W_{imp}T = C - D\ln T \qquad \text{(IV.14)}$$

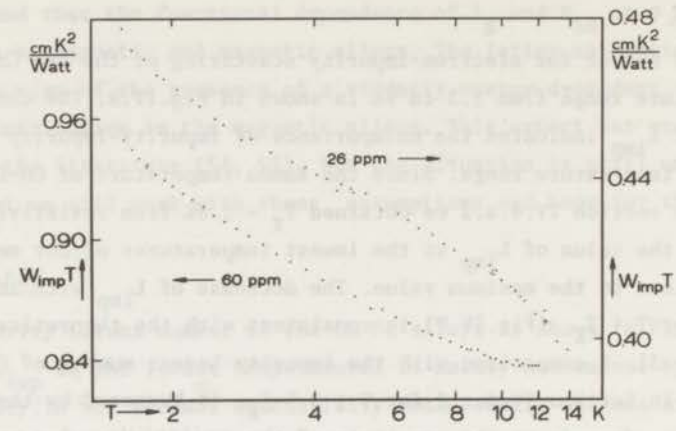

Fig.IV.10. $W_{imp}T$ versus InT for Cu-Mn 26 and 60 ppm.

The departures from this functional dependence on T may be attributed to the use of incorrect values for the ideal thermal resistivity (Table IV.2). This may become important at higher temperatures, since at T > 10 K the electron-phonon scattering can account for more than 10% of the total electronic thermal resistivity. At lower temperatures, however, the ideal thermal resistivity is only a small fraction of the total resistivity. Comparison with Eq.(IV.13) and Fig.IV.4 shows that the thermal resistivity behaves in very much the same way as the electrical resitivity. The values of C and D are listed in Tabel IV.1 along with the values of Cu-Mn 270 ppm. The ratio A/C is the impurity Lorenz number at T = 1K. The systematic decrease in the magnitude of the ratios B/A and D/C demonstrates the presence of impurity-impurity interactions. The values of these ratios for each sample are very similar, indicating that spin flip scattering is almost equally effective in both ρ and W. The same conclusion was obtained for the Au-Fe system (42), although one must be cautious in comparing both systems since the Kondo temperature of Cu-Mn is an order of magnitude smaller than that of Au-Fe.

The Lorenz numbers of Cu-Mn 26 and 60 ppm are shown as a function of temperature in Fig.IV.11. The values obtained for both alloys are higher than L_0 and L_{imp} decreases slowly with increasing temperature. The peculiar behaviour of L_{imp} at the highest temperatures of the measurements is due to the importance of the ideal thermal resistivity (Fig.IV.10). The impurity Lorenz number at lower temperatures can be represented by

$$L_{imp} = \frac{A - B\ln T}{C - D\ln T} \qquad \text{(IV.15)}$$

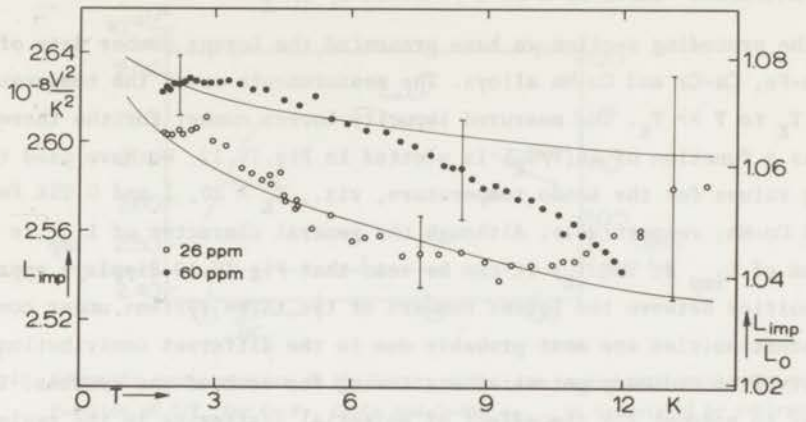

Fig.IV.11. The Lorenz number for impurity scattering of Cu-Mn 26 and 60 ppm as a function of temperature. The solid lines are obtained from Eq.(IV.15) using the coefficients from Table IV.1. The Lorenz number data at T > 8.5K are calculated under the assumption that at these temperatures the electrical resistivity is represented by Eq.(IV.13) with the constants as listed in Table IV.1.

where A, B, C and D are listed in Table IV.1. The differences in magnitude of L_{imp} for Cu-Mn 26 and 60 ppm are never larger than 1.5% and are a result of several factors such as impurity-impurity interactions, the experimental error and the error introduced by the method of analysis (Section IV.4.c.1).

An impurity Lorenz number which exceeds L_0 was observed in dilute Au-Fe (42) and Ag-Mn (43) alloys. Both systems have a low Kondo temperature ($T_K < 1K$) and have been investigated below T = 4K. The Lorenz number at these temperatures is reported to be approximately constant and about 3-4% higher than L_0, which is about half the effect we observe in Cu-Mn (Fig.IV.11). This may be accounted for by the fact that the temperature dependence of the electrical resistivity of Cu-Mn is stronger than that of Au-Fe and Ag-Mn. The ration B/A is 0.044 and 0.04 for the most dilute Au-Fe (42) and Ag-Mn (43) alloy, respectively, whereas B/A = 0.073 for Cu-Mn 26 ppm. The enhancement of the Lorenz number for these systems can be calculated from Eq.(IV.11). One obtains $L/L_0 \approx 1.07$, 1.03 and 1.03 for Cu-Mn, Au-Fe and Ag-Mn, respectively. The agreement with the experimental data must be considered as accidental, however, in view of the restricted validity of Eq.(IV.11). We mention once again the neglect of DMR and the condition $\ln(T/T_K) \gg 1$, which in particular for Au-Fe ($T_K \approx 10^{-1}K$) does not hold at liquid He-temperatures.

IV.5. A 'universal' curve of L as a function of T/T_K

In the preceding section we have presented the Lorenz number data of some dilute Cu-Fe, Cu-Cr and Cu-Mn alloys. The measurements cover the temperature range from $T < T_K$ to $T >> T_K$. The measured impurity Lorenz number for the three alloy systems as a function of $\ln(T/T_K)$ is plotted in Fig.IV.12. We have used the following values for the Kondo temperature, viz., T_K = 20, 1 and 0.05K for Cu-Fe Cu-Cr and Cu-Mn, respectively. Although the general character of L_{imp} is obtained (a maximum of L_{imp} at $T \approx T_K$) it can be seen that Fig.IV.12 displays apparent discontinuities between the Lorenz numbers of the three systems under consideration. These discontinuities are most probably due to the different contributions to the resistivity from ordinary potential scattering for each of the systems. The most simple way to account for the effect of potential scattering in the resistivity is to subtract a temperature independent term from the total impurity resistivity. This term may be obtained from the high temperature value of resistivity or from resistivity data on concentrated alloys. In Fig.IV.13 we have plotted the Lorenz number for exchange scattering, defined as $L_{exch} = \rho_{exch}/(WT)_{exch}$, where $\rho_{exch} = \rho_{imp} - \rho_{pot}$ and $(WT)_{exch} = (WT)_{imp} - (WT)_{pot}$, as a function of $\ln(T/T_K)$, using ρ_{pot}(Cu-Fe) = 8μΩcm/at.%, ρ_{pot}(Cu-Cr) = 5μΩcm/at.%, ρ_{pot}(Cu-Mn) = 2μΩcm/at.% and $(WT)_{pot} = \rho_{pot}/L_0$. This subtraction procedure neglects, however, the effect of DMR due to the interference of a strongly and weakly energy dependent scattering process. In order to get some insight into the error introduced by this subtraction procedure we have calculated the DMR in the electrical and thermal resistivity and

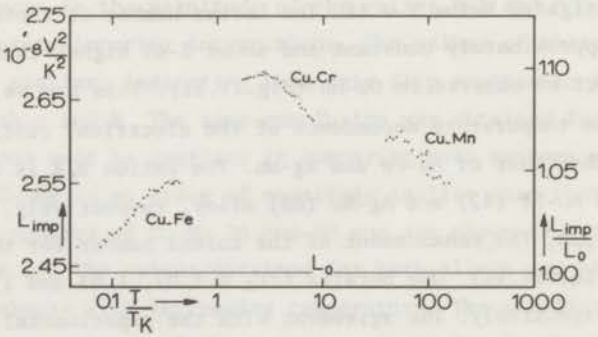

Fig.IV.12. The impurity Lorenz number of Cu-Fe (T_K = 20K), Cu-Cr (T_K = 1K) and Cu-Mn (T_K = 0.05K) as a function of $\ln T/T_K$. The data plotted are those of Cu-Fe 15 ppm, Cu-Cr 10 ppm and Cu-Mn 26 ppm and are characteristic for the behaviour of L_{imp} in the three alloy systems.

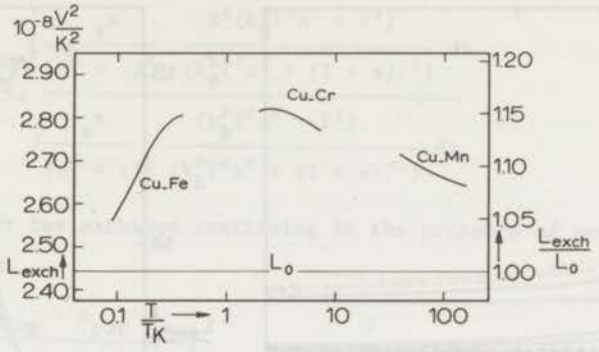

Fig.IV.13. Schematic representation of the Lorenz number due to exchange scattering as a function of T/T_K for Cu-Fe, Cu-Cr and Cu-Mn. L_{exch} is calculated by subtracting the resistivity term due to ordinary potential scattering from the impurity resistivity.

their effect on the Lorenz number for the case of a resonance in the scattering amplitude at ε_F (See also Section II.2.a). We use a relaxation time of the form:

$$\tau_{exch}^{-1} = \tau_{exch}^{-1}(0)\ (1 + a\ \frac{\Gamma^2}{\omega^2 + \Gamma^2}) \qquad \text{(IV.16)}$$

where $\omega = \varepsilon - \varepsilon_F$. The potential scattering is accounted for by adding the reciprocal of an energy independent relaxation time to τ_{exch}^{-1}:

$$\tau_{imp}^{-1} = \tau_{exch}^{-1} + \tau_{pot}^{-1} \qquad \text{(IV.17)}$$

Although we do not expect that this simple form of τ_{imp} gives a correct description of the behaviour of the resistivity in the entire temperature range, we note that substitution of Eq.(IV.17) into the transport-integrals (Eqs.(II.9) and (II.10)) yields the general features of the observed behaviour of the impurity resistivities of dilute magnetic alloys, viz., ρ_{imp} and $(WT)_{imp}$ decrease as T^2 from their zero temperature values, the resistivity curves show an inflection point at a temperature of the order Γ/k_B, if Γ/k_B is identified with the Kondo temperature, and a slow decrease with increasing temperature towards a high temperature plateau. Fig.IV.14 shows that the interference between exchange and potential scattering significantly affects the behaviour of the resistivity. The DMR, $\Delta = \rho_{imp} - (\rho_{exch} + \rho_{pot})$ and $\Delta' = (WT)_{imp} - ((WT)_{exch} + (WT)_{pot})$, vary as T^4 at $T \ll \Gamma/k_B$, reach a maximum at $T \approx \Gamma/k_B$ and gradually decrease with increasing temperature.

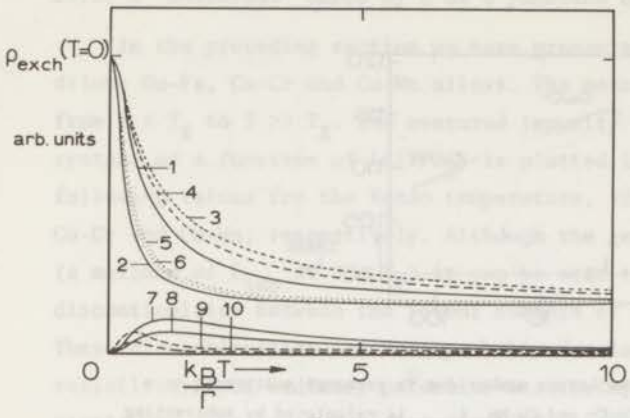

Fig.IV.14

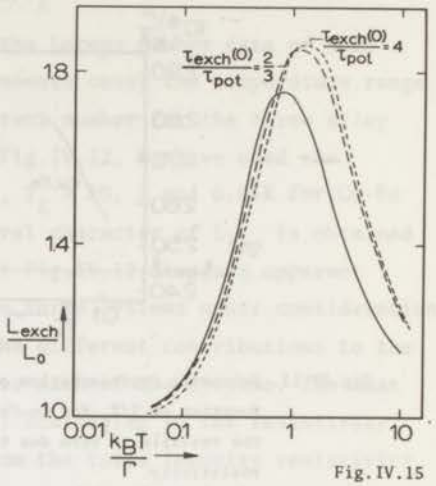

Fig.IV.15

Fig.IV.14. The effect of DMR on the temperature dependence of ρ_{exch} and $(WT)_{exch}$. The numbers have the following meaning:
1: ρ_{exch}; 2: $L_0(WT)_{exch}$; 3: $\rho_{exch} + \Delta$, $\tau_{exch}(0)/\tau_{pot} = 4$; 4: $\rho_{exch} + \Delta$, $\tau_{exch}(0)/\tau_{pot} = 2/3$; 5: $L_0(WT)_{exch} + L_0\Delta'$, $\tau_{exch}(0)/\tau_{pot} = 4$; 6: $L_0(WT)_{exch} + L_0\Delta'$, $\tau_{exch}(0)/\tau_{pot} = 2/3$; 7: Δ, $\tau_{exch}(0)/\tau_{pot} = 4$; 8: Δ, $\tau_{exch}(0)/\tau_{pot} = 2/3$; 9: $L_0\Delta'$, $\tau_{exch}(0)/\tau_{pot} = 4$; 10: $L_0\Delta'$, $\tau_{exch}(0)/\tau_{pot} = 2/3$.

Fig.IV.15. The Lorenz number due to exchange scattering. The solid curve is obtained from Eq.(IV.18). The dashed curves are calculated from Eq.(IV.19).

For the numerical computations we have used a = 5 and $\tau_{exch}(0)/\tau_{pot} = 4$ and 2/3. The total impurity resistivities ρ_{imp} and $(WT)_{imp}$ have been calculated from Eqs.(II.9) and (II.10) with

$$\tau_{imp} = \frac{\tau_{pot}\,\tau_{exch}}{\tau_{pot} + \tau_{exch}}$$

A similar calculation has been performed by Smith and Wilkins (57) for the electrical resistivity. They included the energy independent part of τ_{exch}^{-1} into the potential scattering and obtained a maximum of about 20% in $\Delta/\rho_{exch}(T = 0)$ at $T = \Gamma/k_B$ for $\tau_{pot}/\tau_{exch} = 0.2$.

The effect of DMR on L is shown in Fig.IV.15. The Lorenz number for exchange scattering is obtained by substituting the relaxation time Eq.(IV.15) into Eq. (II.12) (we note that Eq.(IV.16) leads to a vanishing thermopower).

$$L_{exch} = \frac{3}{\pi^2} L_0 \frac{\int \frac{e^x}{(e^x+1)^2} \frac{x^2(k_B^2T^2x^2 + \Gamma^2)}{(k_B^2T^2x^2 + (1+a)\Gamma^2)}\,dx}{\int \frac{e^x}{(e^x+1)^2} \frac{(k_B^2T^2x^2 + \Gamma^2)}{(k_B^2T^2x^2 + (1+a)\Gamma^2)}\,dx} \qquad \text{(IV.18)}$$

The Lorenz number for exchange scattering in the presence of potential scattering is obtained from

$$L'_{exch} = \frac{\rho_{imp} - \rho_{pot}}{(WT)_{imp} - (WT)_{pot}} \qquad \text{(IV.19)}$$

Up to first order in Δ and Δ', L'_{exch} may be written as:

$$L'_{exch} = L_{exch}\left(1 + \frac{\Delta}{\rho_{exch}} - \frac{\Delta'}{(WT)_{exch}}\right) \qquad \text{(IV.20)}$$

where L_{exch} is given by Eq.(IV.18). Fig.IV.15 shows that the neglect of DMR has a pronounced effect on the magnitude of L_{exch} at $T \gtrsim \Gamma/k_B$, which can be understood by considering the magnitude of Δ/ρ_{exch} and $\Delta'/(WT)_{exch}$ as shown in Fig.IV.14. For $T \ll \Gamma/k_B$ and $T \gg \Gamma/k_B$ DMR have become small so that L'_{exch} is close to L_{exch}.

Hence, returning to Fig.IV.13, we remark that the 'universal' curve of L_{exch} (which in fact is L'_{exch}(Eq.(IV.19))) vs. $\ln(T/T_K)$ must be considered with some caution. Although the correct relaxation time, which describes the spin dependent scattering in dilute magnetic alloys, will be different from that given in Eq. (IV.16) (it should contain logarithmic terms) we expect that the general features as displayed in Fig.IV.14 and IV.15 will not be altered. This implies that the effect of neglecting DMR will affect the calculated values of L_{exch} as shown in Fig.IV.13 especially at $T \gtrsim T_K$, which applies to Cu-Cr. The lack of a precise knowledge of the functional dependence of τ_{exch} on ω and T prevents the determination of the magnitude of this effect, however. It should furthermore be noted that the uncertainty in L_{exch} is also caused by the fact that both ρ_{pot} and T_K are not accurately known for the three alloy systems. Nevertheless, we may conclude that the general feature of L_{exch} is expressed in Fig.IV.13, viz., an asymmetric peak in L_{exch} at $T \approx T_K$, the magnitude of which exceeds L_0 by about 15%.

IV.6. Discussion of the Lorenz number data

In this section we will discuss our experimental results on Cu-Fe and Cu-Cr on the basis of a simple scattering resonance model. For this purpose we have extended the electrical resistivity measurements on Cu-Cr down to T = 0.06K. Both the lsf model (33) and the s-d model (13, 14, 15) suggest a many body peak in the scattering amplitude with half width Γ ($\approx k_B T_K$ or $k_B T_{sf}$) which, in order to account for the nonsingular behaviour of the transport properties at low temperatures, should have a Lorentzian form at low energies. For our analysis we use the following expression for τ_{imp}:

$$\tau_{imp}^{-1} = A \frac{\Gamma^2}{\omega^2 + \Gamma^2} + \tau_0^{-1} \qquad \text{(IV.21)}$$

where τ_0^{-1} accounts for the potential scattering. Although we realize that the form of the relaxation time given in Eq.(IV.21) is too simple to account for the real situation at all temperatures, it is likely that Eq.(IV.21) is valid at $T << \Gamma/k_B$. A complete expression of the scattering amplitude should account for the temperature dependence of Γ, a proper inclusion of the potential scattering and must display a logarithmic behaviour at high energies.

The behaviour of the Lorenz number due to resonance scattering can be found by substituting Eq.(IV.21) into Eq.(II.12). For $T << \Gamma/k_B$ one obtains

$$L = L_0 \left(1 - \frac{16}{5} \frac{1}{\rho_0} \frac{d\rho}{d(T^2)}\right) - S^2 \qquad \text{(IV.22)}$$

Neglecting the second term in the right-hand side of Eq.(IV.22) (S is of the order of 10^{-6} V/K at these temperatures), the Lorenz number for impurity scattering can be written as:

$$L = L_0 \left(1 + \frac{16}{5} \left(\frac{T}{\theta}\right)^2\right) , \qquad \text{(IV.23)}$$

where θ is obtained from Eq.(IV.12). This is a general result which depends only on the assumption of a Lorentzian form of the resonance and on the assumption $\tau_\sigma = \tau_\lambda$. The latter assumption will be used throughout this section and implies that the scattering is elastic.

We have analysed the data of two Cu-Fe alloys (15 and 100 ppm) and Cu-Cr 30 ppm in the following way. First, the electrical resistivity data were fitted to the expression

$$\rho = \rho(T = 0) \frac{1}{\int \frac{e^x}{(e^x + 1)^2} \frac{x^2 + (\Gamma/k_B T)^2}{x^2 + (1 + A\tau_0)(\Gamma/k_B T)^2} dx} \qquad \text{(IV.24)}$$

where Γ and $A\tau_0$ were treated as adjustable parameters. Eq.(IV.24) is obtained by substituting Eq.(IV.21) into Eq.(II.9). The values obtained for these parameters were then used to compute the Lorenz number for impurity scattering from the expression

$$L + S^2 = \left(\frac{k}{e}\right)^2 \frac{\int \frac{e^x}{(e^x + 1)^2} \frac{x^2 + (\Gamma/k_B T)^2}{x^2 + (1 + A\tau_0)(\Gamma/k_B T)^2} x^2 dx}{\int \frac{e^x}{(e^x + 1)^2} \frac{x^2 + (\Gamma/k_B T)^2}{x^2 + (1 + A\tau_0)(\Gamma/k_B T)^2} dx} \qquad \text{(IV.25)}$$

where S is the measured thermopower and may account for terms containing odd functions of ω in Eq.(IV.21), which are unimportant in the expressions for the electrical and thermal conductivity.

The electrical resistivity data of Cu-Fe could be fitted to Eq.(IV.24) in the entire temperature range of our measurements, whereas the electrical resistivity of Cu-Cr could be described by Eq.(IV.24) only up to $T \approx 0.8K$. Due to the limited experimental accuracy of the electrical resistivity measurements (0.1%) the values obtained for Γ and $A\tau_0$ are not uniquely determined. Some values of these parameters are listed in Table IV.3. The characteristic temperature θ (Eq.(IV.12)) is calculated from

$$\theta = \frac{\sqrt{3}}{\pi} \frac{\Gamma}{k_B} \left(\frac{1 + A\tau_0}{A\tau_0}\right)^{1/2} \qquad \text{(IV.26)}$$

Eq.(IV.26) is obtained by applying the Sommerfeld expansion to the transport integral K_0. The Lorenz number values computed from Eq.(IV.25) with the parameters listed in Table IV.3 have been plotted in Fig.IV.16. The factor S^2 where S is the measured thermopower (Fig.IV.5) has been subtracted from L_{imp}(Cu-Fe). The thermopower of Cu-Cr is an order of magnitude smaller (Fig.IV.7) and can be neglected. One can see from Fig.IV.16 that the agreement between the measured and calculated L_{imp} of Cu-Fe is very good for $T \lesssim 4K$. At higher temperatures the agreement is less satisfactory, which is not surprising in view of the simplicity of the model, but the differences are not larger than about 2%. Furthermore, we

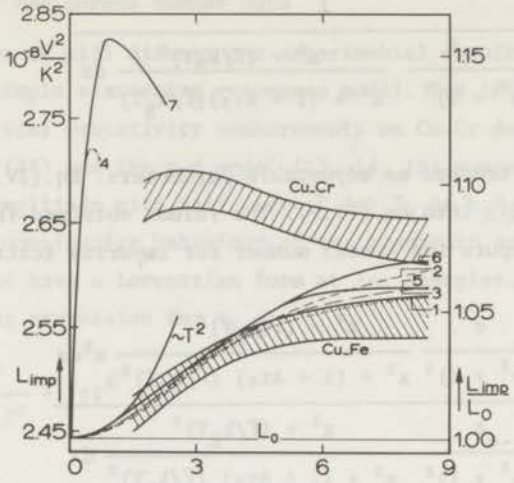

Fig. IV.16. Some numerical results for the impurity Lorenz number of Cu-Fe and Cu-Cr. The shaded regions represent the Lorenz number data of the two systems (Fig. IV.8 and IV.9) taking into account the experimental error. The solid curves are obtained from the relaxation time Eq. (IV.27). The broken curves are computed from Eq. (IV.25). The numbers refer to the parameters from the electrical resistivity fits, as listed in Table IV.3 and IV.4.

Table IV.3

Parameters of a computer fit of the electrical resistivity data to Eq. (IV.24)

Alloy		$\rho(T = 0)$ ($10^{-8}\Omega$cm)	Γ/k_B (K)	$A\tau_0$	θ (K)	Computed Lorenz number curve (Fig. IV.16)
Cu-Fe	15 ppm	1.859	15.0	0.20	20.2	1
	15 ppm	1.859	18.5	0.25	22.8	2
	100 ppm	11.09	15.6	0.218	20.3	3
Cu-Cr	30 ppm	6.82	0.75	0.37	0.80	4

note that the accuracy of the experimental Lorenz number at these temperatures is determined by the analysis employed in order to extract the lattice conductivity and the ideal thermal resistivity from the measured thermal conductivity (Section IV.c.1).

A straightforward comparison between the measured and calculated Lorenz number of Cu-Cr is not possible, since the electrical resistivity could be fitted to Eq.(IV.24) only for $T \leq \Gamma/k_B \approx 0.8K$. The discrepancies appear to be similar to those for the Cu-Fe alloys.

In order to obtain a better approximation of the actual scattering resonance than that given in Eq.(IV.21), one may think of expressing the relaxation time in a power series of ω. Such an expansion should then approximately account for the temperature dependence and the logarithmic terms of the actual scattering amplitude. This was done by Star (44, 45) in order to describe his electrical resistivity data on Cu-Fe. He used a relaxation time which is slightly different from Eq. (IV.21), i.e.,

$$\tau = \tau(\omega = 0)\left(1 + \sum_{n=1}^{m} c(n)\,\frac{\omega^{2n}}{\omega^{2n} + \Gamma^{2n}}\right) \qquad \text{(IV.27)}$$

The coefficients c(n) can be determined by fitting the experimental values of the electrical resistivity to Eq.(II.9) with τ given by Eq.(IV.27). The Lorenz number is calculated in the same way as described above with the coefficients

Table IV.4

Parameters of a computer fit of the electrical resistivity data to Eq.(II.9) with τ given by Eq.(IV.27) and m = 4.

Alloy		$\rho(T=0)$ ($10^{-8}\Omega$cm)	Γ/k_B (K)	c(1)	$\sum_{n=1}^{4} c(n)$ $(= \frac{\rho(T=0)}{\rho(T\to\infty)} - 1)$	θ (K)	Computed Lorenz number curve (Fig.IV.16)
Cu-Fe	15 ppm	1.861	15.0	0.278	0.187	15.7	5
	100 ppm	11.09	18.0	0.333	0.231	17.2	6
Cu-Cr	30 ppm	6.82	1.90	1.77	0.650	0.79	7

c(n) and Γ obtained from the electrical resistivity fit. Some typical numerical results for Cu-Fe 15 and 100 ppm and Cu-Cr 30 ppm are listed in Table IV.4. The characteristic temperature θ (Eq.(IV.12)) is obtained from $k_B\theta = \Gamma(3/(\pi^2 c(1)))^{1/2}$. The computed Lorenz number values are plotted in Fig.IV.16. One can observe that the results are not essentially different from those obtained from Eq.(IV.25). We mention once again that this may be attributed to the limited experimental accuracy of the electrical resistivity measurements, which makes the values of the adjustable parameters somewhat ambiguous.

Although a detailed agreement between the experimental and calculated Lorenz number is lacking, the features shown in Fig.IV.16 suggest that a description of the Kondo state at low temperatures can be given in terms of a scattering resonance, which is Lorentzian in form at low energies.

IV.7. Spin fluctuation effects in the Lorenz number

The essence of the present section is based on some remarks made in Section IV.2.c.2 and IV.2.c.3 regarding the temperature dependence of the transport properties of alloys having a vbs compared to that of the iso-electronic alloys. The scattering of the conduction electrons by the spin density fluctuations, enhanced at the impurity site, in the latter type of alloys can be calculated analogously to the electron-phonon scattering (Section II.3.a.1). The low energy form of the spectral density of the spin fluctuations $A(q,\omega)$ ($\sim \omega$ where $\omega = \varepsilon_k - \varepsilon_{k'}$) and the fact that the q values ($\vec{q} = \vec{k} - \vec{k}'$) of the excited spin fluctuations do not change with temperature give rise to a T^2 and T term in the electrical and thermal resistivity, respectively. The Lorenz number is a very suitable quantity to study the nature of this scattering process as was discussed in Section II.2.c. If the scattering angle is temperature independent (at least at low temperatures) then the Lorenz number for scattering of the conduction electrons by the spin fluctuations, which is in fact an effective electron-electron scattering process, should reach a value somewhere between 0 and L_0 at T = 0, in contrast to the electron-phonon scattering where $L_{id} \to 0$ due to the temperature dependence of the scattering angle.

The spectral density $A(q,\omega)$ has a peak at $\omega = k_B T_{sf}/\hbar$, where T_{sf} is the spin fluctuation temperature (58). This implies that for $T >> T_{sf}$ the scattering is quasi-elastic, as the spinfluctuations have insufficient energy to scatter the electrons through the thermal layer of the FS. With decreasing temperature, inelastic scattering becomes important. The consequences of these scattering processes

for the Lorenz number L_{e-e} are that at $T \gg T_{sf}$ L_{e-e} is close to L_0. With decreasing temperature L_{e-e} is gradually reduced below L_0 until it reaches a finite value at T = 0. The zero temperature value is determined by the angular distribution of the scattering. A simple variational calculation of ρ and W leads to the following expression of the Lorenz number at T = 0 (31, 32):

$$L_{e-e} = L_0 \frac{5}{3 + 12a} \qquad \text{(IV.28)}$$

where

$$a = \frac{\frac{1}{k_F^2} \int_0^{2k_F} q\,|F(q)|^2\, A(q,\omega)dq}{\frac{1}{k_F^4} \int_0^{2k_F} q^3|F(q)|^2\, A(q,\omega)dq} \qquad \text{(IV.29)}$$

F(q) is the form factor of the impurity d-orbital. For uniform angular scattering we neglect the q-dependence of the form factor and of the spectral density and Eq.(IV.29) then gives a = 0.5, which results in $L_{e-e} = 5L_0/9 = 1.36 \times 10^{-8} V^2/K^2$. This value was first obtained by Herring (59) on the basis of Fermi liquid theory using a simple relaxation time of the form $\tau^{-1} \sim (\pi k_B T)^2 + \omega^2$ where $\omega = \varepsilon - \varepsilon_F$. Any aspect of the scattering which peaks the forward scattering would consequently reduce L_{e-e} from the value $5L_0/9$. (we mentioned already the extreme case of electron-phonon scattering).

Rivier and Zlatic (27) have argued that the functional dependence of the electrical resistivity of iso-electronic alloys on the temperature is the mirror image of that of alloys described by the Anderson model. A Lorenz number given by the expression:

$$L_{e-e} = \frac{\rho(T = 0) - \rho(T)}{WT(T = 0) - W(T)T} \qquad \text{(IV.30)}$$

may then be defined (Section IV.2.c.3) analogously to the Lorenz number arising from electron-electron scattering in iso-electronic alloys, the features of which have been discussed above.

We have plotted the Lorenz number given by Eq.(IV.30) in Fig.IV.17 for Cu-Fe, Cu-Cr and Cu-Mn. This figure demonstrates the difference in the nature of the scattering in the three alloy systems. Elastic scattering dominates in Cu-Mn

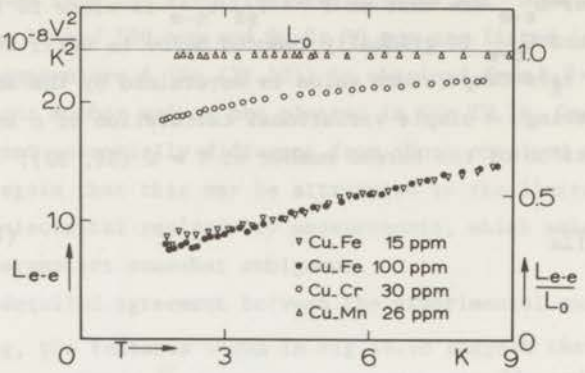

Fig.IV.17. The Lorenz number for 'electron-electron' scattering (Eq.IV.30) of Cu-Fe, Cu-Cr and Cu-Mn as a function of temperature between 2 and 9K.

($\rho(T = 0) = 17.3\mu\Omega cm/at.\%$ (60)), whereas inelastic scattering dominates in Cu-Fe in the present temperature range. Cu-Cr represents an intermediate case. Fig.IV.17, therefore, gives an indication of the magnitude of T_{sf} and, hence, of the position of the peak of $A(q,\omega)$ on the energy scale. The value of L_{e-e} at $T << T_{sf}$ can only be obtained for the Cu-Fe system and is $(0.32 \pm 0.05)L_0$. The low temperature value of L_{e-e} is determined by the q-dependence of the scattering. The values obtained for Cu-Fe are smaller than the value for uniform angular scattering. A similar feature was observed for the Lorenz number of Pd-Ni alloys (31), where $L_{e-e} = 0.45\ L_0$. Schriempf et al. (31) concluded from their measurements that $A(q,\omega)$ is a slowly varying function of q (Eq.(IV.29)). Although a straightforward comparison of the zero temperature value of L_{e-e} obtained for Cu-Fe with Eq.(IV.29) is possibly not justified (we note that Kaiser (32) and Kaiser and Doniach (58) employed a two-band model, current carrying s-electrons and d-band spin fluctuations, in calculating the transport properties in the Born approximation; this pertubation theory breaks down at $T \approx T_{sf}$), we argue that the value of $L_{e-e}(T = 0)$ for Cu-Fe is also determined by the q-dependence of the spectral density of the spin fluctuations, as in the case of Pd-Ni, and may therefore provide information about the extension in space of the vbs.

With respect to the temperature dependence of L_{e-e} (Fig.IV.17) we note that a quantitative comparison with the calculations of Kaiser (32) is not justified either, although the features of the three alloy systems are not inconsistent with conclusions drawn in previous sections, viz., the spin fluctuations temperature of Cu-Mn is apparently far below our measuring range in contrast to the spin fluctuation temperatures of Cu-Fe and Cu-Cr.

IV.8. Impurity interaction effects in Cu-Mn

The effect of impurity-impurity interactions, already mentioned in Section IV. 4.a.3. is clearly visible in the transport properties of Cu-Mn 270 and 1000 ppm. The interaction between the Mn impurities makes the conduction electron-impurity scattering inelastic, since the degeneracy of the impurity states is now removed. Consequently, the Kondo effect (logarithmic behaviour of the transport properties as a function of temperature) is quenched. The occurrence of a maximum in the electrical resistivity vs temperature curve is a typical result of this suppression of elastic spin flip scattering.

The electrical resistivity as a function of temperature of the two concentrated Cu-Mn alloys has been plotted in Fig.IV.18 and IV.19. The data on the 270 ppm alloy show only the onset of the resistivity maximum. From electrical resistivity data (61) at T < 1K on alloys with Mn concentrations comparable to the present ones, a relation between the temperature at which the maximum occurs (T_m) and the concentration is obtained

$$\frac{T_m}{c} = 33 \text{ K/at.\%} \qquad \text{(IV.31)}$$

This suggests that T_m(Cu-Mn 270 ppm) ≈ 1.2K. The observed maximum in the electrical resistivity of Cu-Mn 1000 ppm (Fig.IV.19) is consistent with Eq.(IV.31).

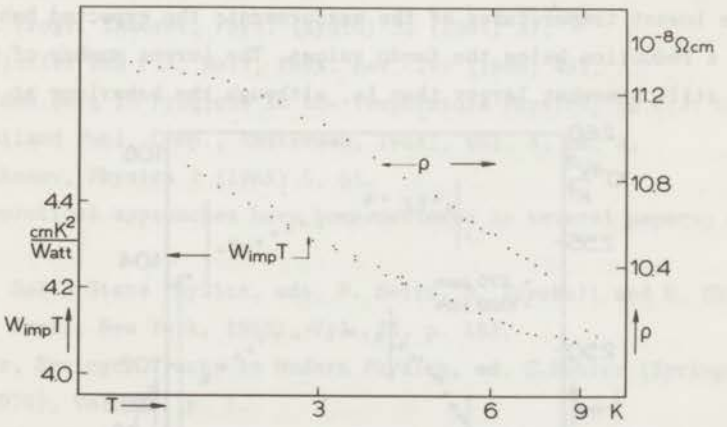

Fig.IV.18. The electrical resistivity ρ and the impurity thermal resistivity times temperature as a function of temperature for Cu-Mn 270 ppm (The pure Cu values have been subtracted). Note the departures from a logaritmic dependence on T of the electrical resistivity at low temperatures.

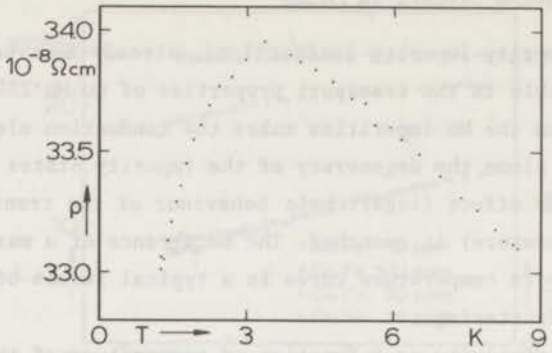

Fig.IV.19. The electrical resistivity of Cu-Mn 1000 ppm versus T. The electrical resistivity of Cu has been subtracted.

The inelastic nature of the spin flip scattering in concentrated magnetic alloys should have a pronounced effect on the Lorenz number, in that the magnitude of L_{imp} is reduced below the values for alloys exhibiting the Kondo effect. L_{imp} may even become smaller than L_0. The inelastic spin flip scattering is frozen out at sufficiently high concentrations or sufficiently low temperatures and L_{imp} should approach L_0.

The impurity Lorenz number as a function of temperature of the 270 and 1000 ppm alloys have been plotted in Fig.IV.20. A comparison with Fig.IV.11 shows at the lowest temperatures of the measurements the expected behaviour of L_{imp}, viz., a reduction below the Kondo values. The Lorenz number of Cu-Mn 1000 ppm is still somewhat larger than L_0, although the behaviour at the lowest

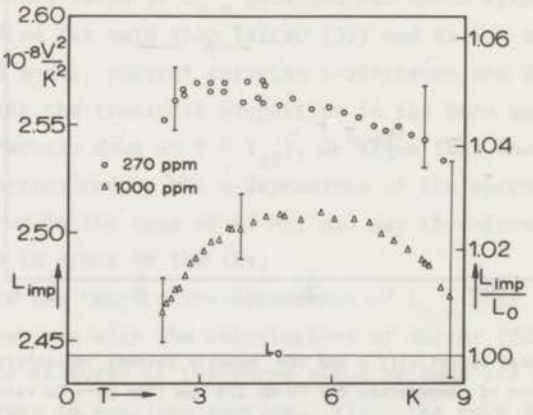

Fig.IV.20. The Lorenz number for impurity scattering of Cu-Mn 270 and 1000 ppm as a function of temperature.

temperatures suggests a reduction of L_{imp} below L_0. It must be noted, however, that the temperature dependence of L_{imp} as displayed in Fig.IV.20 should be considered with caution, in particular for the 1000 ppm alloy, due to the fact that the lattice thermal conductivity forms a large fraction of the total thermal conductivity (at 4K ≈ 6%, at 8K already ≈ 15%). The features of L_{imp} of Cu-Mn as a function of temperature and concentration are similar to those observed in Au-Fe (42) and Ag-Mn (43). At c ≈ 0.1 at.%, L_{imp} is close to L_0 for T< 4K. A reduction of L_{imp} below L_0 (5% in Ag-Mn and 15% in Au-Fe) is observed for higher concentrations. However, it should be mentioned once again that the thermal conductivity data and, hence, the Lorenz number values of more concentrated alloys become unreliable which precludes any quantitative comparison.

References

1. D.K. Wohlleben and B.R. Coles, Magnetism, ed. H. Suhl (Academic Press, New York and London, 1973), Vol. V, p. 3.
2. See for example: J. Friedel, Nuovo Cimento Suppl. 7 (1958) 287.
3. P.W. Anderson, Phys. Rev. 124 (1961) 41.
4. J.R. Schrieffer and D.C. Mattis, Phys. Rev. 140 (1965) A 1412.
5. C. Zener, Phys. Rev. 1 (1951) 440.
6. J. Kondo, Progr. Theoret. Phys. (Kyoto) 32 (1964) 37.
7. J.R. Schrieffer and P.A. Wolf, Phys. Rev. 149 (1966) 491.
8. G.J. van den Berg in Progress in Low Temperature Physics, ed.C.J. Gorter (North Holland Publ. Comp., Amsterdam, 1964), Vol. 4, ch. 4.
9. A.A. Abrikosov, Physics 2 (1965) 5, 61.
10. These theoretical approaches have been reviewed in several papers; see for example:
    J. Kondo, Solid State Physics, eds. F. Seitz, D. Turnball and H. Ehrenreich (Academic Press, New York, 1969), Vol. 23, p. 183.
    K. Fischer, Springer Tracts in Modern Physics, ed. G.Höhler (Springer Verlag, Berlin, 1970), Vol. 54, p. 1.
    and several papers in Magnetism, ed. H. Suhl (Academic Press, New York and London, 1973), Vol. V.
11. W.M. Star and G.J. Nieuwenhuys, Phys. Lett. 30 A (1969) 22.
12. P. Lederer, Proc. Nato Summerschool, La Colle sur Loupe, 1970, to be published.

13. P.W. Anderson, Comments on Solid State Physics 5 (1973) 73.
14. P.W. Anderson and G. Yuval, Magnetism, ed. H. Suhl (Academic Press, New York and London, 1973), Vol. V, p. 217 and references therein.
15. K.G. Wilson, Collective Properties of Physical Systems, Nobel Symposium 24 (Academic Press, 1974),p. 68.
16. A.D. Caplin and C. Rizzuto, Phys. Rev. Lett. 21 (1968) 746.
17. P. Lederer and D.L. Mills, Phys. Rev. Lett. 20 (1968) 1036.
18. N. Rivier and M.J. Zuckermann, Phys. Rev. Lett. 21 (1968) 904.
19. N. Rivier, M. Sunjic and M.J. Zuckermann, Phys. Lett. 28 A (1969) 492.
20. H. Suhl and D. Wong, Physics 3 (1967) 17.
21. Y. Nagaoka, Phys. Rev. 138 (1965) A 1112.
22. D.R. Hamann, Phys. Rev. 158 (1967) 570.
23. P.E. Bloomfield and D.R. Hamann, Phys. Rev. 164 (1967) 856.
24. K. Fischer, Z. Physik 225 (1969) 444.
25. S.B. Nam and M.S. Fullenbaum, Phys. Rev. 186 (1969) 506.
26. N. Rivier and V. Zlatic, J. Phys. F 2 (1972) L 87.
27. N. Rivier and V. Zlatic, J. Phys. F 2 (1972) L 99.
28. R. Bass, J. Phys. F 3 (1973) L 156.
29. M.J. Rice, Phys. Lett. 26 A (1967) 86, Phys. Rev. Lett. 20 (1968) 1439, 21 (1968) 871 (E).
30. A.J. Bennet and M.J. Rice, Phys. Rev. 185 (1969) 968.
31. J.T. Schriempf, A.I. Schindler and D.L. Mills, Phys. Rev. 187 (1969) 959.
32. A.B. Kaiser, Phys. Rev. B 3 (1971) 3040.
33. V. Zlatic, G. Grüner and N. Rivier, Solid State Comm. 14 (1974) 639.
34. A.J. Heeger, Solid State Physics, eds. F. Seitz, D. Turnball and H. Ehrenreich (Academic Press, New York, 1969), Vol. 23, p. 283.
35. C. Rizzuto, Reports on Progress in Physics, 37 (1974) 147.
36. W.M. Star, P.C.M. Gubbens and J.J. de Jong, Phys. Lett. 36 A (1971) 15.
37. R.G. Sharma and M.S.R. Chari, J. Low Temp. Phys. 14 (1974) 365.
38. R.G. Sharma and M.S.R. Chari, J. Low Temp. Phys. 15 (1974) 79.
39. D.A. Spohr and R.T. Webber, Phys. Rev. 105 (1957) 1427.
40. H.L. Malm and S.B. Woods, Can. J. Phys. 44 (1966) 2293.
41. M.S.R. Chari and N.S. Natarjan, Phys. Stat. Sol. 29 (1968) K 69.
42. P.L. Garbarino and C.A. Reynolds, Phys. Rev. B 4 (1971) 167.
43. D. Jha and M.H. Jericho, Phys. Rev. B 3 (1971) 147.
44. W.M. Star, Thesis, University of Leiden, 1971.

45. W.M. Star, F.B. Basters, G.M. Nap, E. de Vroede and C. van Baarle, Physica 58 (1972) 585, Comm. Kamerlingh Onnes Lab., Leiden, No. 390 a.
46. C. Rizzuto, E. Babic and A.M. Stewart. J. Phys. F 3 (1973) 825.
47. M.D. Daybell and W.A. Steyert, Phys. Rev. Lett. 20 (1968) 195.
48. M.D. Daybell, Magnetism, ed. H. Suhl (Academic Press, New York, 1973), Vol. V, p. 121.
49. K. Fischer, J. Phys. Chem. Solids 29 (1968) 1227.
50. Susceptibility measurements and nuclear orientation on Cu-Mn suggest a value of the Kondo temperature of the order of 10 mK.
E.C. Hirschkoff, O.G. Symko and J.C. Wheatley, J. Low. Temp. Phys. 5 (1971) 155.
I.A. Campbell, J.P. Compton, I.R. Williams and G.V.H. Wilson, Phys. Rev. Lett. 19 (1967) 1319.
W.P. Pratt, Jr., R.I. Schermer and W.A. Steyert, J. Low. Temp. Phys. 1 (1969) 469.
J. Flouquet, J. Phys. F 1 (1971) 87.
51. J.R. Cooper, Z. Vucic and E. Babic, J. Phys. F 4 (1974) 489.
52. M. Read and A.M. Guenault, J. Phys. F 4 (1974) 94.
53. I.M. Templeton, J. Phys. F 4 (1974) L 15.
54. M.J. Rice, Phys. Rev. Lett. 23 (1969) 1108.
55. M.J. Rice and O. Bunce, Phys. Rev. B 2 (1970) 3833.
56. H. Smith, Solid State Comm. 8 (1970) 1991.
57. H. Smith and J.W. Wilkins, Phys. Rev. Lett. 24 (1970) 221.
58. A.B. Kaiser and S. Doniach, Intern. J. Magnetism 1 (1970) 11.
59. C. Herring, Phys. Rev. Lett. 19 (1967) 167, 684 (E).
60. J. Souletie, J. Low Temp. Phys. 7 (1972) 141.
61. O. Laborde and P. Radhakrishna, J. Phys. F 3 (1973) 1731.

SAMENVATTING

In dit proefschrift worden de resultaten van het onderzoek naar het gedrag van de elektrische- en warmtegeleiding en de thermospanning van verdunde koperlegeringen bij lage temperaturen beschreven. Het onderzoek werd enkele jaren geleden aangevangen met het doel inzicht te verkrijgen in het gedrag van het Lorenz getal van verdunde magnetische koperlegeringen. Het Lorenz getal is de verhouding tussen de elektrische weerstand en het produkt van de warmteweerstand en de temperatuur. De transporteigenschappen van verdunde magnetische legeringen wijken af van die van niet-magnetische legeringen tengevolge van de verstrooiing van de geleidingselektronen aan de magnetische onzuiverheden (Kondo effect). Het meest bekende verschijnsel is het minimum in de elektrische weerstand. De warmte weerstand (en dus het Lorenz getal) was een van de fysische grootheden waarin het effect van het bovengenoemde verstrooiingsproces lange tijd onduidelijk was, voornamelijk vanwege de experimentele problemen. Het optreden van een extra component in de warmtegeleiding, n.l. de roosterwarmtegeleiding, bemoeilijkt de interpretatie van warmtegeleidingsmetingen. Bovendien geeft de gevoeligheid van het warmtegeleidingsvermogen voor inelastische verstrooiingsprocessen aanleiding tot het optreden van een relatief grotere weerstand t.g.v. de elektron-fonon verstrooiing dan de analoge term in de elektrische weerstand. Dit had tot gevolg, dat het gedrag van de warmtegeleiding van normale (niet-magnetische) verdunde koper legeringen nauwkeurig onderzocht moest worden, alvorens over te gaan tot een analyse van het Lorenz getal van verdunde magnetische koperlegeringen. De resultaten van dit onderzoek zijn beschreven in hoofdstuk III.

De warmteweerstand t.g.v. de elektron-fonon wisselwerking ('ideale' warmteweerstand) van koper kan niet beschreven worden met de uitdrukking afgeleid voor het vrije-elektronen model. Dit wordt veroorzaakt door de wisselwerking tussen de geleidingselektronen en de transversale fononen en door het optreden van afwijkingen van de regel van Matthiessen. De wisselwerking tussen de geleidingselektronen en de transversale fononen leidt tevens tot een gecompliceerd gedrag van de roosterwarmtegeleiding bij lage temperaturen. De resultaten van metingen van de roosterwarmtegeleiding aan zeer verdunde Cu-Ge en Cu-Sn legeringen zijn vergeleken met de theorie van Pippard voor de absorptie van geluidsgolven in metalen. De correlatie tussen de grootte van de roosterwarmtegeleiding en de vrije weglengte van de elektronen zoals die reeds waargenomen was in meer geconcentreerde legeringen blijkt ook in zeer verdunde legeringen te bestaan.

Een interpretatie van het gedrag van de roosterwarmtegeleiding bij hogere temperaturen wordt bemoeilijkt door het feit dat bij deze temperaturen de elektronenwarmtegeleiding niet nauwkeurig bekend is. De onzekerheid in de waarde van de elektronenwarmtegeleiding ontstaat door het optreden van afwijkingen van de regel van Matthiessen. Een nauwkeurige analyse van de meetresultaten bracht aan het licht dat deze afwijkingen van dezelfde orde van grootte zijn als die welke gevonden zijn in meerwaardige metalen. De voornaamste oorzaak voor de beperking van de roosterwarmtegeleiding bij hogere temperaturen ($10K \lesssim T \lesssim 30K$) bleek de verstrooiing van de fononen aan puntfouten (in dit geval Ge en Sn atomen) te zijn.

De resultaten voor de niet-magnetische legeringen zoals die beschreven zijn in hoofdstuk III, zijn in hoofdstuk IV gebruikt om de warmteweerstand, t.g.v. de verstrooiing van de geleidingselektronen aan de magnetische gast-atomen, van verdunde Cu-Fe, Cu-Cr en Cu-Mn legeringen te bepalen. Deze weerstandsterm werd gecombineerd met de gemeten elektrische weerstand (de 'ideale' elektrische weerstand is voor $T < 10K$ te verwaarlozen) om het Lorenz getal voor onzuiverheidsverstrooiing te verkrijgen. De drie bovengenoemde systemen zijn gekozen om hun verschillende waarden van een karakteristieke temperatuur T_K (Kondo temperatuur). Dit maakt het mogelijk om het gedrag van transporteigenschappen (i.h.b. het Lorenz getal) te bestuderen in het gebied $T < T_K$ (Cu-Fe), $T \approx T_K$ (Cu-Cr) en $T >> T_K$ (Cu-Mn). Een van de belangrijkste resultaten van de metingen is het optreden van een maximum in het Lorenz getal voor $T \approx T_K$, zoals theoretisch reeds voorspeld was. De bestaande theorieën geven evenwel nog geen bevredigende beschrijving van het experimenteel gevonden gedrag van de transport eigenschappen voor $T < T_K$. Een analyse van de Lorenz getal metingen aan Cu-Fe en Cu-Cr suggereert dat de elektrische- en warmteweerstand beschreven kunnen worden met eenzelfde relaxatietijd die de verstrooiing van de geleidingselektronen aan de onzuiverheidsatomen karakteriseert.

Een interpretatie van de metingen op basis van het lokale spin fluctuatie model leidt tot het definiëren van een Lorenz getal voor elektron-elektron verstrooiing. Dit Lorenz getal, waarvoor de waarde $0.32\ L_0$ (L_0 is de Sommerfeld waarde van het Lorenz getal) voor Cu-Fe bij lage temperaturen gevonden wordt, kan mogelijk informatie verschaffen omtrent de vorm van het spin fluctuatie spectrum in deze legeringen.

Op verzoek van de faculteit der Wiskunde en Natuurwetenschappen volgt hier een overzicht van mijn studie.

Nadat ik in 1963 het diploma H.B.S.-B had behaald aan het Christelijk Lyceum "Zandvliet" te Den Haag, begon ik in hetzelfde jaar aan mijn studie aan de Rijksuniversiteit te Leiden. In 1967 legde ik het kandidaatsexamen Natuurkunde en Wiskunde met bijvak Sterrekunde (a') af, waarna ik mijn werkzaamheden begon op het Kamerlingh Onnes Laboratorium. Aanvankelijk assisteerde ik Drs. J.P. Kaper bij zijn onderzoek omtrent de verankering van magnetische flux in supergeleiders. Sinds begin 1969 ben ik werkzaam in de werkgroep 'F.O.M.-metalen Mt IV', waarvan tot 1 november 1973 Prof. Dr. C.J. Gorter de leiding had. De dagelijkse leiding van de groep berust bij Dr. G.J. van den Berg en bij Dr. B. Knook.

In 1969 ben ik samen met Drs. P.C.M. Gubbens begonnen aan een onderzoek betreffende het Lorenz getal van Cu-Fe legeringen bij lage temperaturen. Eind 1970 legde ik het doctoraal examen af, waarna ik als wetenschappelijk medewerker van de Stichting voor Fundamenteel Onderzoek der Materie (F.O.M.) het bovenvermelde onderzoek voortzette.

Sinds 1969 ben ik als assistent betrokken geweest bij het natuurkunde-praktikum voor prekandidaten.

Velen hebben een bijdrage geleverd aan het tot stand komen van dit proefschrift. Bij het van de grond komen van dit onderzoek zijn de waardevolle adviezen en suggesties van Dr. W.M. Star van grote betekenis geweest. De bijzonder plezierige samenwerking met Drs. P.C.M. Gubbens heb ik reeds gememoreerd. Bij het uitvoeren van de metingen heb ik de medewerking van Drs. J. Hansen en Drs. C.G. van Went zeer op prijs gesteld. De vele discussies met Dr. J.E. van Dam dienen niet onvermeld te blijven. De medewerking van Drs. C.J. de Pater en M.J. Zuilhof bij het uitwerken van enkele van de meetresultaten heb ik zeer gewaardeerd.

De legeringen werden vervaardigd door de heren C.E. Snel, H.J. Tan en T.J. Gortemulder. De chemische analyse van enkele preparaten werd uitgevoerd door mevr. M.A. Otten-Scholten en mevr. B.M. Aarts-van den Ende. De heer G.L.E. van Vliet ben ik zeer erkentelijk voor enkele suggesties omtrent het verbeteren van de elektronika van de meetopstelling. De samenwerking met de heren J. Turenhout en J.F. Bennink is steeds zeer prettig geweest.

De tekeningen in dit proefschrift werden vervaardigd door de heren W. Rijnsburger en W.J. Brokaar, terwijl de heer W.F. Tegelaar voor de foto's zorgde.

STELLINGEN

1. Simons geeft een verklaring voor het bestaan van een universeel verband tussen het gereduceerde warmtegeleidingsvermogen λ^* $(=\lambda/\lambda_{max})$ van niet-metallische vaste stoffen en de gereduceerde temperatuur $T^*(=T/T_{max})$. Dit kan tot een onjuiste interpretatie van het gedrag van de warmtegeleiding bij temperaturen in de buurt van T_{max} leiden.

S. Simons, J.Phys. C 6 (1973) 2947

2. De betekenis van het vraagteken, dat Kao c.s. plaatsen in de titel van hun artikel, "PdV: A System with a High Spin-Fluctuation or Kondo Temperature?", is om verschillende redenen onduidelijk.

F.C.C. Kao, M.E. Colp en G. Williams,
Phys.Rev. B 8 (1973) 1228

3. Het verband tussen de anisotrope polariseerbaarheid van symmetrische tol-moleculen en de depolarisatie-verhouding voor het verstrooide licht, zoals gegeven door Rowell c.s., is onjuist.

R.L. Rowell, G.M. Aval en J.J. Barrett,
J.Chem.Phys. 54 (1971) 1960

4. De invloed van elektron-elektron verstrooiing op het warmtegeleidingsvermogen van wolfraam bij lage temperaturen wordt door Wagner c.s. overschat.

D.K. Wagner, J.C. Garland en R. Bowers,
Phys.Rev. B 3 (1971) 3141

5. De theoretische kromme, die Abkowitz en Honig geven voor de temperatuurafhankelijkheid van het antiferromagnetische resonantieveld in $MnCl_2.4H_2O$ bij een resonantiefrequentie van 9.2 GHz voor het magneetveld in de ordeningsrichting, is niet correct.

M. Abkowitz en A. Honig, Phys.Rev. 136 (1964) A 1003

6. De overeenkomst tussen de door Klein en Brout berekende en de experimenteel bepaalde waarde van de soortelijke warmte van een "spin glass" bij lage temperaturen berust in een aantal gevallen op toeval.

M.W. Klein en R. Brout, Phys.Rev. 132 (1963) 2412

7. Uit Mössbauer-effect metingen aan Cu-Fe hebben Steiner c.s. het bestaan van een T^2 term in de lokale susceptibiliteit aangetoond. De vergelijking die zij maken van deze term met het Curie-Weiss gedrag van dit systeem, zoals gevonden door Tholence en Tournier, is inconsequent.

P. Steiner, W. v. Zdrojewski, D. Gumprecht en S. Hüfner, Phys.Rev.Lett. 31 (1973) 355.
J.L. Tholence en R. Tournier, Phys.Rev.Lett. 25 (1970) 867

8. Wanneer in 1976 een nieuwe ^{4}He-temperatuurschaal zal worden vastgesteld, is het gewenst deze in de vorm van één of meer analytische vergelijkingen te geven. Deze vergelijkingen zouden bij het λ-punt en het kritisch punt van helium een thermodynamisch consistente vorm moeten hebben.

H. Montgomery, Cryogenics 5 (1965) 229.
G.L. Jones, Physica 76 (1974) 181

9. De overeenkomst tussen de experimenteel bepaalde roosterwarmteweerstand $(1/\lambda_g)$ van een zeer verdunde legering en de berekende $1/\lambda_g$ van het zuivere metaal door middel van een door Klemens afgeleid verband tussen $1/\lambda_g$ en de ideale warmteweerstand is toevallig.

10. Een onderzoek naar het gedrag van het Lorenz getal van Al-Mn legeringen als functie van de temperatuur kan informatie verschaffen omtrent de vorm van het spin-fluctuatie spectrum en is daarom van groot belang voor een waardebepaling van de huidige spin-fluctuatie theorieën.

11. Het optreden van de door Watanabé c.s. waargenomen rosetvormige dislokatie patronen in verdunde Cu-Al éénkristallen kan worden verklaard door de aanwezigheid van Al_4C_3 clusters.

J. Watanabé, Y. Imashimizu, H. Nagumo en K. Tsukamoto, J.Cryst.Growth 24 (1974) 414

12. Het veelal ontbreken van gambieten in het openingsrepertoire van schakers kan worden toegeschreven aan onjuiste opvattingen omtrent de waarde van de gambietopening.

11 december 1974

J.J. de Jong